

**Matter wave interferences of potassium molecules
and the influence of collisions with potassium atoms
in the ground state**

Von der Fakultät für Mathematik und Physik der
Gottfried Wilhelm Leibniz Universität Hannover

zur Erlangung des Grades

**Doktor der Naturwissenschaften
Dr. rer. nat.**

genehmigte Dissertation

von

Dipl.-Phys. Ivan V. Sherstov
geboren am 10.11.1979 in Moskau (Russland)

2006

Referent: Prof. Dr. E. Tiemann
Korreferent: Prof. Dr. J. Großer

Tag der Promotion: 21. Juli 2006

To my wife Yulia and son Alexander

Abstract

Ivan V. Sherstov

Materiewelleninterferenzen von Kaliummolekülen und der Einfluß von Stößen mit Kaliumatomen im Grundzustand

Das Ziel der vorliegenden Arbeit ist, die Eignung und die Präzision von molekularer Materiewellen-Interferometrie für das Studium von schwachen Wechselwirkungen wie kalten Stößen zu untersuchen. Dafür wurde ein Ramsey-Bordé Aufbau eines molekularen Materiewellen-Interferometers mit vier Laserstrahlteilern an einem Überschall-Atomstrahl von Kalium verwendet, in welchem einige Prozent K_2 Moleküle verdünnt sind. Die beobachteten Signale sind eine Superposition von zwei unterschiedlichen Interferenzmustern: Eines ist die Interferenz vom Ramsey-Bordé Typ entsprechend einer Verschiebung der molekularen Wellenpakete gegeneinander in Längsrichtung in der Richtung des Überschallstrahls, die durch zwei gegenläufige Paare von Laserstrahlen erzeugt wird. Das zweite ist eine rein optische Ramsey Interferenz: ein räumlicher Überlapp der verhältnismäßig großen molekularen Wellenpakete in der transversalen Richtung verursacht durch ein Paar von Laserstrahlen. In der vorliegenden Konfiguration unseres molekularen Materiewellen-Interferometers konnten die möglichen Ausgänge im Grund- und angeregten Zustand unabhängig verwendet werden. Ein Vergleich der Eigenschaften des Ausgangs im angeregten Zustand und des Grundzustandsausgangs wurde für verschiedene Molekülübergänge durchgeführt. Der neu entwickelte Grundzustandsausgang bietet den Vorteil der Beobachtung von Interferenzen einzeln aufgelöster Hyperfeinstrukturkomponenten

. Die Materiewellen-Interferometrie wird hier angewendet, um niederenergetische Stöße zwischen Atomen und Molekülen in einem Überschallstrahl von Kalium zu untersuchen. Die K_2 -Moleküle bewegen sich in einem atomaren Medium und bekommen dabei eine zusätzliche Phasenverschiebung entsprechend den kalten Stößen mit den Atomen (die Relativgeschwindigkeit zwischen Atomen und Molekülen entspricht 16 K). Die Verschiebung der Interferenzmuster bei Änderungen der Eigenschaften des Mediums, d.h. bei Veränderung der Dichte der Atome im Atomstrahl, wurde untersucht. Mit Ablenkung der Atome aus Molekülstrahl war es möglich, die Atomdichte um eine Größenordnung zu ändern und eine Phasenverschiebung der Interferenzstruktur zu beobachten, die einer Druckverschiebung von ungefähr 10 kHz für den Molekülübergang des Kaliums entspricht. Systematische Untersuchungen zeigten keine Abhängigkeit der Druckverschiebung von Vibrations- und Rotationsquantenzahl in dem untersuchten Bereich. Als ein alternativer Weg, die Druckverschiebung auf Grund von Stößen zwischen Atomen und Molekülen zu studieren, wurden absolute Frequenzmessungen von Molekülübergängen, mit ein- und ausgeschalteter atomarer Dichte, unter Anwendung des Frequenzkammes eines Femtosekundenlasers durchgeführt. Die Ergebnisse der direkten Messungen der Druckverschiebung zeigte keinen Widerspruch zu den interferometrischen Messungen innerhalb der experimentellen Unsicherheiten und der Effizienz der Ablenkung der Atome.

Schlagworte zum Inhalt

Materiewellen-Interferometrie, K_2 , kalte Stöße, absolute Frequenzmessungen

Abstract

Ivan V. Sherstov

Matter wave interferences of potassium molecules and the influence of collisions with potassium atoms in the ground state

The aim of the current work is to investigate the suitability and the precision of molecular matter wave interferometry for study of weak interactions like cold collisions. For this a Ramsey-Bordé setup of a molecular matter wave interferometer with four laser beam splitters was realized in a supersonic atomic beam of potassium with a few percent of K_2 molecules diluted in it. The observed signals are a superposition of two different interference patterns. One is the Ramsey-Bordé type interference due to a longitudinal displacement of molecular wave packages in the direction of the supersonic beam produced by two pairs of counter propagating laser beams. The second one is pure optical Ramsey fringes: a spatial overlap of relatively large molecular wave packages in the transversal direction created by only two laser beam splitters.

In the present configuration of our molecular matter wave interferometer both possible exits in the ground and excited states could be independently used. A comparison of the properties of excited state exit and ground state exit operated on different molecular transitions was done. The newly developed ground state exit gives the advantage to observe fully resolved hyperfine interferences.

The matter wave interferometry is applied to examine low energy collisions in a supersonic potassium beam between atoms and molecules. K_2 molecules propagate through an atomic medium and hence gain some additional phase shift due to cold collisions (relative atom-molecule velocity corresponding to 16 K) with the atoms. By changing the properties of the medium, i.e. varying the density of the atoms in the beam, the shift of the interference patterns was investigated.

By deflecting atoms out of molecular beam we were able to change the atomic density by one order of magnitude and observed a phase shift of the interference structure relating to a pressure shift of about 10 kHz for the molecular transition of potassium. Systematic investigations did not show any dependence of the pressure shift on vibrational and rotational quantum in the limit range studied.

As an alternative way to study the pressure shift due to atom-molecular collisions absolute frequency measurements of the molecular transitions with atomic density in the beam switched on and off were carried out applying the frequency comb of a fs-laser. The results of the direct measurements of the pressure shift did not show a contradiction to the interferometric measurements within experimental uncertainties and efficiency of the atomic deflection.

Keywords of the contents

matter wave interferometer, K_2 , cold collisions, absolute frequency measurements

Table of Contents

Table of Contents	- 1 -
List of Figures	- 5 -
1. Introduction.....	- 9 -
2. Principles of matter wave interferometry	- 13 -
2.1. Manipulation of matter waves (beam splitters by resonant light fields). - 13 -	
2.2. Ramsey-Bordé matter wave interferometer with four laser beam splitters	- 15 -
2.3. Optical Ramsey matter wave interferometer with two laser beam splitters	- 18 -
2.4. Simultaneous observation of two and four laser beam splitter matter wave interferometers	- 19 -
2.4.1. Transversal and longitudinal coherence in a supersonic molecular beam	- 23 -
3. Experimental setup.....	- 27 -
3.1. Molecular beam machine	- 28 -
3.1.1. Vacuum apparatus.....	- 28 -
3.1.2. Fluorescence detection.....	- 30 -
3.1.3. Data acquisition system	- 33 -
3.2. Laser source for molecular matter wave interferometer	- 33 -
3.2.1. External cavity diode laser system.....	- 34 -
3.2.2. Frequency stabilization	- 36 -
3.2.3. Optical arrangement of molecular matter wave interferometer	- 39 -
3.3. Laser systems used in applications of matter wave interferometry	- 41 -
3.3.1. Deflection laser system	- 41 -
3.3.2. Detection laser system	- 44 -
3.3.3. He-Ne frequency stabilization	- 45 -
4. Experimental study of molecular matter wave interferometer	- 49 -
4.1. Potassium dimers as a base for molecular matter wave interferometer..	- 50 -
4.1.1. Production of long living states	- 50 -
4.1.2. Observed hyperfine structures in the molecular beam of K_2	- 53 -

4.2.	Experimental study of molecular matter wave interferometers with two and four laser beam splitters	- 56 -
4.2.1.	Excited state exit detection and analysis of observed signals.....	- 57 -
4.2.2.	Investigation of the matter wave interferometer with four laser beam splitters	- 61 -
4.2.3.	Investigation of the matter wave interferometer with two laser beam splitters	- 64 -
4.2.4.	Comparison between two and four laser beam splitter molecular matter wave interferometers.....	- 65 -
4.3.	Detection on different exits of the molecular matter wave interferometer.....	- 66 -
4.3.1.	Ground state exit of molecular matter wave interferometer observed on the B-X transition.....	- 68 -
4.3.2.	Ground state exit of molecular matter wave interferometer observed with the b-X transition	- 70 -
4.3.3.	Excited vs. ground state exit: experimental advantages and complications	- 72 -
5.	Cold collisions observed in a supersonic potassium beam	- 75 -
5.1.	Theoretical background	- 75 -
5.2.	Switching atomic density inside supersonic potassium beam	- 79 -
5.2.1.	Potassium supersonic beam	- 80 -
5.2.2.	Experimental arrangement of the optical setup	- 81 -
5.3.	Low energy collisions examined by matter wave interferometry method.....	- 83 -
5.4.	Stability and precision of the interferometric measurements	- 87 -
6.	Absolute frequency measurements of molecular transitions for matter wave interferometer.....	- 89 -
6.1.	Optical setup for the measurements with the frequency comb	- 89 -
6.2.	Frequency measurements with femtosecond comb	- 90 -
6.3.	Results of the absolute frequency and relative measurement	- 93 -
6.4.	Uncertainty budget for the absolute frequency measurements of molecular transitions.....	- 94 -
7.	Summary and outlook	- 97 -
7.1.	Matter wave interferometry with potassium molecules.....	- 97 -

Table of contents

7.1.1.	Detection on ground state exit of interferometer	- 97 -
7.1.2.	Observation of different types of interferences	- 98 -
7.2.	Collisional experiments with molecular matter wave interferometer and absolute frequency measurements	- 99 -
7.3.	Outlook	- 101 -
Literature	- 105 -
Curriculum Vitae	- 111 -
Study	- 111 -
Thanks, Danke, Спасибо	- 113 -

List of Figures

Figure 2.1 Optical beam splitter.....	- 14 -
Figure 2.2 Ramsey-Bordé interferometer	- 16 -
Figure 2.3 Ramsey matter wave interferometer.....	- 18 -
Figure 2.4 Scheme of the spatial overlap of the wave packets for Ramsey-Bordé setup	- 21 -
Figure 2.5 Enlarged picture for the resulting overlap of the wave packages in the Ramsey-Bordé setup	- 22 -
Figure 3.1 General scheme of experiment	- 27 -
Figure 3.2. Vacuum apparatus.	- 29 -
Figure 3.3. Principal scheme of interferometer chamber.....	- 31 -
Figure 3.4 Residual magnetic field inside μ -metal box. Coordinate = 0 corresponds to the center of the μ -metal box	- 32 -
Figure 3.5 Principal scheme of interferometer laser system.....	- 35 -
Figure 3.6 PDH stabilization sutup.....	- 37 -
Figure 3.7 frequency drift of master 1	- 38 -
Figure 3.8 Optical arrangement of the Ramsey-Bordé matter wave interferometer..	- 39
-	
Figure 3.9 Ti-Sa laser system.....	- 42 -
Figure 3.10 Formation of deflection beam	- 43 -
Figure 3.11 Principal scheme of dye laser setup.....	- 45 -
Figure 3.12, Principal scheme of He-Ne stabilization	- 46 -
Figure 4.1 Lowest electronic states of potassium dimer.....	- 51 -
Figure 4.2 Lifetimes of mixed states for some v' and J' numbers of the coupled system $b^3\Pi_u(0^+) + A^1\Sigma_u^+$	- 52 -
Figure 4.3 Resolved hyperfine structure for two cases in the $27 - 0$ band of the $b^3\Pi_u(0^+) \leftarrow X^1\Sigma_g^+$ transition in the molecular beam. (A) and (B) corresponding to even and odd J'' number.....	- 54 -
Figure 4.4 Saturation spectroscopy of the R(25) $27 - 0 b^3\Pi_u(0^+) \leftarrow X^1\Sigma_g^+$ transition	- 56 -

Figure 4.5 Experimental scheme to observe excited state exit of molecular Ramsey-Bordé interferometer - 57 -

Figure 4.6 Interferences observed in potassium molecular beam - 58 -

Figure 4.7 Fourier spectrum of a recording like the right art of Figure 4.6 - 59 -

Figure 4.8 Digital filtering of studied spectra of the molecular matter wave interferometer in the Ramsey-Bordé configuration. The lower trace indicates longitudinal interferences after band pass digital filter while the upper part shows remaining incoherent background and optical Ramsey interferences. - 60 -

Figure 4.9 Signals of the Ramsey-Bordé molecular matter wave interferometer observed for different separations between the pair of the copropagating laser beams. - 62 -

Figure 4.10 Interference signals of the Ramsey-Bordé interferometer after digital filtering for some beam separations D . The part A indicates fringes corresponding to different hyperfine components; the part B is zoom on the highest in frequency hyperfine component. - 63 -

Figure 4.11 Interference signals of the optical Ramsey interferometer after digital filtering for some beam separations D - 64 -

Figure 4.12 Dependence of the frequency interval $1/P$ on the beam separation D for the optical Ramsey and Ramsey-Bordé molecular matter wave interferometers. The results for the optical Ramsey interferometer were fitted by formula $1/P = v/D$, while for the Ramsey-Bordé interferometer by $1/P = v/2D$ - 65 -

Figure 4.13 Scheme of the experimental setup for simultaneous observation of both exits of molecular matter wave interferometer - 67 -

Figure 4.14 Simultaneous spectra of the interference patterns for the ground state and excited state exits of the two laser beam splitter interferometer. The ground state exit is realized by excitation on the $Q(25) 4-0 B^1\Pi_u \leftarrow X^1\Sigma_g^+$ transition of K_2 .- 69 -

Figure 4.15 Simultaneous records of matter wave interference patterns from ground state exit detected by laser induced fluorescence on the highest frequency hyperfine component of the $R(25) (27-0) b-X$ transition, and on the excited state exit. Note that the ground state exit shows the interference pattern and the background due to only one hyperfine component. - 71 -

Figure 4.16 Result of narrow-band (0.7 μ s) Fourier-filtering of the Ramsey-Bordé interferences of both interferometer exits	- 72 -
Figure 4.17 The optical Ramsey interferences observed for the ground and excited state exits of the molecular matter wave interferometer at different beam separations D.....	- 73 -
Figure 5.1 Indexes of refraction for the Ramsey-Bordé setup.....	- 77 -
Figure 5.2 level diagram of ^{39}K D2 line	- 80 -
Figure 5.3 The optical setup for the collisional experiment	- 81 -
Figure 5.4 Sequence of the experiment to observe atom-molecule collisions in the potassium beam.....	- 83 -
Figure 5.5 Observed phase difference between ^{39}K atoms present and deflected for the R(25) 27-0 b-X line measured for the dark zone length $D=400\ \mu\text{m}$ by the Ramsey-Bordé setup	- 84 -
Figure 5.6 Dependence of the difference in the phase for the atomic density switched off/on as a function of the dark zone D observed for R(25) 27-0 b-X line by the Ramsey-Bordé setup	- 85 -
Figure 5.7 Observed phase difference between ^{39}K atoms present and deflected for several lines in the $b\ ^3\Pi_u(0^+) \leftarrow X\ ^1\Sigma_g^+$ system of K_2 measured for the dark zone length $D=400\ \mu\text{m}$	- 86 -
Figure 5.8 “Zero” measurement for the Ramsey-Bordé setup operated on the R(25) 27-0 b-X line with the dark zone length $D=400\ \mu\text{m}$	- 88 -
Figure 6.1 Scheme of the laser stabilization of the laser used for spectroscopy	- 89 -
Figure 6.2 Frequency scheme for determination of absolute frequencies with the frequency comb.....	- 90 -
Figure 6.3 Spectrum of the highest frequency hyperfine component of the R(24) (27-0) line of $b\ ^3\Pi_u(0^+) \leftarrow X\ ^1\Sigma_g^+$ of K_2 . The Lamb dip in the line centre has a width of about 500 kHz due to natural linewidth and time of flight broadening....	- 92 -
Figure 7.1 Perspective setup for study collisions with K atoms in Rydberg states and influence of near resonant light on the properties of molecular matter wave interferometer.....	- 102 -

1. Introduction

The field of the matter wave interferometry our days is a well developed tool and widely used for many applications [1, 45]. As a definition, interferometer uses the wave character of a particle; it does not matter if it is pseudo particle like photon, or “normal” one like atom or molecule. According to the particle-wave dualism formulated by de Broglie in 1924 interferometer can, in principle, be built for all sorts of particles. The essential condition to observe interference is that the particle-wave has to be by some means coherently split and recombined in indistinguishable paths.

While the 19th century was the golden age of interferometers with light, the twentieth century, definitely, became the era of the matter wave interferometers. Matter wave interferometers are proposed and constructed for variety of particles: starting with small and light like electrons [2] and neutrons [3, 4], through variety of different atoms [1, 5, 29, 36] and finishing by large and heavy particles like molecules [31, 39] or fullerenes [10]. For instance a typical de Broglie wavelength of complex and heavy particles like atoms and molecules at room temperature is much smaller than the size of the particles, what makes the matter wave interferometry with atoms and molecules so interesting. Another interesting feature of atoms and molecules is that these particles have internal degrees of freedom which can be utilized for matter wave interferometry. The real breakthrough in this field happed after a significant development of technology when lasers and nanofabrication became common tools in the lab life. The necessary coherent manipulation with atoms or molecules is realized today by mechanical gratings [6] or by applying laser light like resonant radiation [23, 30] or standing waves [11].

Since the invention, first the light interferometry and later the matter wave interferometry were implemented as an irreplaceable tool for precise measurements. The matter wave interferometry has been applied when the highest accuracy and sensitivity to weak interactions are needed like in cases of frequency standards [7], gravito-inertial sensors [23, 46] or for a search of a dipole moment of the electron [8].

Our interest in matter wave interferometry focuses on the interferometry with potassium dimers. We use the simple and elegant way of molecular interferometry where the splitting of the molecular wave package is realized by the energy and

momentum transfer during an interaction with laser radiation. The matter wave interferometer based on $^{39}\text{K}_2$ with laser beams as molecular matter wave beam splitters is the main subject of this thesis. We use the Ramsey-Bordé setup with four laser beam splitters [21] to obtain molecular matter wave interferences in well defined quantum state. The Ramsey-Bordé setup is realized in the potassium beam of atoms coming out of a heated oven with a few percent of dimers diluted in it. This work is extension of the studies done by Ch. Lisdat [35] who setup the first interferometer in our group, M. Frank [37] who built diode laser system for the interferometer, and S. Jung [32] who constructed the first laser systems for deflecting K atoms out of the supersonic beam. With the first setup of the matter wave interferometer with $^{39}\text{K}_2$ initial experiments to observe collisions with potassium atoms in ground and Rydberg (8s, 12s) states were presented [35].

The utilization of the K_2 molecules for a Ramsey-Bordé interferometer in the beam has several advantages compared to atoms. For example, due to the spin-orbit coupling between $A\ ^1\Sigma_u^+$ and $b\ ^3\Pi_u(0^+)$ molecular states there are, easily accessible by diode lasers, long living molecular states which are required for the Ramsey-Bordé interferometer setup. Or by using molecules for matter wave interferometry it is much simplified to observe simultaneously the two exits of molecular matter wave interferometer, namely in ground and excited states because according to the Franck-Condon principle the molecules in excited state will decay with very low probability to the original ground state [18].

Due to high collimation ratio in the particle jet we have quite narrow transversal and longitudinal velocity distributions compared to the mean velocity in the beam. So for our Ramsey-Bordé interferometer setup where the spatial separations between the wave packages are relatively small we expect to observe two types of molecular matter wave interferences: longitudinal Ramsey-Bordé and transversal optical Ramsey interferences.

Recent progress reported on the molecular BEC [13] stimulated the interest of many research groups worldwide to investigate low energy atom-molecule collisions. A brilliant investigations of collisions by matter wave interferometry method were done by D. Prichard with coworkers at the MIT, USA. In [26, 29] they studied atom-molecular and molecule-molecule collisions in a sodium supersonic beam by matter wave interferometer with nanofabricated gratings as coherent beam splitters. In these

experiments phase shift of interferometric signals due to collisions with particles injected externally were observed and an interesting model of attributing to the scattering medium an index of refraction was established.

In the current work we want to utilize the wave nature of the K_2 molecules to study weak interactions like cold collisions with K atoms in the supersonic beam. K_2 molecules propagate through this atomic medium and hence gain some additional phase shift due to cold collisions (relative atom-molecule velocity corresponding to 16 K) with the atoms. We want to change the properties of the scattering medium by varying the density of the atoms in the beam and observe a shift of the interference patterns.

In section 2 an introduction to the field of the matter wave interferometry is given and the principles of our molecular interferometer in the Ramsey-Bordé configuration are described. Section 3 presents the current status of the complete experimental setup including all laser systems and vacuum apparatus used. In section 4 the detailed analysis and comparison of the longitudinal Ramsey-Bordé and the transversal optical Ramsey interferences are done. Also in the same section a detailed investigation of the detection of the ground state exit on different molecular transitions and comparison with the typical detection of the excited state exit of the interferometer are presented. Section 5 contains the description and results of the collisions within the supersonic potassium beam studied by matter wave interferometry method with $^{39}K_2$. Section 6 presents absolute frequency measurements with a fs-comb of molecular transitions as an alternative way to interferometric measurements to study cold atom-molecular collisions within potassium jet. The final section concludes with summary and outlook of the matter wave experiment.

2. Principles of matter wave interferometry

The matter wave interferometry with light induced beam splitters is a well established field in high precision laser spectroscopy. It was first suggested by Ramsey in [19] to use a microwave radiation in spatially separated interaction zones for spectroscopy. The proposed configuration allows producing interferometric signals by tuning the excitation frequency with the periodicity inversely proportional to the flight time between the interaction zones.

In this chapter an introduction to the field of matter wave interferometry is given. The basic element of any matter wave interferometer is a beam splitter for matter wave. Different types of beam splitters for matter waves exist like mechanical gratings [6] or light fields [5]. The case of light fields will be discussed in chapter 2.1. The Ramsey-Bordé scheme for a matter wave interferometer with four laser beam splitters will be discussed in chapter 2.2. The qualitative background for optical Ramsey fringes produced by only two laser beam splitters will be considered in chapter 2.2.

2.1. Manipulation of matter waves (beam splitters by resonant light fields)

Since de Broglie first described a particle with mass m and velocity v by a matter wave with a wavelength λ_{dB} given by the equation (2.1)

$$\lambda_{dB} = \frac{h}{mv} \quad (2.1)$$

the term matter wave appeared. For example the de Broglie wavelength λ_{dB} for potassium dimer $^{39}\text{K}_2$ with $v = 1000$ m/s will be about 10^{-12} m = 1 pm.

The thermal velocity v is proportional to $v \propto \sqrt{\frac{T}{m}}$ so to reach large values of the de Broglie wavelength λ_{dB} in the order of 1 μm low temperatures of only few mK are needed. Such temperatures are easily accessible now in a magneto-optical trap or some other types of traps due to development of the laser cooling and trapping

techniques for atoms and molecules [53]. They are also accessible by the process of deceleration of the supersonic particle beam with polar molecules [48].

Normally, we do not have a monochromatic particle beam like an atom laser so another parameter of the matter wave which should be mentioned is a size of the wave package for a particle beam out of an oven. In some cases we have an ensemble of particles with a very narrow velocity distribution, the size of the wave package could be rather large. It could even reach the size of the confining potential for the case of the Bose-Einstein condensate [54]. A large size of the wave package could be achieved also in a well collimated supersonic jet. Although the mean velocity in the beam could be several thousands of meters per second, the longitudinal or/and transversal distribution of the velocity could be only some meters or centimetres per second. In section 3.1 our supersonic potassium beam will be described where we had a mean velocity for the potassium atoms and dimers of about 1000 m/s while the transversal and longitudinal distributions were about 1 m/s and 50 m/s correspondingly.

We will use a supersonic beam of potassium molecules interacting with resonant laser fields. So to explain how our molecular matter wave interferometer functions one should first mention a beam splitter for potassium molecules produced by a resonant radiation. The mechanical interpretation of such beam splitter is described in [1, 35].

Let first consider a two-level molecule which could be in a ground state $|g\rangle$ and an excited state $|e\rangle$, both interacting with laser radiation (Figure 2.1). The separation between the levels is $\hbar\omega_0$ and the laser frequency is ω_L ; we also assume that laser and molecular beams are perpendicular to each other.

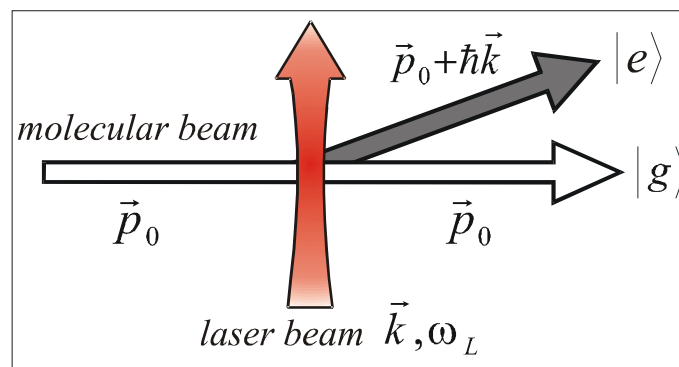


Figure 2.1 Optical beam splitter.

The energy of the system of molecule light field will be conserved and we can write the condition for the energy conservation

$$\frac{\vec{p}_0^2}{2M} + \hbar\omega_L = \frac{(\vec{p}_0 + \hbar\vec{k})^2}{2M} + \hbar\omega_0 \quad (2.2)$$

$|\vec{k}| = \frac{\omega_L}{c}$ gives the wave vector of the absorbed photon and evaluation of the equation

(2.2) leads to

$$\frac{\vec{k} \cdot \vec{p}_0}{m} = \Delta - \frac{\hbar k^2}{2m} \quad (2.3)$$

where $\Delta = \omega_L - \omega_0$ is the detuning of the laser and $\frac{\hbar k^2}{2m}$ is the recoil energy due to the absorbed photon.

One can see that the momentum of the photon is transferred to the molecule. Thus the molecule matter wave can be split in space (compare Figure 2.1) with a desired probability (for instance 50/50) if the laser intensity and detuning is chosen properly. The importance of the laser detuning Δ and the product $\vec{k} \cdot \vec{p}_0$ for the matter wave interferometry will be discussed later.

2.2. Ramsey-Bordé matter wave interferometer with four laser beam splitters

One of the possible realizations of matter wave interferometer in the optical domain could be Ramsey-Bordé matter wave interferometer with four laser beam splitters. This type of matter wave interferometer was realized in our working group [35] and in this chapter I would like to give an overview of its principle with Figure 2.2.

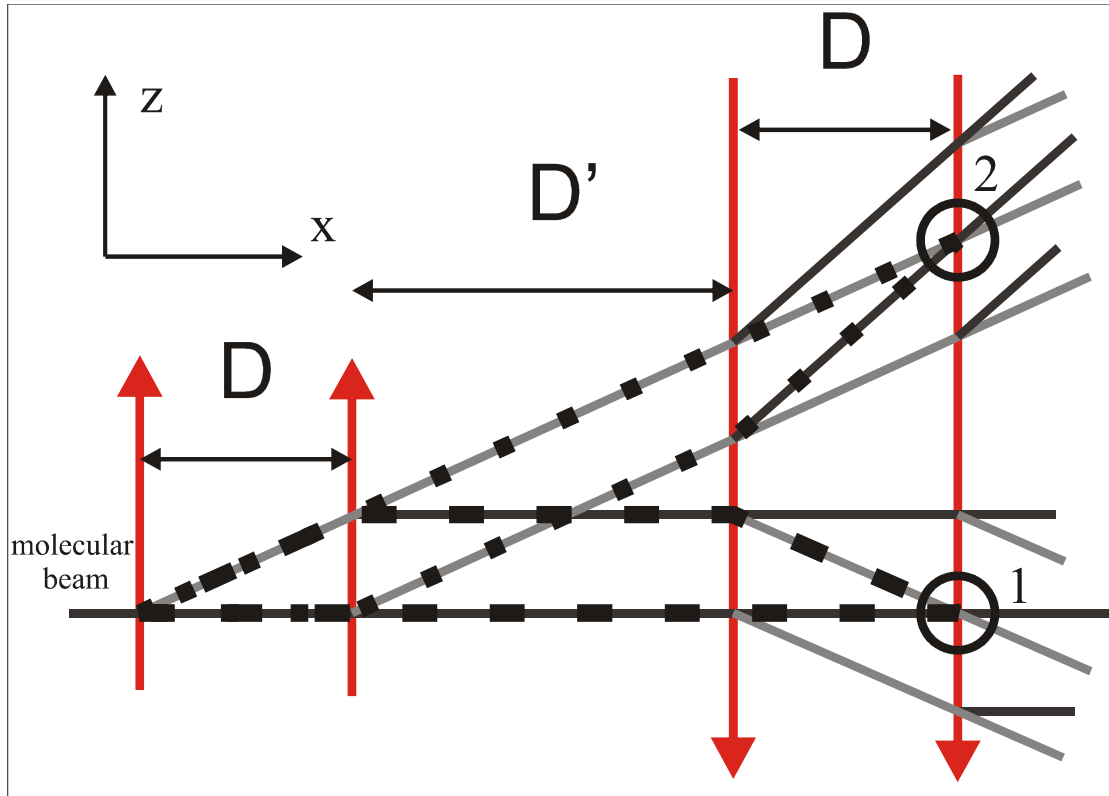


Figure 2.2 Ramsey-Bordé interferometer

Let us consider two pairs of counter propagating laser beams interacting with the molecular beam propagating in the x direction (Figure 2.2). The separation between copropagating laser beams in each pair is D , while the spacing between the two pairs of counter propagating beams is D' . The laser beams are acting as a beam splitter for molecular wave packets the same manner as described in chapter 2.1. By each interaction process an incoming molecular matter wave is split into two parts. The result will be 16 partial waves after the last fourth laser beam where only the two circled pairs could, in principle, form closed paths to produce an interferometer. The two possible matter wave interferometers, indicated on Figure 2.2 as dashed and dotted lines, use different quantum states, given as black line for state $|g\rangle$ and as grey line for $|e\rangle$, during their travel through the beam pair separations D and the central distance D' . The interferometer marked with dotted line uses only the excited state in one arm with switching to ground state on distances D in the second arm while in the dashed interferometer the molecular partial wave propagates in one arm only in the ground state.

The theoretical description of the Ramsey-Bordé interferometer can be found in [1,21,30,35] so here I would like to mention only some key points of it. The first

important point is a longitudinal (in the direction of the molecular beam) displacement (phase shift) of the produced partial molecular waves. The laser beam for beam splitter does not have a shape of ideal plane wave; it is normally a localized beam which has Gaussian distribution so its momentum composition consists of some variety of wave vectors. According to equation (2.3) the molecule absorbs a photon with the momentum compensating the laser detuning. Thus for the case $\Delta - \delta \neq 0$ the wave vector \vec{k} will have a component in direction of \vec{p}_0 and therefore accelerate the molecule in the longitudinal direction. This change of the velocity for one molecular partial wave will cause a relative longitudinal displacement on the whole path through the interferometer [49]

$$\Delta x = 2 \frac{D}{v_x} (\Delta \pm \delta) / k \quad (2.4)$$

where $\delta = \frac{\hbar k^2}{2m}$ is the recoil shift in equation (2.3). The plus and minus signs are corresponding to matter wave interferometers marked by dashed and dotted lines in Figure 2.2. Because we do not know which path the molecule will take we are expecting interference of molecular partial waves at the points on Figure 2.2 marked with circles. The interference term of both possible molecular matter wave interferometers will be (neglecting second order Doppler effect) [47]

$$\langle e | e \rangle_{\text{int}} = A_1 \cos[2T(\Delta - \delta) + \varphi_{\text{tot}}] + A_2 \cos[2T(\Delta + \delta) + \varphi_{\text{tot}}] \quad (2.5)$$

where A_1 and A_2 denote the amplitude of the two recoil components and $T = \frac{D}{v_x}$. The

term $\varphi_{\text{tot}} = \varphi_2 - \varphi_1 + \varphi_4 - \varphi_3$ is present because each interaction between molecules and laser beam will imprint on the phase of the molecular wave function some additional phase φ_i by the corresponding laser beam. The Ramsey-Bordé interferometer signal given in the formula (2.5) is visible while the coherence length

$l_{\text{coh}}^x \equiv \frac{\hbar}{2\Delta p}$ of a wave packet with momentum spread Δp is larger than the displacement Δx .

2.3. Optical Ramsey matter wave interferometer with two laser beam splitters

As it was mentioned above the simplest construction of a matter wave interferometer consists only of one pair of copropagating laser beams (Figure 2.3). It was first proposed and realized by N. Ramsey [19] using excitation frequencies for which the momentum transfer is negligible for the transversal splitting.

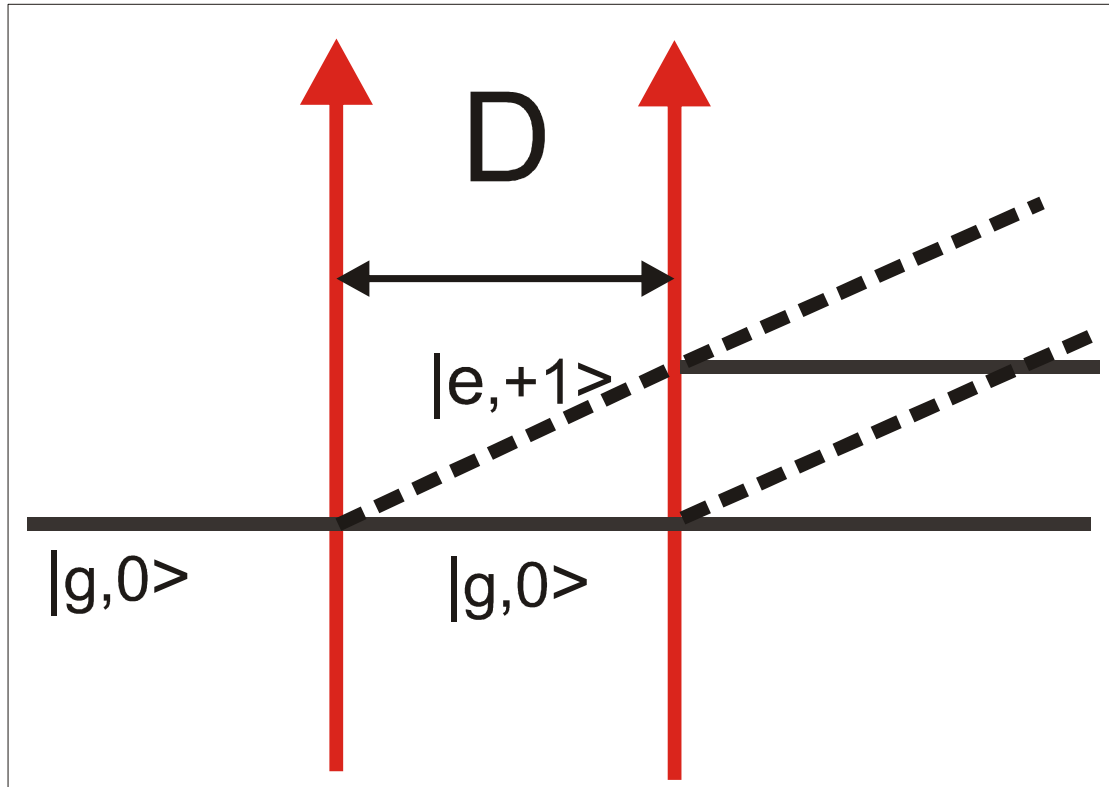


Figure 2.3 Ramsey matter wave interferometer

I will discuss the more general case of two interaction zones. The wave packets here are recombined the same way as was mentioned in section 2.2 but the two exits of the interferometer have now some displacement in the direction of laser beams

$$\Delta z = \frac{D}{v_x} \frac{\hbar k}{m} \quad (2.6)$$

where $\frac{D}{v_x}$ denotes the time molecules need to reach the second laser beam and $\frac{\hbar k}{m}$

shows the recoil velocity component in z direction.

This type of the matter wave interferometer is sensitive to the transverse coherence length of the molecular beam $l_{coh}^z = \frac{\hbar}{2m\Delta v_z}$ [1]. For microwave radiation the transferred photon momentum will be quite small and thus the displacement Δz is negligible compared to l_{coh}^z . Interference patterns could be easily observed by scanning the excitation frequency while when we are going to the optical domain a high collimation ratio for the molecular beam or small Δv_z and large l_{coh}^z is needed. The interference term will be

$$\langle e|e \rangle_{int} \propto \cos[T(\Delta - \delta) + \varphi_2 - \varphi_1] \quad (2.7)$$

where T is the same quantity as in eq. (2.5)

2.4. Simultaneous observation of two and four laser beam splitter matter wave interferometers

Our matter wave interferometer with potassium dimers has an additional feature compare to other atomic and molecular matter wave interferometers – it is possible to observe simultaneously two different types of molecular matter wave interferences. Due to high collimation of the molecular beam and application of supersonic expansion we have quite narrow velocity distribution in longitudinal and transversal direction. This leads to an enormous coherence length of the matter wave packet compare to de Broglie wave length for potassium molecules in the supersonic beam, which is about 5 pm in our case.

The scheme of the overlap of the wave packets of the different partial waves from Ramsey-Bordé setup is presented on the Figure 2.4. From the high collimation ratio of the molecular beam we know that the transverse velocity spread is less than 1 m/s, and the transverse coherence length of the matter wave packet which travels with a speed of about 1000 m/s results to about 5 nm. The total width Δv_l of the longitudinal velocity v_l was determined [35] to be about $\Delta v_l \approx 120$ m/s, corresponding to a longitudinal coherence length of the matter wave packet of 42 pm. Thus the spatial shape of the wave packet can be visualized by a very thin disk with large extension of

about 5000 pm perpendicular to the molecular beam axis and relatively small extension of about 42 pm along the direction of the beam. The lifetime τ of the upper state is about 1 μ s and requires, that the separation D between the two laser beams, acting as coherent beam splitters for the matter wave, have to be less than about one mm giving a travel time of less than 1 μ s, in order not to lose too many particles due to spontaneous decay of the molecules within the dark zones D , where part of the matter wave is in the excited state. By the interaction with the laser beam the transverse momentum equal to the momentum of the photon $\hbar k$ is added to the momentum of the molecule. This yields on a length D of 600 μ m between laser beams 1 – 2 or 3 – 4 a transverse spatial shift of about 4 nm for the deflected part of the matter wave. This shift is smaller than the transverse coherence length of the wave packet, so that the two parts of the matter wave spatially overlap and can interfere.

The second pair of laser beams acts as beam splitters in the same manner as the first one but with opposite transverse direction and is located about 15 mm downstream the molecular beam, which is a sufficient distance for the molecular excited state to decay. Thus the matter wave paths given as dashed lines in Figure 2.4 will not play any role in the discussion of the interference but may give some incoherent background signal. One can see from the Figure 2.4 the resulting overlap of the packages of the partial matter waves for our molecular Ramsey-Bordé interferometer has a quite complicated structure for exits in the excited as well in the ground state due to superposition of two different types of the matter wave interferences. One is the Ramsey-Bordé type interference due to the longitudinal displacement of molecular wave packages in the direction of the supersonic beam produced by the two pairs of counter propagating laser beams. The second one is an optical Ramsey interference: an interference by the spatial overlap of a relatively large molecular wave packages in the transversal direction where the transversal displacement is created by only the two last laser beam splitters.

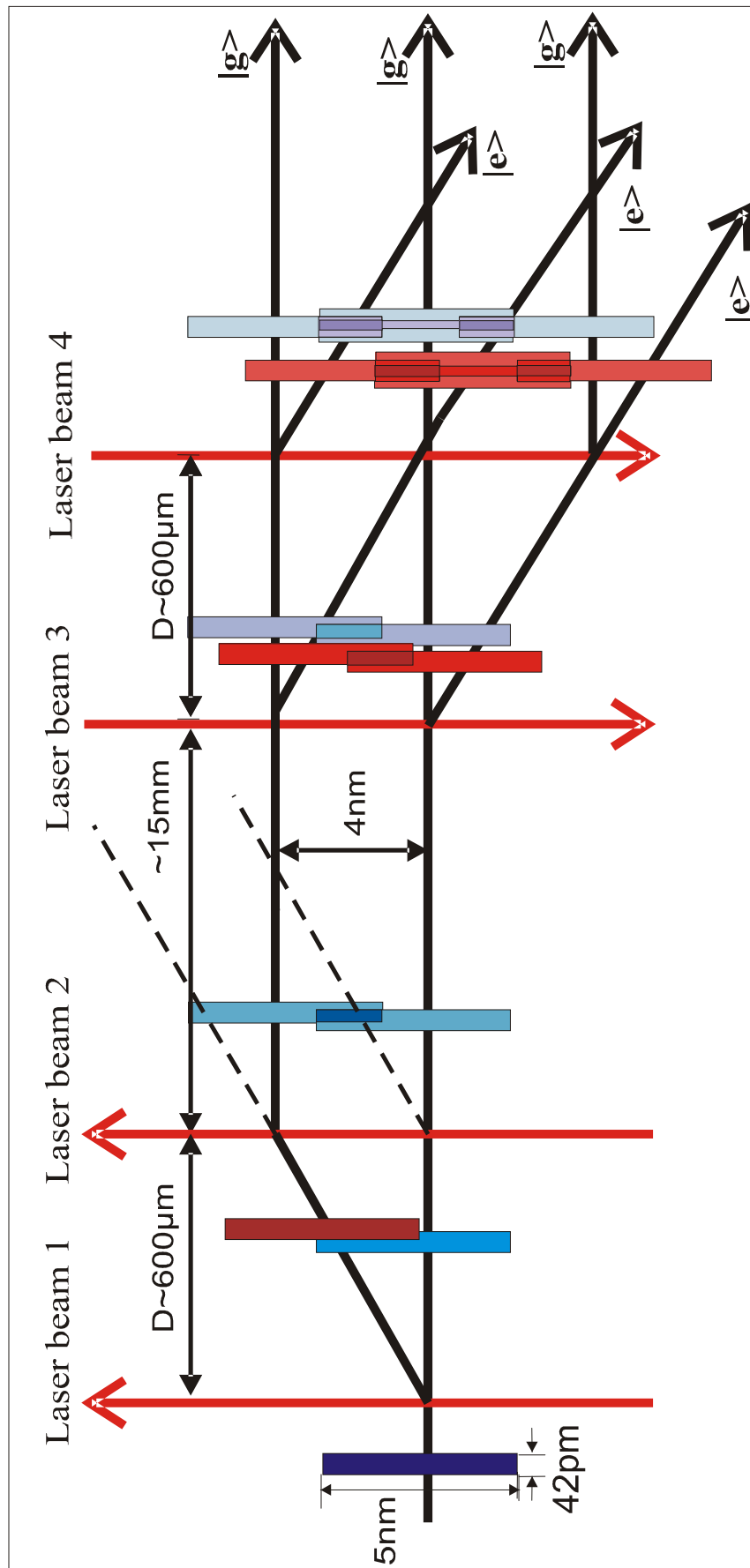


Figure 2.4 Scheme of the spatial overlap of the wave packets for Ramsey-Bordé setup

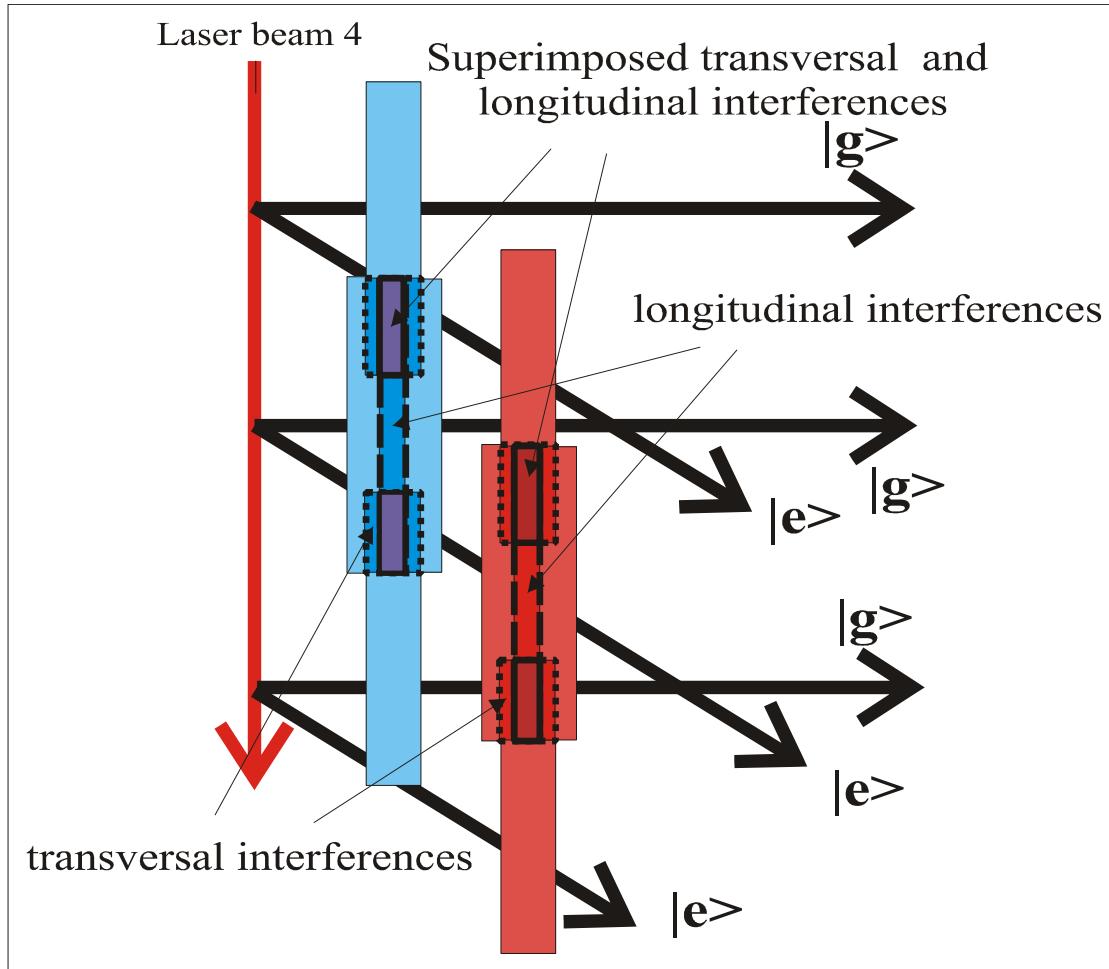


Figure 2.5 Enlarged picture for the resulting overlap of the wave packages in the Ramsey-Bordé setup

The enlarged picture for the resulting overlap of the wave packages in the Ramsey-Bordé setup is shown in Figure 2.5. One can see how the overlapped wave packages for the excited and the ground state exits produce in space regions the molecular interferences. The solid line marks the area of the overlapped wave packets corresponds to the superimposed transversal and longitudinal interferences, while the dashed and dotted lines indicate regions, respectively, of pure transversal and longitudinal interferences.

2.4.1. Transversal and longitudinal coherence in a supersonic molecular beam

Both produced partial matter waves acquire different phases from the phases of the exciting laser beams and the detuning of the laser. Therefore as was mentioned above the matter waves will show up interference patterns in the region, where they spatially overlap. The period of the observed interference pattern, while tuning the laser, is determined by the length of the dark zone D and by the speed of the molecules (eq. 2.5 or 2.7). Under our experimental conditions matter wave interference can already be observed with a pair of two laser beams as beam splitters only (Figure 2.3). The period of such interferences is given by

$$P = \frac{D}{v_l} \quad (2.8)$$

which is half the period of the full four beam Ramsey-Bordé setup. In the Figure 2.4 this spatial overlap situation of the wave packets in the interferometer is schematically shown. The interaction between the molecule and laser beam fulfills the $\pi/2$ condition for the Rabi oscillation, so the molecular matter wave is coherently split into two equal parts. As indicated also in Figure 2.4, after the first laser beam splitter the molecule is in a superposition of excited state and ground state with equal amplitudes. Due to the momentum transfer in the splitting process, the packets of molecules in the different inner states are also split in space. When the laser frequency is tuned off resonant, the molecules in the excited state is also accelerated or decelerated in longitudinal direction. Thus they accumulate a phase shift after the dark zone D with respect to the unaffected reference molecular matter wave in the ground state and the second laser beam removes the transverse momentum. The two wave packets have spatial overlap in the transverse direction and a phase shift in the longitudinal direction, which is indicated in Figure 2.4 and Figure 2.5 as the darker area. Behind the laser beam 4, even three paths with spatially overlapping matter wave packets exist, as shown in the figures, for both the ground state and the excited state. For the ground state exit, there is one wave packet in each of the two outer paths, and there is no relative displacement (phase shift) between these two wave packets in the longitudinal direction, because each wave packet accumulates on the whole the only phase shift of one dark zone D . In the middle path, however, there are

two wave packets. They stem from the closed path of the Ramsey-Bordé scheme and their spatial overlap in the longitudinal direction is thus given by the phase shift accumulated in the two dark zones labeled D. Thus it shows an interference period given by

$$P' = \frac{2D}{v_l} \quad (2.9)$$

The transverse spatial overlap of the central wave packets with the outer paths gives an interference pattern with the frequency tuning interval $1/P$ corresponding to one dark zone length D . The same situation appears also for the wave packets in the excited state. Thus the detected interference pattern should contain two frequency tuning intervals which differ by a factor of two and they appear both, as long as the transverse separation is smaller than the transverse spread of the wave packets.

By increasing the dark zone length D , the transverse separation between the two paths is enlarged and the overlap of the wave packets between different paths decreases. Therefore, the amplitude of the interference with period P will decrease according to the transverse spatial distribution, but that appearance of the Ramsey-Bordé interferences with period P' will be dominated by the lifetime of the upper state and thus will change in a different manner.

Let us discuss in more detail the influence of the phases of the laser fields on the interference patterns. When the molecules interact with the laser beam, a phase shift φ_i ($i=1,2,3,4$) is introduced, i marks the different laser beams. The accumulated total phase shifts of two interfering matter wave packets in a Ramsey-Bordé setup according to eq. 2.5 is

$$\varphi_{tot} = \varphi_2 - \varphi_1 + \varphi_4 - \varphi_3 \quad (2.10)$$

while for packets after traversing two laser beams of the same direction we have (see eq. (2.7))

$$\varphi_{tot} = \varphi_2 - \varphi_1 \quad (2.11)$$

$$\text{or } \varphi_{tot} = \varphi_4 - \varphi_3 \quad (2.12)$$

for copropagating laser beams, depending on the pair of parallel laser beams they have interacted with. For counter propagating laser beams, the case of saturation spectroscopy, there are no resulting partial matter waves with common direction, which would give stationary interferences.

In the case of the Ramsey-Bordé setup, equation (2.10), where the laser beams 1 and 2 are converted to beams 4 and 3 in a retroreflector, any phase change from one of the beams 1 or 2 is transferred to a phase change of the same magnitude, but with opposite sign, from the corresponding beams 4 or 3, so that such changes cancel in the final total phase. This gives better stability of the interference phase with respect to mechanically induced phase changes in the four beam splitter setup. Such cancellation is not present in the two beam splitter arrangement. Moreover, the first order Doppler shift cancels in the Ramsey-Bordé setup, while it changes the total phase in the two beam splitter arrangement, for details see [1, 21, 47].

3. Experimental setup

For experiments on the matter wave interferometry I begin first with the description of the experimental conditions. The separate experimental parts are discussed in the following sections and only improvements done in connection with conducted interferometric measurements are considered in details. For more particular details please look in [32, 33, 35, 37].

In Figure 3.1 the principal sketch of our molecular matter wave interferometer experiment is presented. The potassium molecules, the internal state structure of which will be discussed in the section 4.2, are produced by supersonic expansion into a vacuum chamber where the beam conditions could be changed by means of deflection laser. A molecular matter wave interferometer is realized by implementing two pairs of counter propagating beams of an interferometer laser which also acts as a probe laser for the excited state exit of the interferometer. The signal is detected by photomultiplier PM1. Downstream from the matter wave interferometer an independent detection laser is used for simultaneous recording of the ground state exit of the molecular matter wave interferometer. This signal is recorded by photomultiplier PM2. The circles indicate the viewing area of the imaging system of the photomultipliers (Figure 3.1).

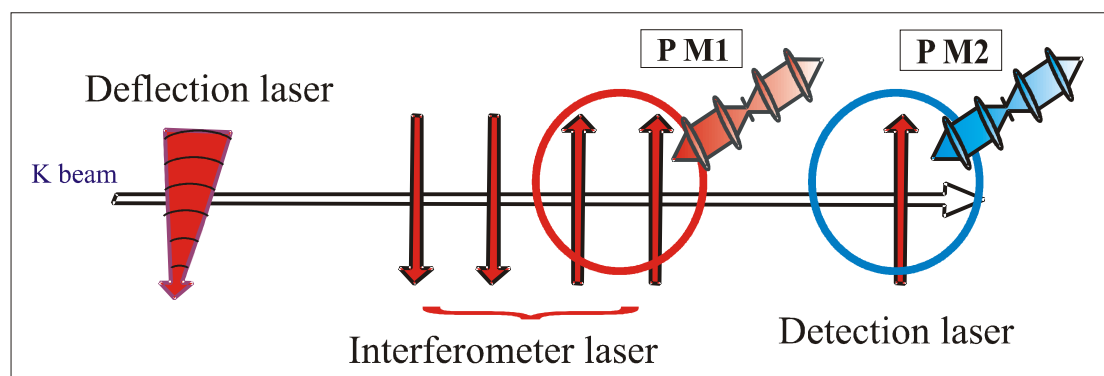


Figure 3.1 General scheme of experiment

The vacuum apparatus arrangement and fluorescence detection system will be described in section 3.1 while the laser systems and coherent source for the matter wave interferometer will be discussed in sections 3.2 and 3.3 respectively.

3.1. *Molecular beam machine*

The basic part of our experiment is a molecular beam machine. It consists particularly of vacuum apparatus itself and different fluorescence detection systems.

3.1.1. Vacuum apparatus

The key segment of our molecular beam machine is the evacuated chamber with a heated oven for potassium. It must possess a source, which produces a supersonic jet with sufficient density, in order to ensure signal-to-noise ratio. As follows from the theoretical overview of the molecular matter wave interferometry, the distribution of velocities of the molecules inside the supersonic beam, especially the spread, is of great importance. A narrow distribution is of advantage here, since a larger number of oscillations in the interference signal can be observed (see chapter 2). This is desirable for the interferometric observation of collisions. Since we have a small difference in velocities between the impact partners, which leads to larger phase shifts of the interferences, the investigation of low energy collisions ("cold collisions") becomes possible.

The demanded characteristics are fulfilled well by a supersonic expansion. It is formed, if the molecules in the gas phase from a reservoir expand through an opening into a vacuum, whereby the mean free path should be small within the reservoir compared to the size of the opening [17]. This leads to multiple collisions and thus a rearrangement of the internal energy of the sample particles into kinetic energy. The process can take place thereby under its own vapor pressure or supported by a carrier gas of higher pressure (seeded beam).

The full-length description of our vacuum apparatus was already discussed in [35], so here I would like only briefly mention the most important details of experimental arrangement.

The schematic picture of vacuum apparatus is presented in Figure 3.2. The potassium oven is placed in the so-called "oven chamber" {1} which is pumped by two diffusion pumps down to the pressure of some 10^{-5} mbar. The oven is heated in the experiment to approx. 380 - 420 °C and the vapor pressure of potassium inside is approximately 10^{-2} bar [42]. In order to prevent blockage of the nozzle with an

opening of 200 μm in diameter its temperature range is about 100° higher than the oven itself.

The supersonic jet of K/K_2 passes a heated skimmer {2} with an opening of 1 mm in diameter into the intermediate chamber. The intermediate chamber is evacuated by a turbo-molecular pump and the background pressure there is kept in the order of 10^{-7} mbar. In this chamber manipulations with the supersonic beam are done (like switching atomic density of ^{39}K within molecular beam). For this purpose a cooling trap {3}, a blade mounted on micrometer screw {4} and view ports {5}, which provide access to potassium beam for observation and laser manipulation, are installed. The blade is specially designed for atomic density switching experiment and allows controlling its position up to 5 μm . Through the cooling trap operated on liquid nitrogen it is possible to decrease background pressure in the intermediate chamber by an order of magnitude which prevents appearance of an unwanted potassium cloud in beam path and the deposition of potassium on the view ports.

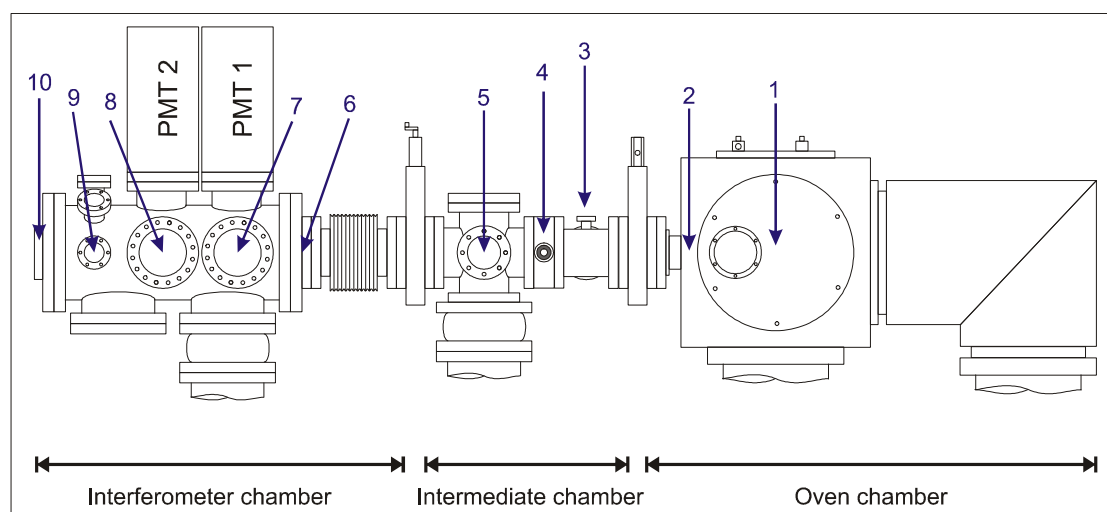


Figure 3.2. Vacuum apparatus.

1 – oven position; 2 – position of first skimmer; 3 – cooling trap; 4 – blade mounted on micrometer screw; 5 – view ports used for preparation of molecular beam; 6 – position of second skimmer; 7 - view ports used for operating matter wave interferometer (MWI) and detecting excited state exit of MWI; 8 - view ports used for detecting ground state exit of MWI; 9,10 - view ports used for online checking quality of atomic density switching.

Intermediate and interferometer chamber are connected via the second skimmer {6} which has 2 mm diameter. The separation between the two skimmers is approximately 1 m and thus in the interferometer chamber a collimation ratio for the molecular beam of 1/1000 is reached, which corresponds to a remaining Doppler

widths of K_2 transitions in transversal direction of less than 2 MHz. The interferometer chamber has several AR coated view port sets for operating molecular matter wave interferometer {7}, probing the exit of matter wave interferometer in the ground state {8} and detecting the quality of deflection of atoms out of the molecular beam {9-10}.

The mean longitudinal velocity of our supersonic molecular beam is about 1000 m/s with the velocity distribution of ± 50 m/s [35]. The very narrow transversal and longitudinal velocity distributions (by collimation) together with vibrational and rotational cooling of potassium molecules within a supersonic jet are the key points for operating our molecular matter wave interferometer.

3.1.2. Fluorescence detection

Detection of the fluorescence from optically excited potassium molecules and atoms is possible via sets of view ports installed in the intermediate and the interferometer chambers. For the examination of potassium jet two photomultipliers, photodiode and CCD camera were used. All the optical components for collecting fluorescence including view ports have wideband AR coatings (500 - 900 nm for the view ports and 700 - 900 nm for lenses implemented together with photomultipliers and photodiode). The observation direction is oriented perpendicularly to the axes of the molecular beam and the exciting lasers.

The main parts of the detection system are located in the interferometer chamber, except a CCD camera located in the intermediate chamber which was used for an observation of the deflection of potassium atoms out of the molecular beam and which is especially sensitive in the near infrared region. The principle scheme of the interferometer chamber is illustrated of Figure 3.3.

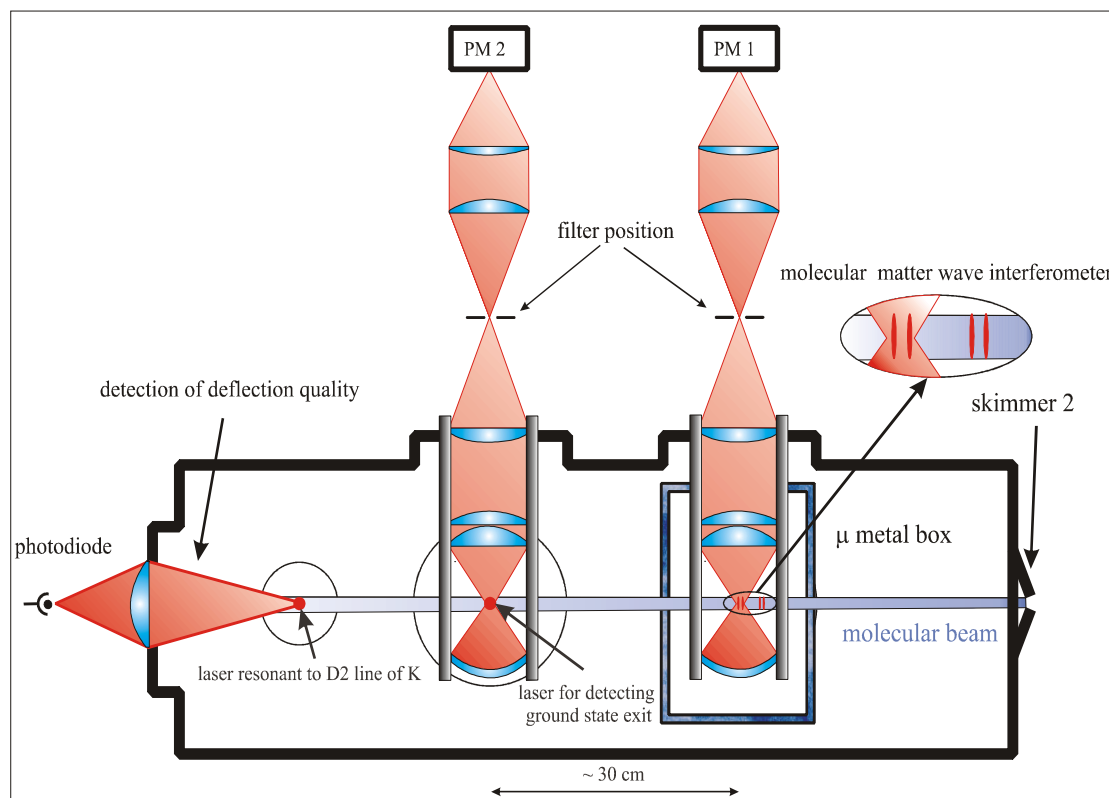


Figure 3.3. Principal scheme of interferometer chamber

As it was mentioned above to examine the exits of the molecular matter wave interferometer in the ground and excited states two independent observation zones were constructed. The fluorescence collecting optics images the laser-molecule interaction region to the detectors which in our case were two Peltier cooled photomultiplier tubes (Hamamatsu R943-02). This type of photomultiplier has a sensitivity range going from 400 nm down to 900 nm and is particularly well suited for the observation of the fluorescence from K_2 A or B states (1100 nm and 700 nm respectively). The solid angle viewed by the photomultiplier tubes is 1.4 sr and the fluorescence spot imaged on the photocathode has a diameter of 1 mm. This last mentioned circumstance is of special importance because in the present experimental configuration it is impossible to distinguish or separate fluorescence from the last two laser beam splitters used for a molecular matter wave interferometer which normally has a separation of several hundreds μm (Figure 3.3).

In addition, different filters can be used in order to suppress the scattered light from excitation lasers. If not mentioned other, a colored glass filter RG 850 (3 mm or 2 mm thick) from the Schott company as well as an interference filter 42-7914 with a central wavelength of 878 nm and a full half width of 51 nm were always used for the

PM 1. In the PM 2 part filter set was varied depending on excitation laser implemented for ground state exit detection: in connection with dye laser oscillating about 633 nm we used an interference filter 42-7757 with a central wavelength of 671.4 nm and a full half width of 36.3 nm and holographic notch filter NFPP8299 with a central wavelength of 632.8 nm and a full half width of 1 nm, while together with 818 nm diode laser the similar set of interference filter 42-7914 and colored glass filter RG 850 was installed.

In order to reduce the lab magnetic field in the region of the molecular matter wave interferometer a passive shielding of external magnetic field was implemented. For this purpose a box made of μ -metal was installed around the area of the interferometer. The magnetic shield is obtained by a 1.5 mm thick μ -metal and has sizes of $145 \times 95 \times 70 \text{ mm}^3$ so it covers the interferometer region completely and has small openings for laser and molecular beams and PM 1 imaging system. The attenuation in the center of the μ -metal box is 20 dB and residual magnetic field gradient is less than $2 \text{ } \mu\text{T}$. In Figure 3.4 results of direct measurements inside the μ -metal box for two components (x is the direction of the potassium beam; y – the direction determined by the fluorescence collecting optics) of the lab magnetic field done with a magnetometer.

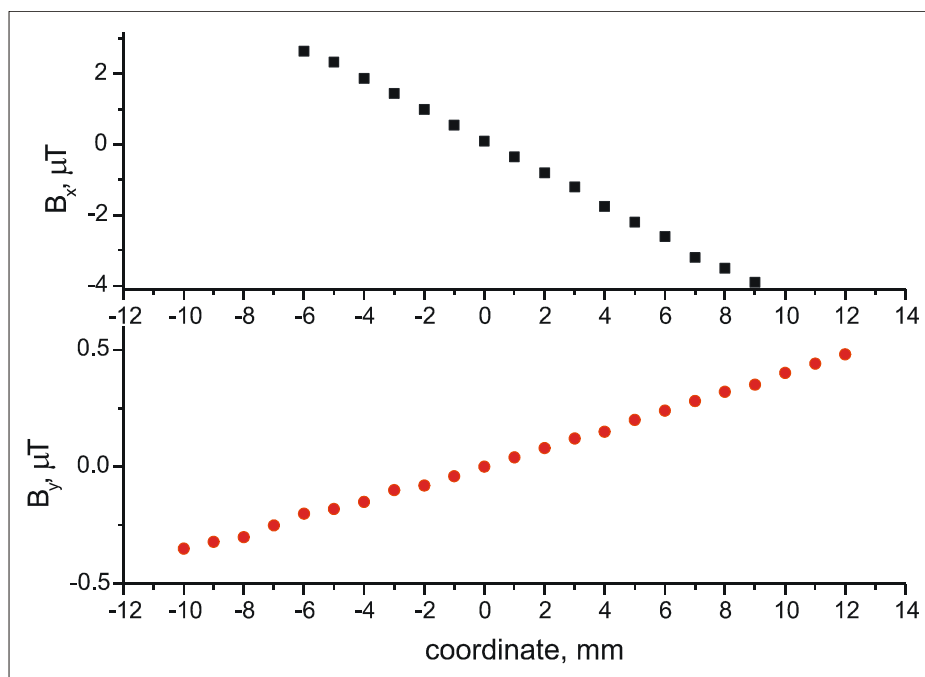


Figure 3.4 Residual magnetic field inside μ -metal box. Coordinate = 0 corresponds to the center of the μ -metal box

For the on-line control for switching of atomic density of ^{39}K in the molecular beam atoms were excited downstream of the location of the PM 2 and atomic fluorescence was collected by flat-convex lenses to a photodiode as detector. The utilization of simple photodiode was adequate for current experiment because of its simplicity and because the fluorescence spot was bright enough to record sufficiently large signals.

3.1.3. Data acquisition system

All obtained signals from photomultipliers and photodiode were detected by independent picoamperemeters, fed to an analog-digital converter and finally recorded by a computer using the LabView software. The implemented data acquisition system could record simultaneous recording of up to 8 different parameters measured during experiment. There was also a build-in option to control on-line parameters of running experiment by software means like sweeping radio frequency of AOM or integrating recorded signals with a defined time constant before storage.

3.2. *Laser source for molecular matter wave interferometer*

The concept of our molecular matter wave interferometer uses laser beams for splitting matter waves. Thus we need a source of laser radiation of good absolute frequency and phase stabilities and therefore relatively small line width at the resonance of the molecular transitions lying in the infrared region to (around 820 nm) long living potassium state. This part of my thesis describes the most recent characteristics and the experimental arrangement of the interferometer laser system based on a frequency stabilized external cavity diode laser as master laser and for sufficient output power injection locked to a slave laser.

3.2.1. External cavity diode laser system

A single mode diode laser with external cavity in Littrow configuration was developed (Master 1) [37] lasing in the 820 nm region. In this geometry a reflecting grating and the rear end face of the laser chip form an external laser resonator (ECDL). The position of the grating is selected in such a way that the -1st diffraction order runs back into the chip and couples it to the grating, while the 0th order is used as a radiation output. So the emitted laser frequency can be easily controlled and tuned by the attitude of the grating.

For this purpose the grating is mounted on a PZT drive which allows to adjust mechanically a grating position by applying DC voltage. In addition to this “slow” control the emitted wavelength can be manipulated by changing the laser diode current and temperature. The laser wavelength is normally tuned by synchronously changing the current through the laser chip and the voltage of the PZT drive of the grating which provides us with an opportunity of a single mode frequency sweeping for 30 GHz. To avoid uncontrolled drift of the laser frequency the laser diode temperature as well as the temperature of the complete external cavity box is temperature stabilized with the precision of 0.01 K.

The optical arrangement of ECDL system is presented in Figure 3.5. A 7 mW laser beam from the Master 1 is beam shaped via a cylindrical telescope in order to have a symmetrical round beam profile and uncoupled from other optical components by a 60 dB Faraday isolator. The 4 % of the total intensity of the Master 1 is coupled to a confocal Fabry-Pérot interferometer to frequency stabilize the laser on the reflection peak by Pound-Drever-Hall method. This stabilization setup will be discussed in a following subsection 3.2.2.

3.2.2. Frequency stabilization

The concept of our frequency stabilization system is to stabilize with the help of the Pound Drever Hall method master 1 to a transversal mode of some confocal Fabry Pérot coupling cavity which itself is stabilized to another stable laser source with good long term stability characteristics which in our case was an ECDL master 2. This should provide the master laser 1 with good short and long term stability of the laser frequency.

The setup for a Pound Drever Hall (PDH) stabilization is presented on figure 3.6. The details of the PDH method are described in [41]. In our experimental realization of the PDH stabilization scheme a modulation signal of 20 MHz is applied to the injection current of master lasers 1 and 2. The modulated light passes through a polarizing beam splitter so only light with one defined linear polarization is reflected to the coupling cavity. As coupling cavity a confocal Fabry Pérot interferometer with a free spectral range of 150 MHz was used. Due to the small line width (approx. 1 MHz FWHM) of the implemented coupling cavity when a laser frequency matches with transversal mode of the cavity sidebands separated by 20 MHz apart from the carrier will be reflected. The detecting sensor which in our case was fast photodiode was placed behind the polarizing beam splitter orthogonally to the incoming light. To permit reflected from coupling cavity light pass through polarizing beam splitter and be detected by the photodiode $\lambda/4$ plate was installed. To improve signal to noise ratio for the photodiode and shield it from transmitted light coming from another laser coupled to the same cavity interference filters with a transmission maximum of 820 nm and 780 nm were used. This basic scheme was implemented to stabilize master 1 and master 2 diode lasers to the same confocal FP coupling cavity. The slow and fast parts of an error signal were fed back to the grating voltage and injection current correspondently. The coupling of lasers to the cavity was done very close to mode matching condition for TEM_{00} in order to have maximally coincident optical paths inside the FP interferometer for both master lasers.

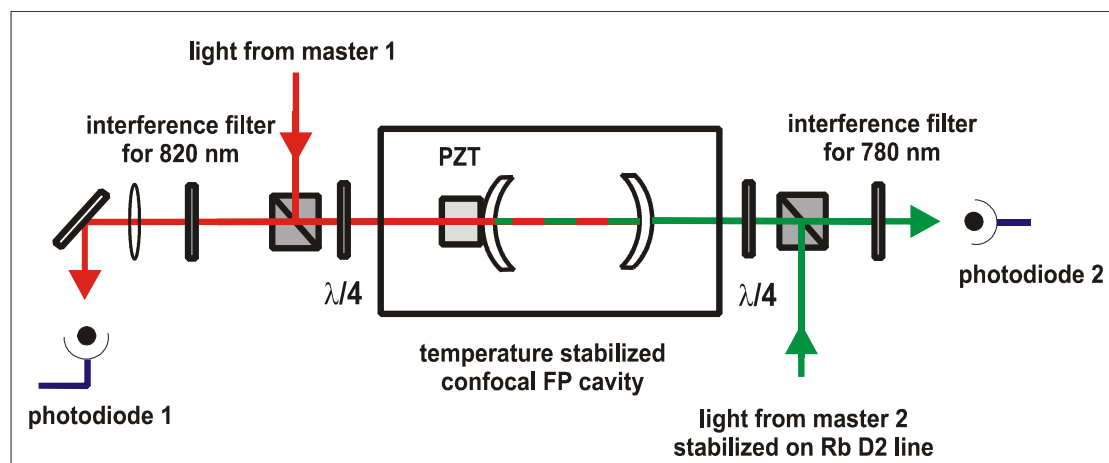


Figure 3.6 PDH stabilization setup

To improve the long term stability of the coupling cavity the position of its transversal modes in the frequency domain was stabilized to a hyperfine component of the rubidium D2 line. For this another external cavity diode laser in the Littrow configuration was get into operation (master 2). The wave length for the laser was chosen to be around 780 nm to be resonant to the rubidium D2 line. The master 2 was prestabilized by PDH stabilization method by the coupling cavity as it was discussed above and its radiation was used to realize a saturation spectroscopy scheme in a gas cell with rubidium of natural abundance. For the production of an error signal from the saturation dip within the spectrum of the D2 line, detected with a photodiode, the 20 MHz sidebands produced for Pound Drever Hall stabilization were used. As a servo a lock-in amplifier system constructed identically to a PDH stabilization servo was applied [37]. The remaining Doppler background was subtracted by chopping the pumping beam in the saturation spectroscopy setup and using lock-in amplifier detection at 440 Hz modulation frequency. The error signal is then produced with a simple PI-controller and fed back to the PZT driver built into the FP coupling cavity.

The line width of master 1 was measured to be less than 30 kHz by means of an optical discriminator. For this purpose master 1 coupled to another 150 MHz confocal Fabry-Pérot cavity via double path AOM. The laser frequency was scanned over the wing of a 1 MHz FWHM transmission peak of FP interferometer by changing RF of the AOM with the step size of 10 kHz.

The long term stability of the laser frequency was measured by recording a position of saturation dips on a molecular transition. The result is shown in Figure 3.7.

One laser beam of the interferometer laser together with counter propagating beam produced by a retroreflector were forming a saturation setup within the supersonic molecular beam. The laser frequency was swept over the center of one hyperfine component of the molecular line $R(25) 27-0 b^3\Pi_u(0^+) - X^1\Sigma_{g^+}$ included saturation dip in order to make an analysis of recorded signals by fitting a position of a Gaussian profile of the hyperfine transition with an overlapped Lorentzian profile of the saturation dip. The recordings were done during approximately one hour which allows as conclude that the frequency drift of the interferometer laser was better then 260 Hz/min.

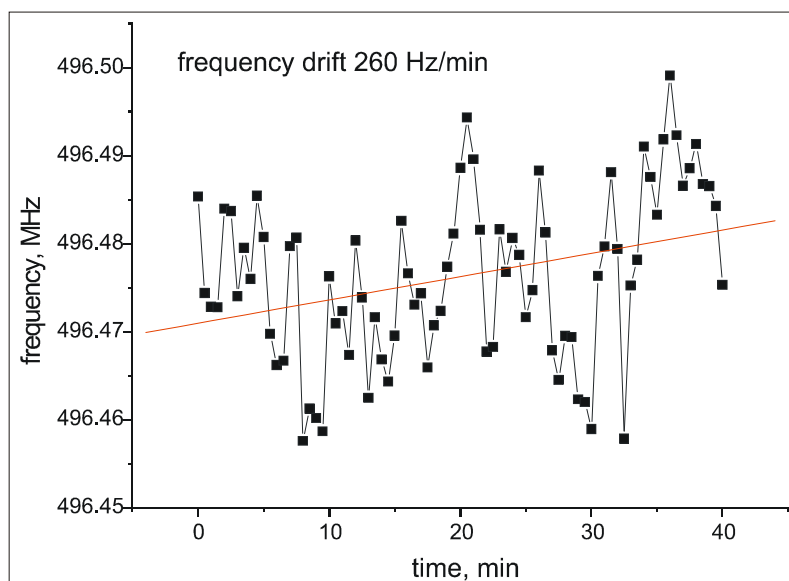


Figure 3.7 frequency drift of master 1

As a result we got a low cost laser system with good short and long term stability suited to reach a resolution of better than 30 kHz. The scanning of the master 1 frequency over 80 MHz by the double path acousto-optical modulator together with the possibility to stabilize the laser at any frequency position within its oscillation range provides us a laser system which perfectly matches the requirements of molecular matter wave interferometry.

3.2.3. Optical arrangement of molecular matter wave interferometer

The light from the interferometer laser was transported to the vacuum system via single mode optical fibers that allow us to uncouple the noisy vacuum lab with several all day running mechanical pumps from laser systems which are very sensitive to any acoustics, and so to fulfill the high demands on their characteristics. The remaining necessary optical components close to the interferometer vacuum chamber were placed on optical tables mounted on rubber support to damp unwanted vibrations coming from the vacuum apparatus.

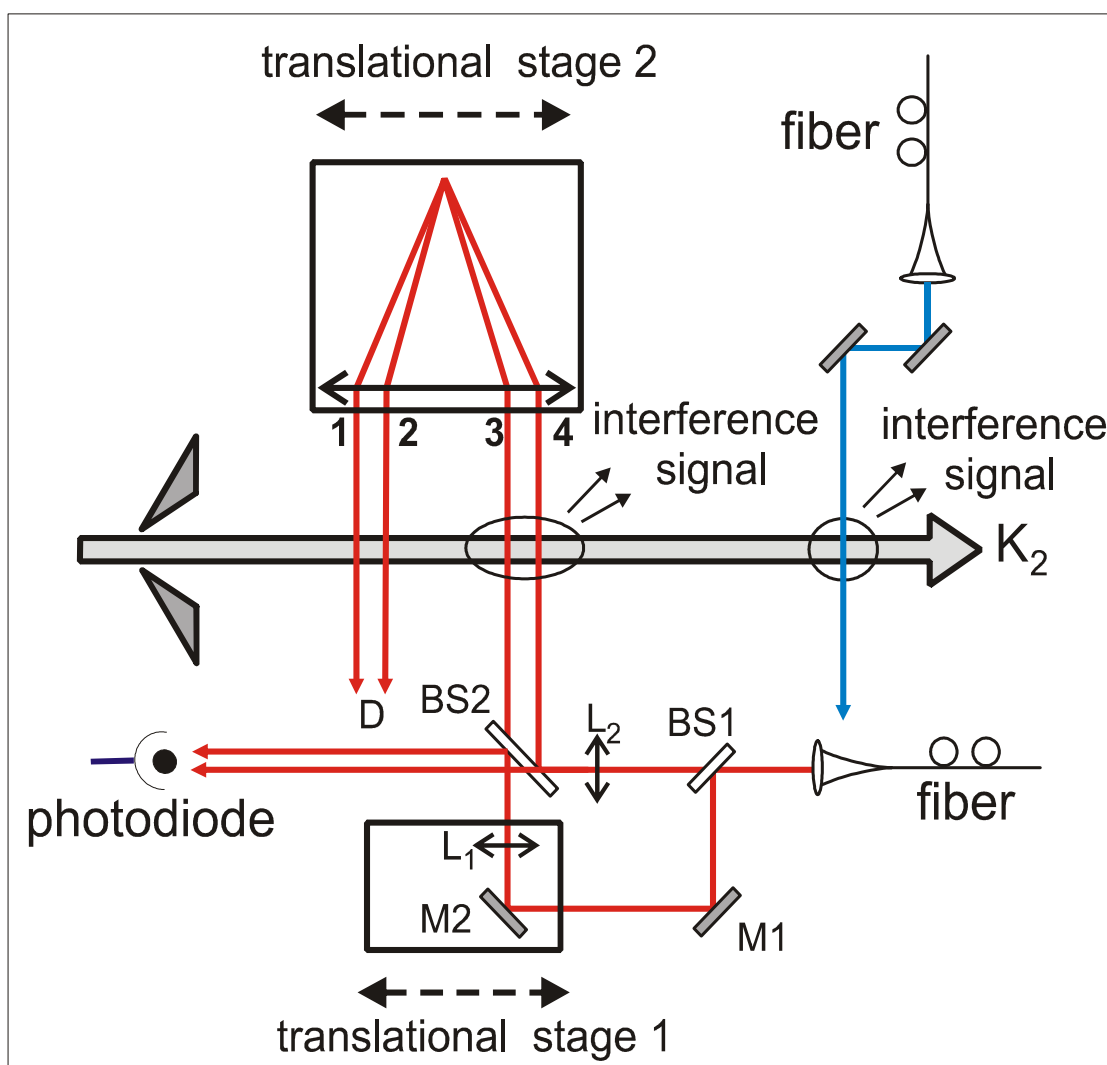


Figure 3.8 Optical arrangement of the Ramsey-Bordé matter wave interferometer

In Figure 3.8 the optical arrangement of molecular matter wave interferometer is illustrated. The beams 3 and 4 of the molecular matter wave interferometer are formed by dividing the light coming out of the optical fiber on beam splitter 1 into two parts which are transmitted into the vacuum chamber via beam splitter 2 and lenses L_1 and L_2 . The ratio between transmission and reflection for the beam splitters 1 and 2 were chosen such that the intensity of the laser beams 3 and 4 are equal when they are entering the vacuum chamber. Mirrors 1 and 2 are high quality dielectric mirrors. The second pair of laser beams for the molecular matter wave interferometer in the Ramsey-Bordé configuration was produced by a retroreflector. The retroreflector in our experiment consists of an achromatic lens and a plane high reflecting mirror placed in the focal plane of the lens. The retroreflector could be parallel shifted (translational stage 2) to the axis of molecular beam with the help of a micrometer screw which has a precision of 10 μm . To correct independently an orientation of laser beams 3 and 4 the adjustment screws of mirror 1 and beam splitter 2 were mounted on a mechanical step motors with the step size of 0.5 μm .

In the present optical setup it was possible to change the dark zone length of the molecular matter wave interferometer by parallel shift of mirror 2 and lens 1 which were mounted on a translational stage 1. The translational stage 1 was powered by a high precision remote controlled step engine, so in connection with a usage of the retroreflector this allows us to control the separation within the pairs of counter propagating beams with the accuracy of 0.5 μm .

As it was mentioned in section 2 the maximum separation between the laser beam splitters 1 – 2 and 3 – 4 at a given mean velocity of the potassium molecules in the supersonic beam is limited by the molecular lifetime of the excited state and in our case is about 1 mm for the velocity of around 1000 m/s. The size of the laser beam out the fiber was 3.3 mm, so we have to focus our laser beams in the direction parallel to the molecular beam axis. For this purpose cylindrical lenses L_1 and L_2 with the focal length of 500 mm were used. They produced a Gaussian beam with the waist of 75 μm which could be controlled on-line by a portable CCD camera connected to a computer.

To control intensity fluctuation of the interferometer laser radiation a photodiode was installed. The position of the photodiode was chosen to be in the focusing point of cylindrical lenses L_1 and L_2 to avoid optical interferences on the facet of the detector which can be interpreted as a change of the laser intensity.

The ground state exit of the molecular matter wave interferometer could be observed by implementing an additional excitation radiation which in our case was either light from a dye laser resonant to one of the transitions in the B-X molecular system or just radiation of the interferometer laser frequency shifted by the AOM 2. To transport this radiation we used optical single mode fiber and the outgoing beam was adjusted to the vacuum system by a pair dielectric mirrors.

3.3. Laser systems used in applications of matter wave interferometry

Apart of the interferometer laser system to conduct many of our relative phase measurements of the molecular matter waves several additional laser systems have to be implemented. In this section supporting laser systems used in the experiment will be discussed.

3.3.1. Deflection laser system

To examine cold collisions between potassium atoms and molecules in well defined quantum states and to distinguish them from other observed phase differences we will switch the atomic density within the molecular beam. For this purpose we used a Ti-Sa laser in the ring configuration (Teknoscan company) pumped by 10 W of a frequency doubled Nd-YAG solid state laser (Coherent Verdi 10). The maximum output power in single mode regime was more than 1.4 W and it was possible to achieve lasing in the wave length region from 700 to 950 nm.

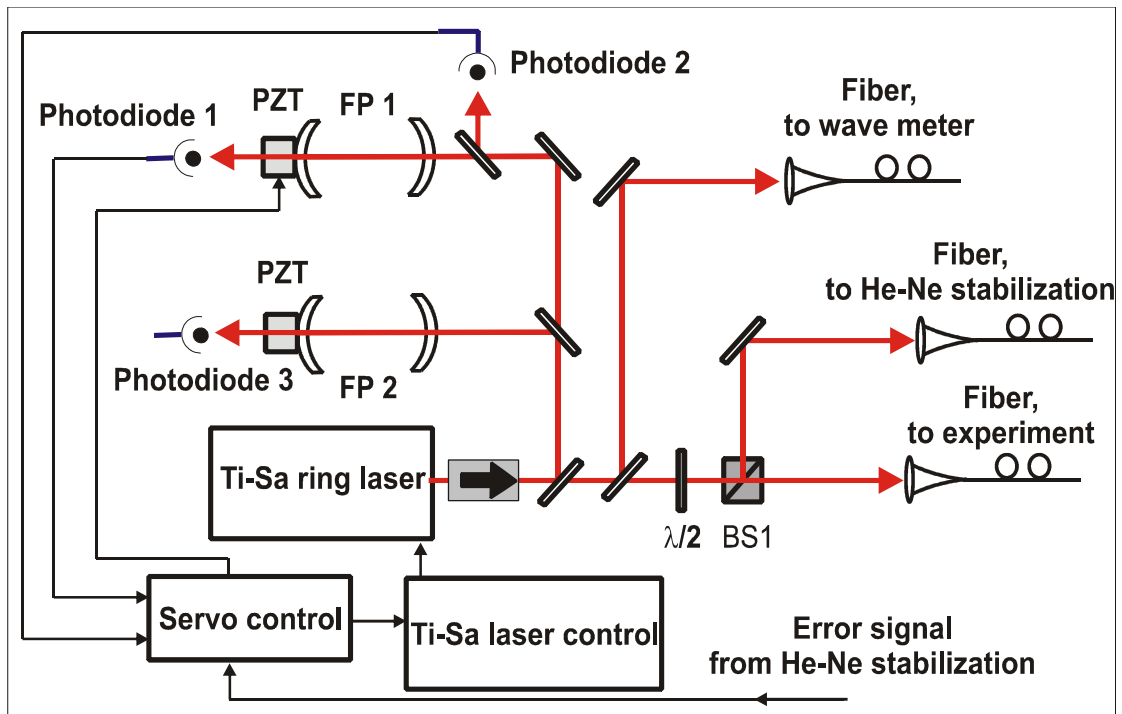


Figure 3.9 Ti-Sa laser system

The principal stabilization scheme of the Ti-Sa laser system is presented in Figure 3.9. The light of the Ti-Sa ring laser is divided with a polarizing beam splitter (BS 1) into two parts which are coupled to two single mode fibers going to the vacuum apparatus and to a He-Ne stabilization setup. The ratio of the power split to the experiment and to the stabilization circuit could be controlled by a position of a $\lambda/2$ plate placed before the beam splitter. The examination of the mode structure of the Ti-Sa laser was done by splitting a small fraction of the total output power to the confocal Fabry-Pérot interferometer (FP2) which transmission picks were scanned by a PZT drive and detected by photodiode 3. To measure the wave length of the Ti-Sa a small part of its radiation was coupled to another single mode fiber and transported to a wave meter with a resolution of 300 MHz.

In order to narrow the line width of the Ti-Sa laser a so called “prestabilization” circuitry was put into operation. A basic element of this stabilization setup is a low finesse confocal Fabry-Pérot cavity (FP1) where the stabilization point is defined to be at a middle of one of the slopes of the transmission pick. An error signal is created by measuring transmitted signal with photodiode 1 and a reference signal with photodiode 2. The correction signal from the servo control is applied to selective elements and the cavity length of the Ti-Sa laser via the Teknoscan laser control unit.

Experimental setup

To avoid a long term drift a part of Ti-Sa radiation is coupled to the single mode fiber and transported to a He-Ne stabilization setup where it is stabilized on the transmission peak of a long term stabilized Fabry-Pérot interferometer. The detailed description of the He-Ne stabilization setup is provided in subsection 3.2.3. The error signal produced by the He-Ne stabilization is fed into the laser and reference cavity.

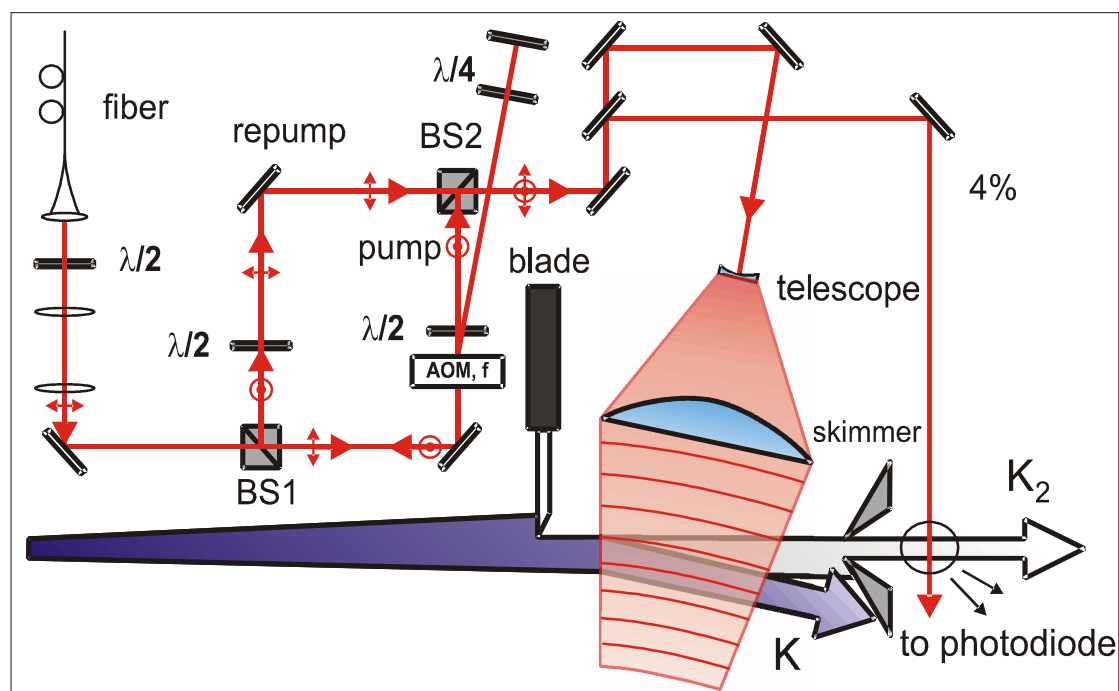


Figure 3.10 Formation of deflection beam

The 150 mW of the Ti-Sa radiation with the wave length of 767 nm (transition $F=2 \rightarrow F'=3$ of the potassium D2 line) comes out of a single mode fiber (Figure 3.10) at the optical table close to the vacuum chamber. The polarization of the laser beam is linear and it is adjusted to have a maximum transmission through beam splitter BS1 by a $\lambda/2$ plate. The passed light is split by an AOM which produces the necessary repump radiation by the first order deflected beam, followed by another $\lambda/2$ plate to polarizing beam splitter BS2. The size of the laser spot going out of the fiber is 3.6 mm so we first focus it to the size of about 1 mm by a telescope in order to have a good matching between the laser beam and a running acoustic wave inside the AOM.

To avoid optical pumping of the potassium atoms instead of the deflection a repump beam was produced by passing through a double path AOM. The radio frequency of the AOM was chosen 221.5 MHz in order that the repump is resonant to

$F=1 \rightarrow F'=2$ transition of the potassium D2 line when the pump beam is resonant to $F=2 \rightarrow F'=3$ transition. The two beams are overlapped on the polarizing beam splitter BS2, have orthogonal to each other polarizations and a typical ratio of pump to repump intensity between 7 and 10. A small part of this mixed radiation is split for the detection of the deflection quality downstream behind the matter wave interferometer region.

To prepare the curved wave front of the deflection laser to improve the deflection quality by a maximal enlargement of the resonant interaction region between ^{39}K and laser light a cylindrical telescope is implemented [32]. A cylindrical concave-plane lens with $f = -6.4$ mm first diverges the laser beam while the convex-plane cylindrical lens with $f = 200$ mm focuses it afterwards. That produces an interaction region between atoms and Ti-Sa radiation of about 5 cm.

3.3.2. Detection laser system

To detect a ground state exit of the molecular matter wave interferometer a laser running in the wave length region of potassium molecular B-X system (around 630 nm) is needed. A Coherent 599 linear dye laser is applied with which the transition Q(25) 4-0 band of the B-X system is reached (15553 cm^{-1}) when the molecular matter wave interferometer operates on the line R(25) 27-0 of b-X molecular system. This allows to observe in addition to the excited state the ground state exit of the interferometer.

The general scheme of the dye laser setup is shown in Figure 3.11. The dye laser system is in some sense a twin sister of the Ti-Sa laser system: the main difference is the linear dye laser while all other basic components like scanning Fabry-Pérot interferometer or single mode fibers are the same.

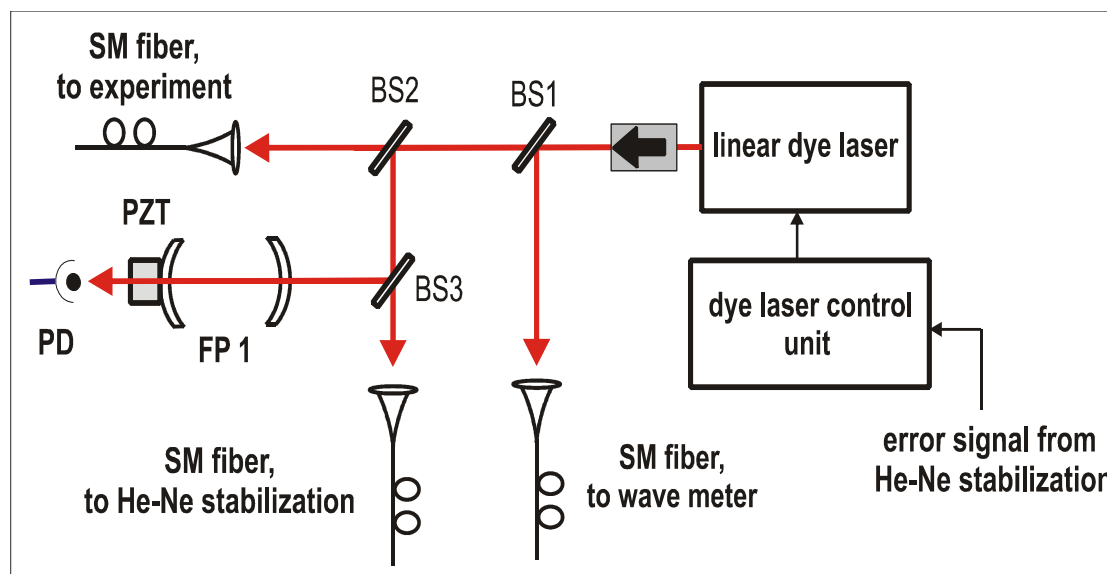


Figure 3.11 Principal scheme of dye laser setup

The linear dye laser produces about 80 mW single mode radiation at 634 nm pumped by 4.5 W of a Coherent Argon-ion laser. The main output power of the dye laser is coupled to a single mode fiber with taps for the scanning FP cavity and two single mode fibers which are used for laser diagnostics and frequency stabilization. By passing through the single mode fiber the light of the dye laser is shaped by a Linos output coupler to have a parallel beam with symmetrical round profile of 3.6 mm in the diameter.

As in case of the Ti-Sa laser system the frequency of dye laser is stabilized to a low finesse cavity for short term frequency stability and to the He-Ne stabilization setup for long term. The only difference compare to the Ti-Sa laser system is that the low finesse cavity unit is a built-in part of the Coherent linear dye laser system.

3.3.3. He-Ne frequency stabilization

To obtain the long term stability of the lasers used for the deflection ^{39}K atoms out of the potassium beam and the detection of the ground state exit of the matter wave interferometer we have used the He-Ne frequency stabilization setup. This setup is discussed in details in [52] has a long term frequency drift better than 1 MHz/h. The basic principle of this stabilization scheme is to transfer to some laser (“laser for

stabilization”) the long term stability of the iodine stabilized He-Ne laser by stabilizing it to the transmission peak of an intermediate cavity, which is already stabilized to the He-Ne laser.

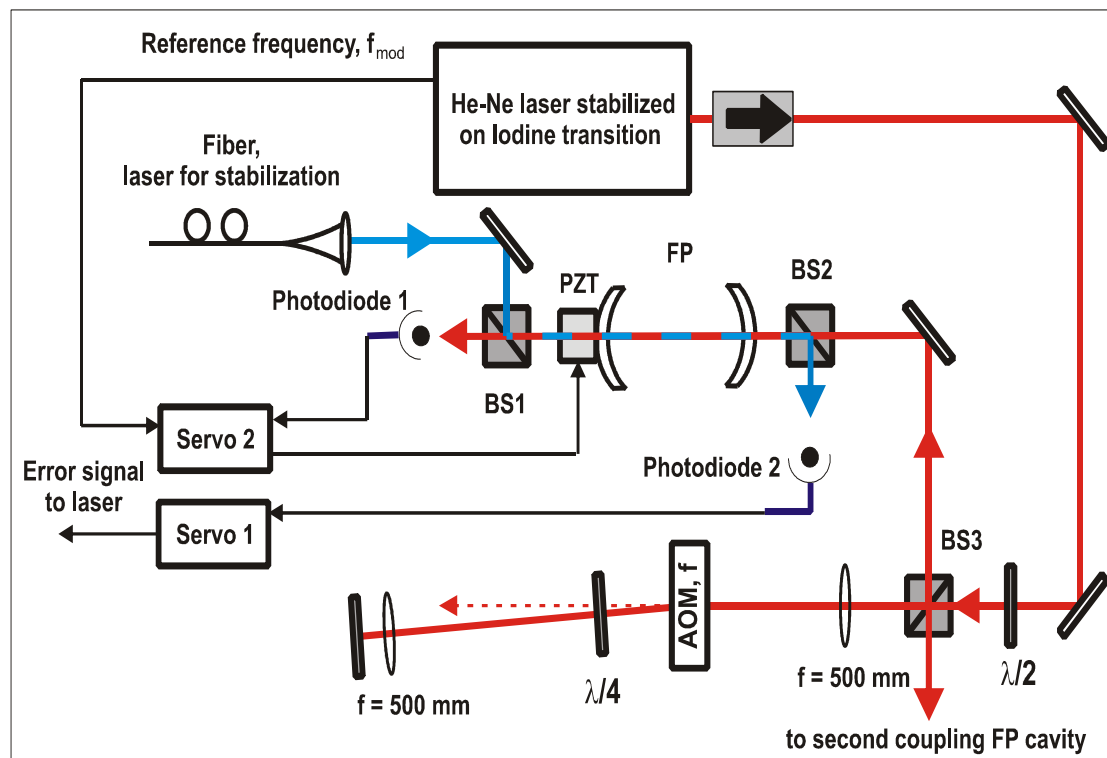


Figure 3.12, Principal scheme of He-Ne stabilization

The principal scheme of it is shown in Figure 3.12. We use an Iodine-stabilized helium neon laser of the PMT company. Its oscillation frequency is stabilized by intra cavity absorption method to the hyperfine component "i" (11-5) of the R(127) line of the I_2 molecule with absolute uncertainty better than 10 kHz and frequency drift under 5 kHz/h. For this the length of the cavity of the He-Ne laser is modulated by $f_{mod} = 477$ Hz. The 80 μ W of the He-Ne radiation is divided into two equal parts with a $\lambda/2$ plate and beam splitter BS3. The split radiation is frequency shifted by passing through a double path AOM setup and feed into a 150 MHz coupling Fabry-Pérot interferometer (FP) by reflecting on a mirror and beam splitters BS2 and BS3.

The transmission peaks of intermediate cavity FP, which finesse is of about 50, are frequency stabilized using lock-in technique. For this frequency modulated light of the He-Ne laser is detected by photodiode 1 and Servo 2 included lock-in amplifier and integrator produces error signal which is fed back to PZT of the cavity.

Experimental setup

The similar stabilization scheme is used to lock a laser which frequency requires good long term stability to the intermediate coupling cavity. “Laser for stabilization” is coupled to intermediate cavity FP with a mirror and beam splitter BS1 and the transmitted light is detected by photodiode 2. The length of coupling cavity FP is modulated by PZT and Servo 1, similar to Servo 2, is used to obtain an error signal for “laser for stabilization“.

4. Experimental study of molecular matter wave interferometer

In this chapter experimental observations are presented from the new investigations of the matter wave interferometer with potassium molecules since its realization in our experimental group [35]. In the section 4.1 potassium dimers as a base for the molecular matter wave interferometer are discussed with some examples of high resolution spectra of potassium molecular transitions obtained in the supersonic beam.

The section 4.2 describes the special situation of our molecular matter wave interferometer where we are able to observe signals resulting from two superimposed interference patterns produced by different types of matter wave interferometers. One is the Ramsey-Bordé type interferometer due to a longitudinal displacement of molecular wave packages in the direction of the supersonic beam produced by interaction with two pairs of counter propagating laser beams. The second one is an optical Ramsey interference: a spatial overlap of relatively large molecular wave packages in the transversal direction created by the interaction of only two laser beams. The evaluation of overlapping interferometric signals needs a special procedure for the data analysis which is described in the section 4.2 as well. In this a section also comparison between the two different interferometric signals is done.

As our molecular interferometer is quantum state sensitive it is possible to detect its two exits in ground and excited state independently and simultaneously by spectroscopic means. In section 4.3 the detection of the interference signals on different exits of the molecular matter wave interferometer is presented and the comparison between observed signals on the excited state and ground state exits using various molecular transitions is done.

4.1. Potassium dimers as a base for molecular matter wave interferometer

As it was mentioned in chapter 2 to construct a molecular matter wave interferometer in the optical domain we have to use a state with sufficiently long lifetime in order to avoid loss of coherence during the flight of a molecule through the two zones D between the pair of laser beams. It is also desirable to have a relatively strong transition moment for easy detection. The potassium molecules are a good base for molecular matter wave interferometer. It is easy to prepare a supersonic beam of potassium for the experiment and desired transitions could be reached by a low cost diode laser system.

4.1.1. Production of long living states

The potassium molecules are produced by heating an oven containing metallic potassium and expanding through a 200 μm nozzle into the vacuum. The description of the experimental setup can be found in section 3. The produced molecules are mainly in the $X^1\Sigma_g^+$ electronic state with low v and J numbers. The Figure 4.1 illustrates the lowest electronic states for potassium dimer. The states $A^1\Sigma_u^+$ and $b^3\Pi_u(0^+)$ are coupled via spin-orbit interaction. So it is possible to observe not only bands from the $A^1\Sigma_u^+ \leftarrow X^1\Sigma_g^+$ system, but also sufficiently strong bands from the $b^3\Pi_u(0^+) \leftarrow X^1\Sigma_g^+$ as well [40].

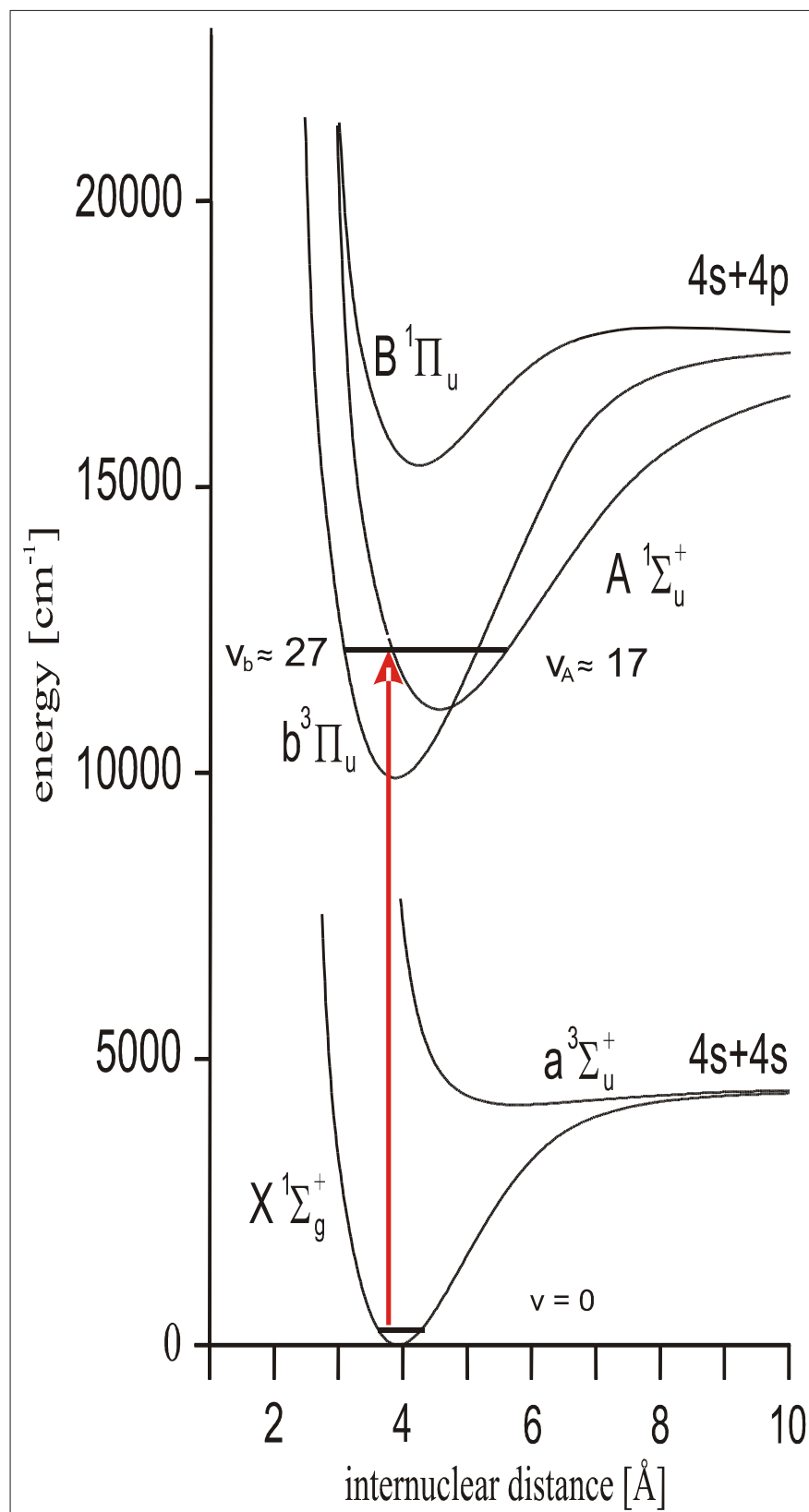


Figure 4.1 Lowest electronic states of potassium dimer

An appropriate transition for molecular matter wave interferometry could be chosen in one of the bands from $b^3\Pi_u(0^+) \leftarrow X^1\Sigma_g^+$ system which has an energy

difference about 12200 cm^{-1} (corresponding to 820 nm). The partial deperturbation analysis was applied for states A and b [40] and mixing coefficients a and b of the rotational and vibrational levels for both states were obtained. In this case the observed level $\Psi(J, \nu')$ can be represented as

$$\Psi(J, \nu') = a(J) \left| {}^1\Sigma_u^+ \right\rangle + b(J) \left| {}^3\Pi_u(0^+) \right\rangle \quad (4.1)$$

where $a(J)$ and $b(J)$ are the amplitudes of the Born-Oppenheimer states and ν' is approximately quantum number ν_b .

Originally the $b \ {}^3\Pi_u(0^+) \leftarrow X \ {}^1\Sigma_g^+$ transition is spin forbidden and the state b has a lifetime in the order of 1 ms [39] while the $A \ {}^1\Sigma_u^+ \leftarrow X \ {}^1\Sigma_g^+$ transition is strong and the state A has a lifetime of about 20 ns . Using this information one can estimate the lifetime of mixed states (for instance with a mixing in the order of 1%) to be about $2 \text{ }\mu\text{s}$.

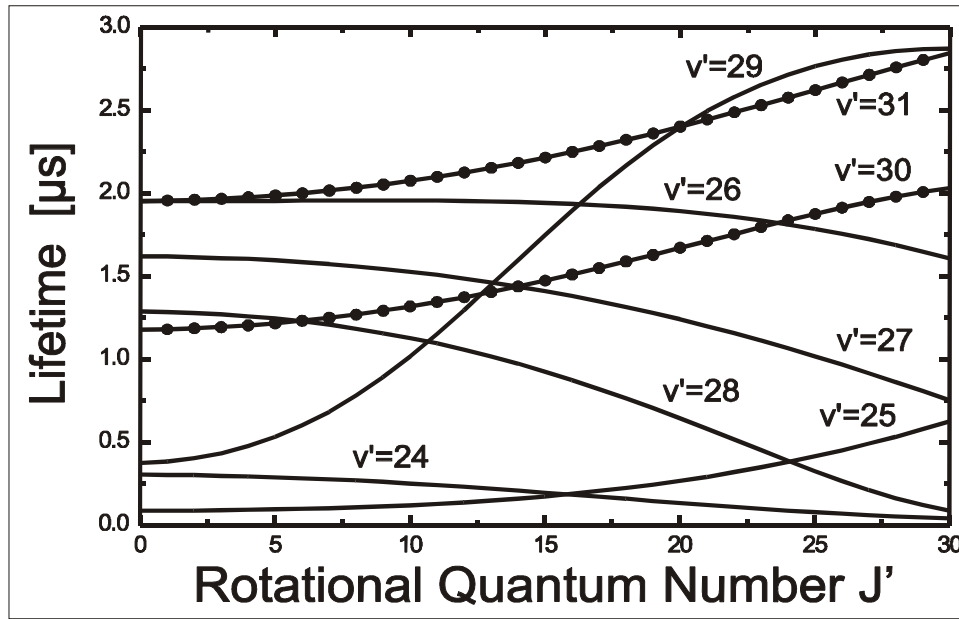


Figure 4.2 Lifetimes of mixed states for some ν' and J' numbers of the coupled system $b \ {}^3\Pi_u(0^+) + A \ {}^1\Sigma_u^+$

In Figure 4.2 the lifetimes for some ν' and J' numbers of the perturbed ${}^3\Pi_u(0^+)$ state are presented [40]. In the experiment the bands $27 - 0$ and $28 - 0$ with J' numbers between 9 and 25 were accessible by our laser system and the lifetimes of the excited levels were typically between 0.5 and $1.5 \text{ }\mu\text{s}$, read from Figure 4.2.

4.1.2. Observed hyperfine structures in the molecular beam of K_2

As it was mentioned in section 3 the molecular beam used in the experiment is highly collimated with the collimation ratio about 1000. Thus the residual transverse velocity spread is less than 1 m/s. The typically observed excitation spectra in the supersonic potassium beam are presented in Figure 4.3. The excitation laser was perpendicular to the molecular beam and had a Gaussian profile with a diameter of 3.2 mm. The power of the laser was chosen to be below the saturation power of the molecular transition. The laser frequency was scanned stepwise over the range of about 60 MHz with a frequency step between 30 and 50 kHz and the integration time of 0.2 s for one point.

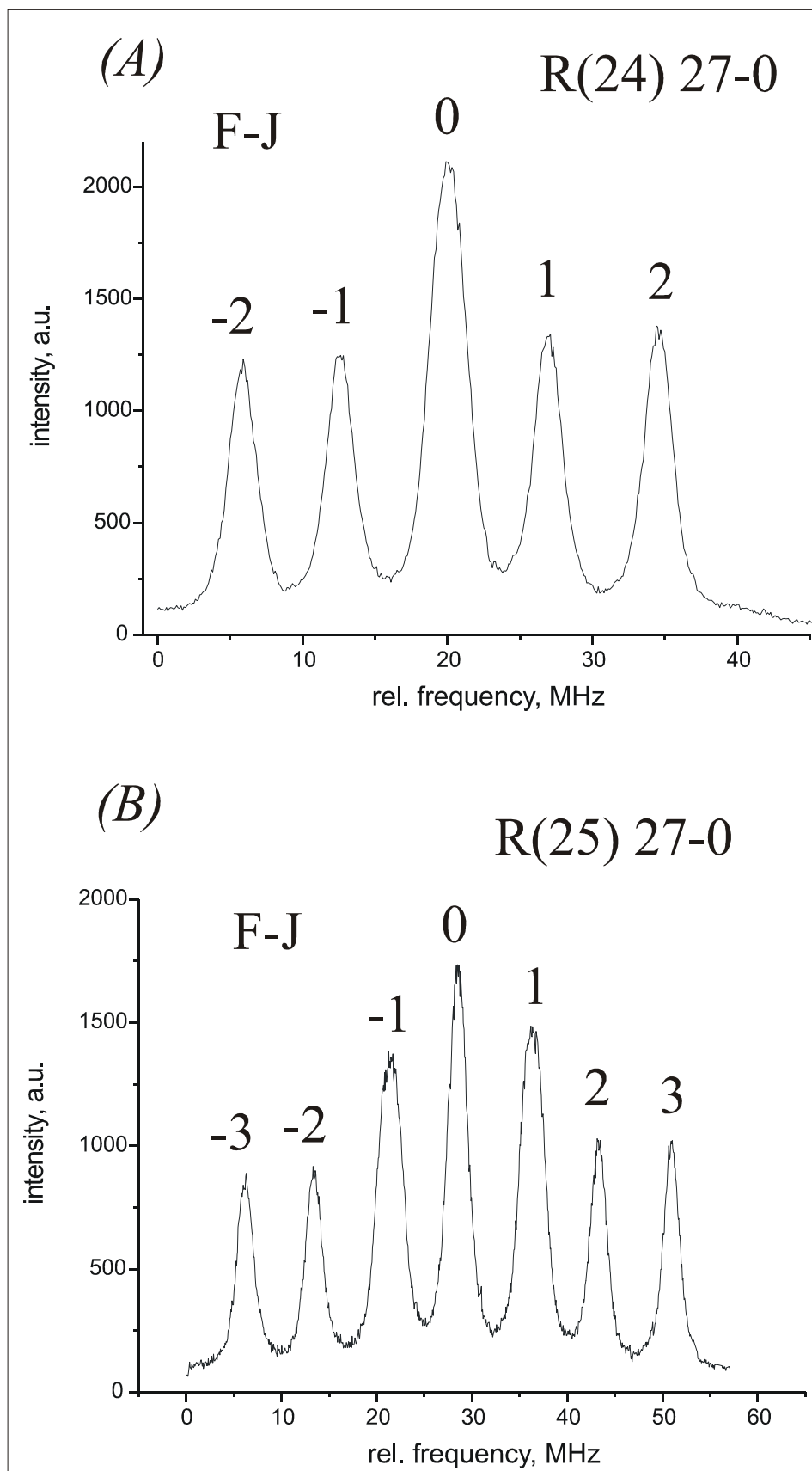


Figure 4.3 Resolved hyperfine structure for two cases in the 27 – 0 band of the $b^3\Pi_u(0^+) \leftarrow X^1\Sigma_g^+$ transition in the molecular beam. (A) and (B) corresponding to even and odd J'' number

The potassium molecule $^{39}\text{K}_2$ with nuclear spin $3/2$ has an antisymmetric wave function with respect to exchange of the nuclei [40]. The selection rules for the total nuclear spin $\vec{I} = \vec{I}_K + \vec{I}_K$ are, respectively, 1 and 3 for odd rotational quantum numbers J'' of the ground state with electronic symmetry g and 0, 2 for even J'' . For the excited state, which in our case has symmetry u , the situation is reversed.

On the part **(A)** one can see in total 6 hyperfine components for $I = 0, 2$, corresponding to $F'' = I + J'', \dots, I - J''$ for the even number $J'' = 24$. The central peak consists of two overlapped hyperfine components from $I = 0$ and 2. In part **(B)** a similar observation for odd $J'' = 25$ is illustrated. In this case we observe 10 hyperfine components for $I = 1, 3$ where three for $F'' - J'' = -1, 0, 1$ are superimposed. It is worthwhile to mention that in the present case the hyperfine splitting of the ground state is quite small []. One can also see in Figure 4.3 that the residual Doppler broadening after collimation of the supersonic beam is still dominant for the linewidth of the observed hyperfine components and is about 2 MHz for both transitions presented in the parts **(A)** and **(B)**.

Figure 4.4 presents the same molecular transition as in Figure 4.3, **(B)** but now with saturation spectroscopy setup. The probe and the pump beams were produced by an unfocused laser beam with a diameter of 3.2 mm crossing the molecular beam perpendicularly to its direction and by a counter running beam shifted 1.5 cm upstream the supersonic beam by means of a retroreflector. The absorption due to the low molecular density in the potassium beam could be neglected so the intensities of the two counter propagating beams are practically equal.

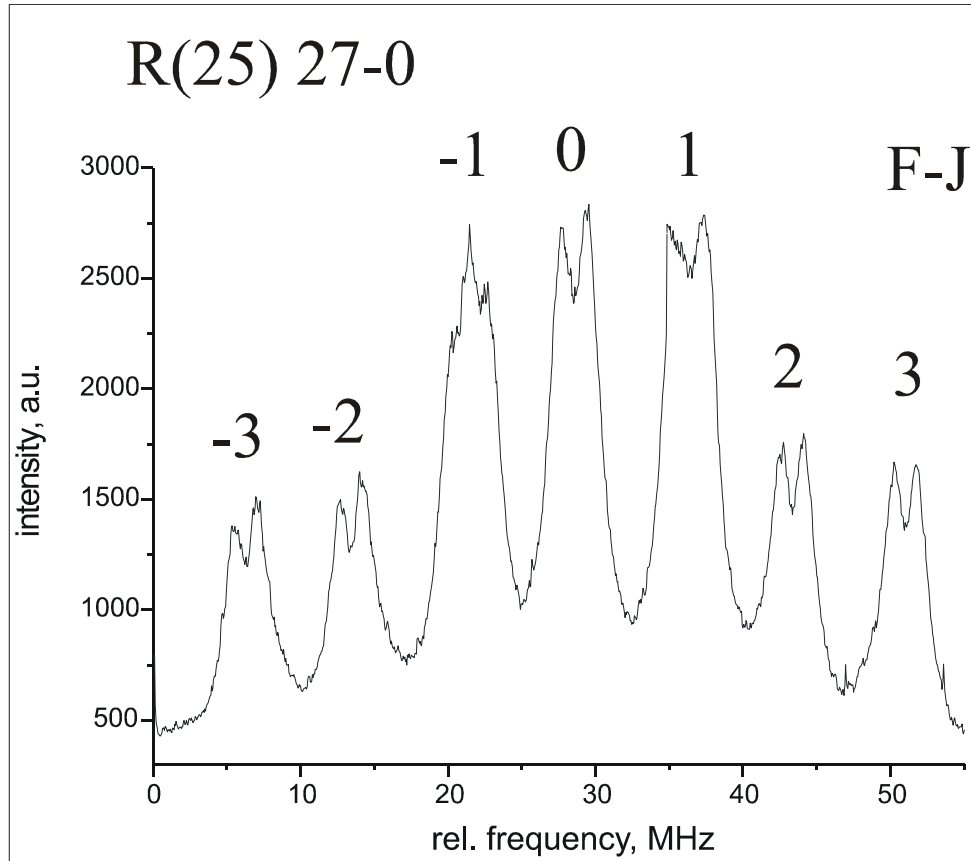


Figure 4.4 Saturation spectroscopy of the $R(25) 27 - 0 \ b \ ^3\Pi_u(0^+) \leftarrow X \ ^1\Sigma_g^+$ transition

As in Figure 4.3, in Figure 4.4 it is possible to see the residual Doppler broadening of about 2 MHz for each resolved hyperfine component of the $R(25) 27 - 0 \ b \ ^3\Pi_u(0^+) \leftarrow X \ ^1\Sigma_g^+$ transition due to the collimation of the molecular beam. The laser linewidth is about 35 kHz (section 3.2) and negligible. The width of the saturation dip of about 500 kHz is determined by the transit time broadening, possible saturation broadening, and the natural line width of 150 kHz (compare lifetimes in Figure 4.2). This information will be of importance when we analyse data of pressure shift measurements done in the supersonic molecular beam (section 5.4). On the component $F - J = -1$ one can see two saturation dips – this feature is probably due to a small displacement in the positions of hyperfine components for $I = 1$ and 3.

4.2. Experimental study of molecular matter wave interferometers with two and four laser beam splitters

In this section observations with the Ramsey-Bordé interferometer (four laser beam splitters) and the optical Ramsey interferometer (with two laser beam splitters),

described in section 2, are presented. In section 4.2.1 procedures of recording and evaluation of observed spectra is described. Results of the measurements done for the Ramsey-Bordé and optical Ramsey interferometers are presented in sections 4.2.2 and 4.4.3. The comparison between observed signals for two and four laser beam splitter interferometers is described in section 4.2.4.

4.2.1. Excited state exit detection and analysis of observed signals

To obtain interferometric signals we first used the experimental scheme given in Figure 4.5 which was already explained in the sections 3.1 and 3.2. The matter wave interferometer was realized by two pairs of counter propagating laser beams 1 – 4 and the interferometric signals were recorded by the photomultiplier PM1 using an imaging system which looks at the fluorescence from beams 1 and 2 as shown in the right part of Figure 4.5. In present experimental arrangement it was possible to switch easily between the Ramsey-Bordé setup and optical Ramsey setup by blocking the pair of laser beams 3 – 4.

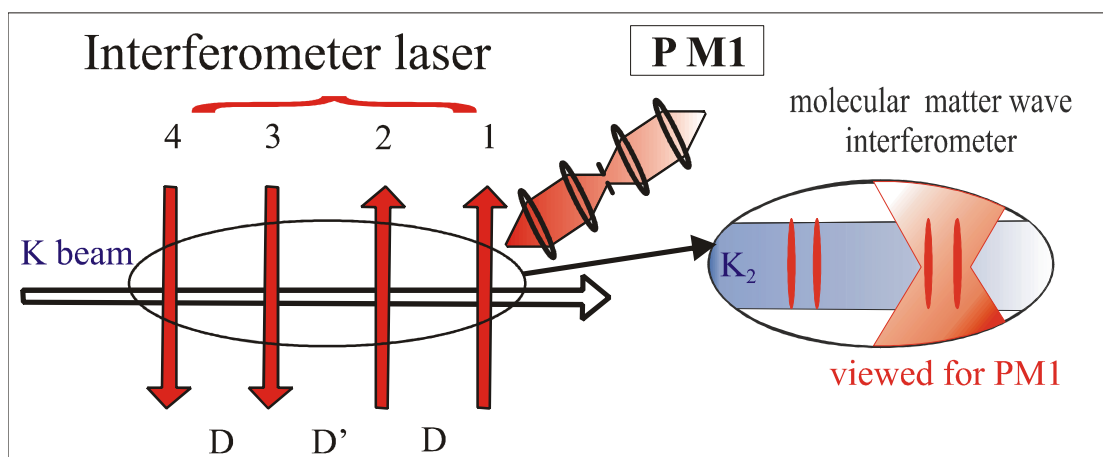


Figure 4.5 Experimental scheme to observe excited state exit of molecular Ramsey-Bordé interferometer

All four laser beams were produced in the way described in the section 3.2.3 and were perpendicular to the direction of the molecular beam (x direction). After focusing by cylindrical lenses each beam has a waist in x direction of about 140 μm . The laser power in one beam was chosen to be typically about 3.5 mW which is close to the value needed to fulfill the condition for the $\pi/2$ Rabi pulse giving 50 % beam splitter.

The separation D in each pair of counter propagating beams was varied between 200 μm to 900 μm while the central distance D' was kept fixed at 15 mm.

Characteristically observed signals with all four laser beam splitters are shown in Figure 4.6. The frequency of the interferometer laser was scanned with steps of 30 kHz and applying an integration time per point of 150 ms. The separation between two copropagating laser beams was 500 μm in the case of Figure 4.6.

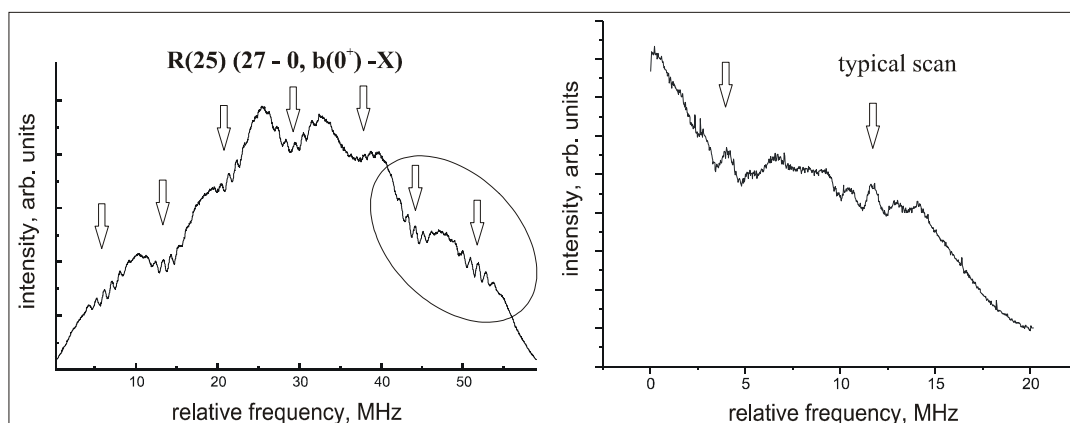


Figure 4.6 Interferences observed in potassium molecular beam

In the left part of Figure 4.6 the interferometric signal observed on all hyperfine components of the transition $R(25) 27 - 0 b^3\Pi_u(0^+) \leftarrow X^1\Sigma_g^+$ is presented. As it is mentioned above we have a 1D-focusing of our interferometer laser beams in the direction of the molecular beam to have sufficiently small size of the laser waist compared to the dark zone length D . Due to this we observe transit time broadening of about 8 MHz for each hyperfine component of the $R(25) 27 - 0 b^3\Pi_u(0^+) \leftarrow X^1\Sigma_g^+$ transition so it is no longer possible to resolve them (Figure 4.6). The positions of unresolved hyperfine components are marked by arrows and one can see interference fringes on top of each hyperfine component. The right part of Figure 4.6 shows a scan over the two high frequency hyperfine components of the $R(25) 27 - 0 b^3\Pi_u(0^+) \leftarrow X^1\Sigma_g^+$ transition circled on the left part of Figure 4.6. The scanning over this particular region was chosen to reduce time needed for one recording and because of largest splitting between the two highest in frequency hyperfine components. If nothing is mentioned specifically this is our “typical scan”.

Although the interferences are clearly visible in the Figure 4.6 the observed signals contain incoherent background. To remove unwanted background signal and to improve signal-to-noise ratio we use a special sequence of data analysis. The

procedure of the following evaluation of the observed traces can be divided into several steps. The recordings normally contain unphysical spikes of 1 to 3 data point width due to fluctuations of the photomultiplier current. So first positions of such peculiarities were analyzed and these data points were replaced by linear extrapolation through nearest points. The stability of our laser source also allows us to average many recorded traces in order to increase effective integration time per one data point.

As was mentioned in section 2 the observed interferometric signals in the Ramsey-Bordé configuration can contain two types of matter wave interferences: longitudinal and transversal. The periods of the Ramsey-Bordé and the optical Ramsey interference fringes are different by factor of 2 because the Ramsey-Bordé interferometer has two times the length of the total dark zone compared to the optical Ramsey interferometer. In order to distinguish these interference fringes we apply the method of digital filtering by Fourier transformation.

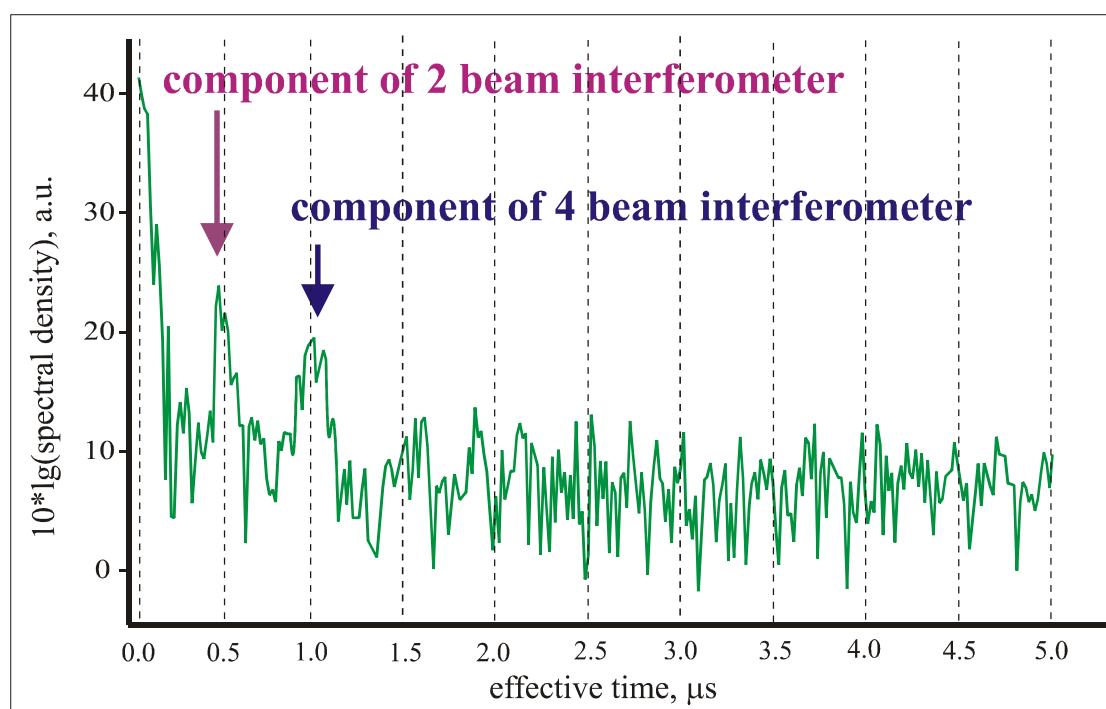


Figure 4.7 Fourier spectrum of a recording like the right art of Figure 4.6

A scan like those shown in the right part of Figure 4.6 are symmetrized by mirroring it at the vertical axis at the start frequency and then calculate the Fourier transform of symmetrized spectrum, interpreted as periodic structure. The Fourier spectrum shows two main peaks, whose frequency ratio is 2, on a noisy background. The incoherent background structure of the interferometer signal is seen as low frequency components located in the domain of the effective time around 0 μ s. The peaks visible

at $0.5 \mu\text{s}$ and $1 \mu\text{s}$ in Figure 4.7 correspond to the optical Ramsey and Ramsey-Bordé interference signals and have widths in time domain between $0.2 \mu\text{s}$ and $0.4 \mu\text{s}$. Selecting an appropriate interval of about $0.7 \mu\text{s}$ around the higher frequency peak, setting the remaining parts of the Fourier transform to zero and transforming back is equivalent to applying a narrow band pass filter with rectangular shape tuned to the frequency of the Ramsey-Bordé interferences. This procedure works well with the signals of both types of molecular matter wave interferometers. The background structure and the noise as well are strongly reduced by this filtering process. We can set the width of the implemented bandpass or highpass filter to be around an expected value for the frequency interval of the interference pattern and thus cut out desired interference components in the recorded spectra from another type of interferences and the incoherent background.

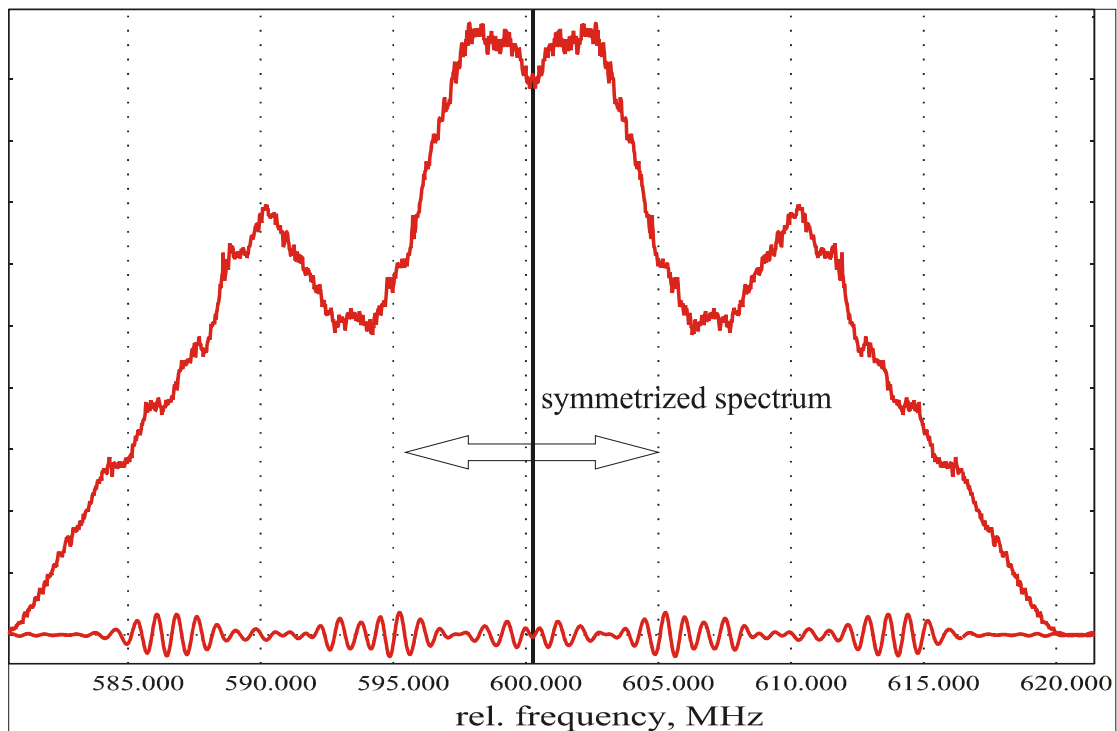


Figure 4.8 Digital filtering of studied spectra of the molecular matter wave interferometer in the Ramsey-Bordé configuration. The lower trace indicates longitudinal interferences after band pass digital filter while the upper part shows remaining incoherent background and optical Ramsey interferences.

We started with a scan similar to the one shown in the left part of Figure 4.6 and symmetrized it, so only the right part of the frequency scale illustrated in Figure 4.8 has a real physical meaning. After obtaining the Fourier transform spectra from the symmetrized scan we set the weights of all frequency components in the time domain to zero except an interval of the frequency components corresponding to studied type

of interference. The result of the digital filtering of the interference signal in the Ramsey-Bordé configuration is presented in Figure 4.8. The lower trace indicates longitudinal interferences after band pass digital filter while the upper part shows remaining incoherent background and optical Ramsey interferences. Even superimposed on the incoherent background signal and the high frequency noise one still can see in the upper trace of Figure 4.8 that the optical Ramsey interferences have twice the period of the Ramsey-Bordé interferences illustrated in the lower trace. The width of the bandpass filter was chosen to be about $0.6 \mu\text{s}$ which is close to the width of the second peak shown in Figure 4.7.

We have made investigations to check the dependence of the fringe position in frequency domain on the choice of the width and position of the bandpass filter. If the width of the bandpass filter in the time domain is not overlapping with nearest peaks the additional phase shift produced by digital filtering is at least an order of magnitude smaller than the experimental uncertainties, which are later discussed for phase shift measurements.

As the next step of evaluation the signal illustrated in the lower part of Figure 4.8 is fitted by formula [35]

$$I(\nu) = U + A \cdot \exp\left(-\frac{(\nu - \nu_0)^2}{\nu_w^2}\right) \cdot \cos(2\pi P(\nu - \nu_0) + \varphi) \quad (4.2)$$

where $I(\nu)$ describes an oscillation damped by a Gaussian envelope with width ν_w , which is determined by the „coherence“ of the wave packet $l_{coh}^x \equiv \frac{\hbar}{2\Delta p}$ and not by the excitation process. In equation (4.2) U represents the residual background after digital filtering, A and φ are the amplitude and phase of the observed interferometric signal.

4.2.2. Investigation of the matter wave interferometer with four laser beam splitters

The experimental study of the four laser beam matter wave interferometer was in detail described in [35, 38, 39] so in this section some examples of recent measurements done for the Ramsey-Bordé molecular interferometer are presented.

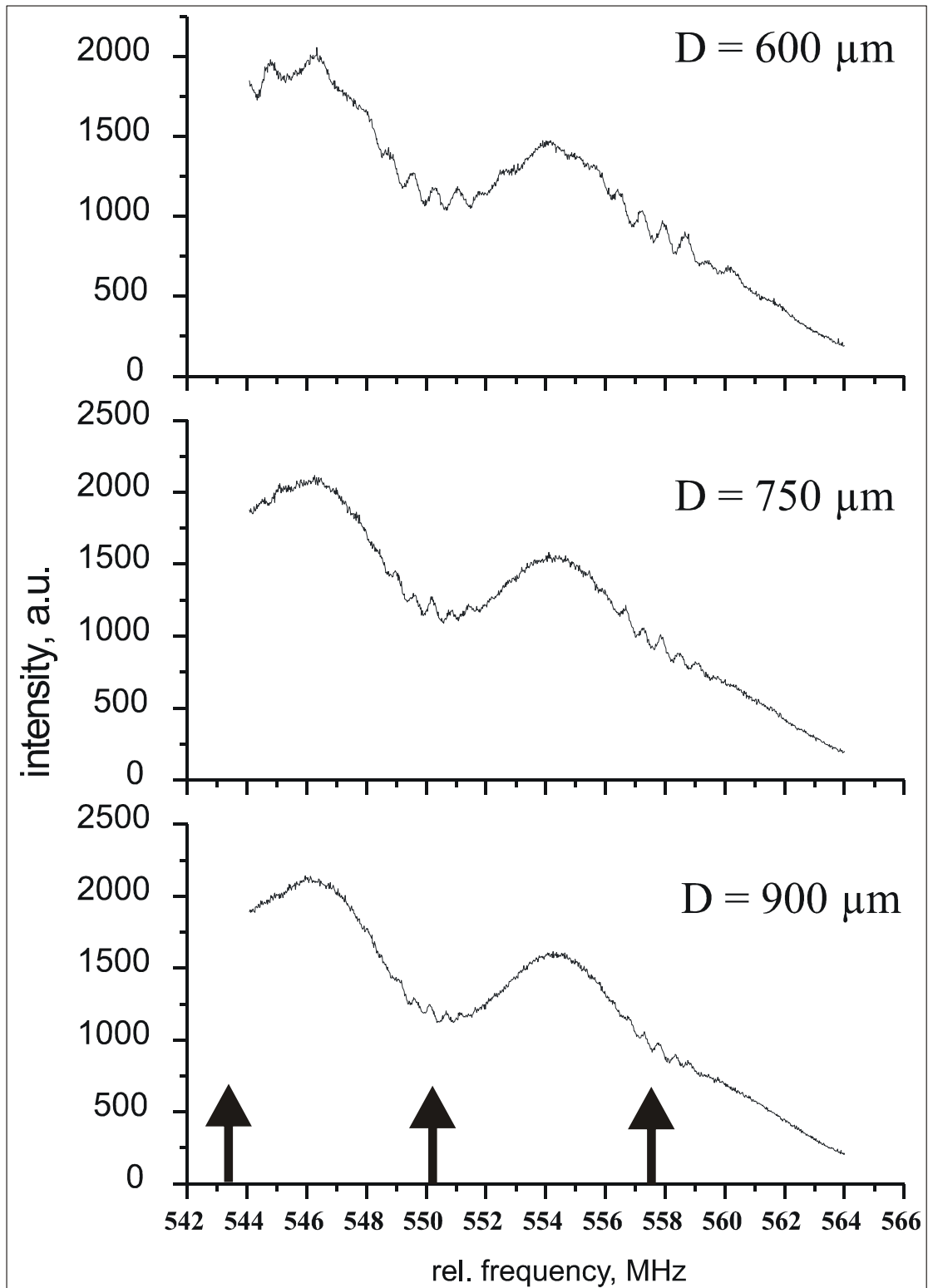


Figure 4.9 Signals of the Ramsey-Bordé molecular matter wave interferometer observed for different separations between the pair of the copropagating laser beams.

The observations for different beam separation D in the pair of copropagating laser beams of the Ramsey-Bordé molecular matter wave interferometer are presented in Figure 4.9. The positions of unresolved hyperfine components are marked by

arrows and located about 543 MHz, 550 MHz and 557 MHz. The recordings were done by scanning interferometer laser with frequency steps of 20 kHz and the integration time per point of 1.8 s. The beam separations D are chosen to be large enough that the optical Ramsey interferences become less visible on the measurements. But one can see even at the beam separation $D = 750 \mu\text{m}$ the resulting interference structure corresponding to one hyperfine component shows reduction of the amplitude for every second interference fringe. That means the optical Ramsey interferences are quite significant and still contributing to the total interference signal.

The filtered Ramsey-Bordé interference patterns of Figure 4.9 are shown in Figure 4.10. The part A shows interference structures corresponding to two different hyperfine components. One can clearly see that envelopes of the interference fringes are not overlapped and can be well localized.

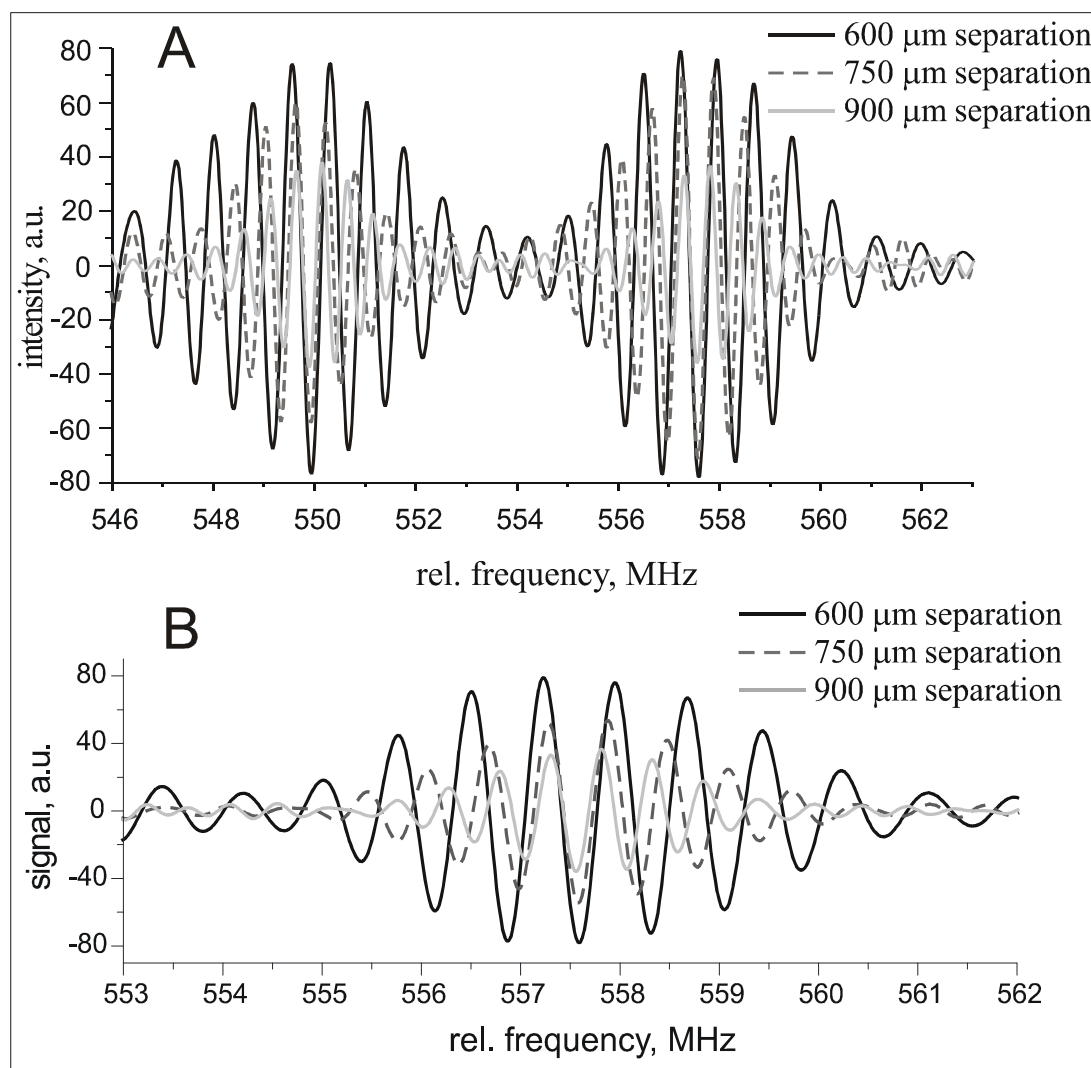


Figure 4.10 Interference signals of the Ramsey-Bordé interferometer after digital filtering for some beam separations D . The part A indicates fringes corresponding to different hyperfine components; the part B is zoom on the highest in frequency hyperfine component.

A zoom of the interference signal corresponding to the last hyperfine component is presented in the part B of Figure 4.10. The change of the contrast and period of interference patterns are clearly visible in the part B. the loss in contrast for increasing D follows the expectations from the lifetime of the excited state and the dependence of the period will be studied in section 4.2.4.

4.2.3. Investigation of the matter wave interferometer with two laser beam splitters

For the signals from the transverse matter wave interferences a similar approach is used to separate them from background and the other interferences, by centering the filter around the low frequency peak in the Fourier transform. Apart from the different period, the result looks similar to the one shown in section 4.2.2, except that these interferences are more widely extended in frequency domain, so that for the excited state exit they appear to cover the whole structure without any visible break between the hyperfine components.

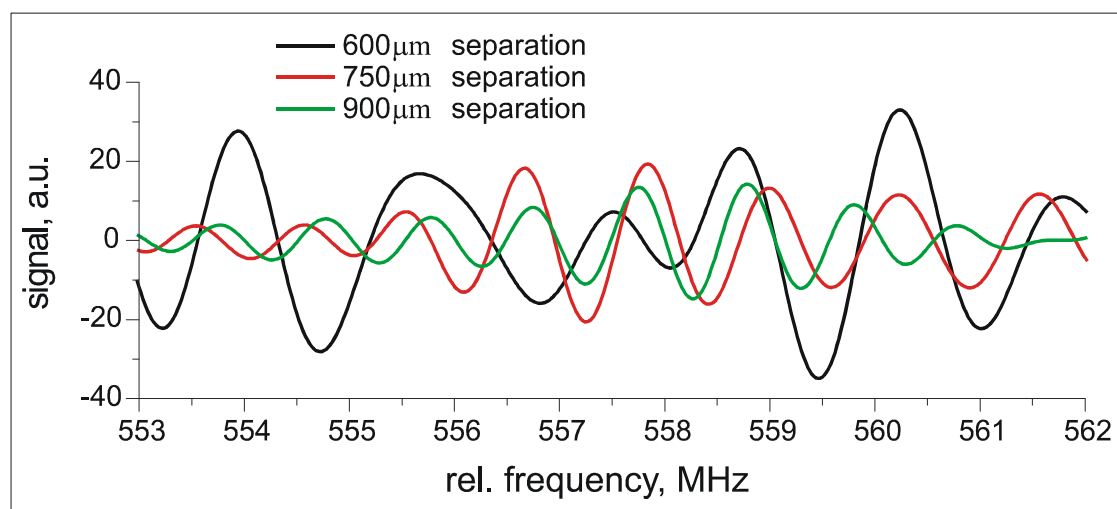


Figure 4.11 Interference signals of the optical Ramsey interferometer after digital filtering for some beam separations D

The interference signals of the optical Ramsey interferometer after digital filtering for the beam separations D as in Figure 4.10 are presented in Figure 4.11. The contrast of the observed interferences is quite low and decreasing with rising D . The determination of the phase of the interference signals produced by the matter wave interferometer with two laser beam splitter is almost impossible in the case of the

excited state exit like shown in Figure 4.11, so for further investigation it is better to use the ground state exit, which will be discussed later.

4.2.4. Comparison between two and four laser beam splitter molecular matter wave interferometers

As derivable from the observations above the interference patterns with two and four laser beam splitters have different width of the confining envelopes. The Gaussian profile of the Ramsey-Bordé interferences has smaller width due to correlation between $1/P$ and longitudinal coherence. This allows in the case of Ramsey-Bordé interferometer to distinguish interference patterns of separated hyperfine components while for the optical Ramsey interferometer the interference structures are overlapped even for the two high frequency hyperfine components.

The analysis of frequency stability of the positions of interference patterns for the two and four beam splitter interferometers shows that optical Ramsey interference fringes are drifting significantly (1MHz within 1 min) while Ramsey-Bordé fringes are quite stable due to symmetrical arrangement of interferometer (laser phases are cancel each other).

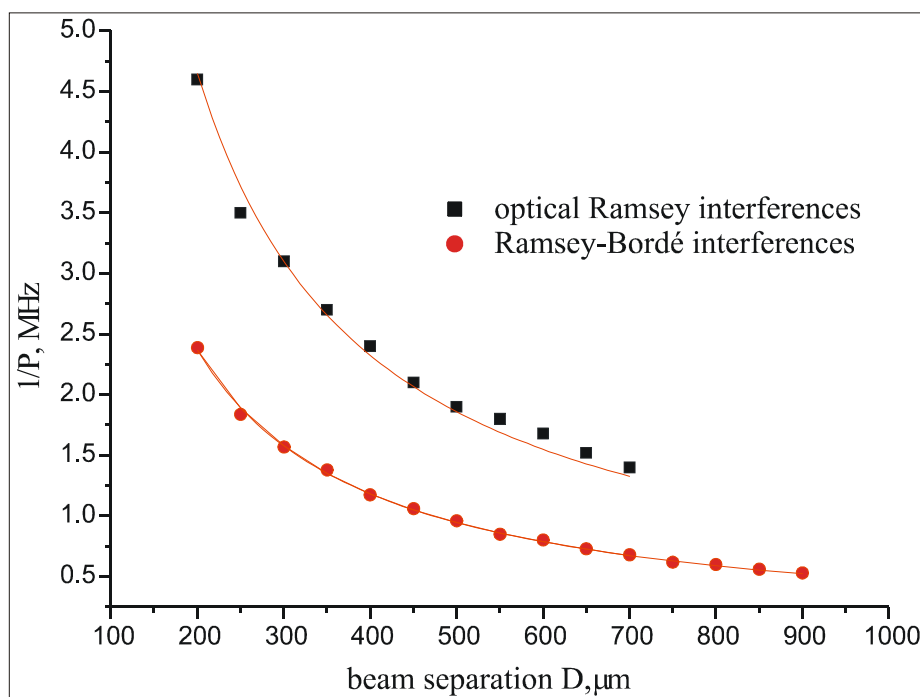


Figure 4.12 Dependence of the frequency interval $1/P$ on the beam separation D for the optical Ramsey and Ramsey-Bordé molecular matter wave interferometers. The results for the optical Ramsey interferometer were fitted by formula $1/P = v/D$, while for the Ramsey-Bordé interferometer by $1/P = v/2D$

The measured dependence of the frequency interval $1/P$ on the beam separation D for the optical Ramsey and Ramsey-Bordé molecular matter wave interferometers is shown in Figure 4.12. The results obtained for the optical Ramsey interferometer were fitted by formula $1/P = v/D$, while for the Ramsey-Bordé interferometer by $1/P = v/2D$. The observations have very good agreement with fitted curves. The measured data points stop for the optical Ramsey interferometer at $D = 700 \mu\text{m}$. At this separation the splitting of the wave packets became larger than the transverse size of the molecular wave packet in the beam and it was no longer possible to identify such interference signals. In case of the Ramsey-Bordé interferometer the observed contrast is limited by the lifetime of the molecular state.

As the Ramsey-Bordé patterns are better localized, we shall concentrate on them for the later measurements of phase shifts due to collisions within the beam (see section 5).

4.3. Detection on different exits of the molecular matter wave interferometer

Up to now the interference signal was detected via the fluorescence, this is the so called excited state exit. In this part of the thesis measurements of ground state exit of the molecular matter wave interferometer are studied. Interesting features of singlet and triplet transitions are discussed and a comparison between two examples of transitions, namely on the $b \ ^3\Pi_u(0^+) \leftarrow X \ ^1\Sigma_g^+$ and $B \ ^1\Pi_u \leftarrow X \ ^1\Sigma_g^+$ molecular systems, are done.

Compared to atoms, molecules have a higher number of internal degrees of freedom. According to the Franck-Condon principle, mostly the molecules in the excited state decay with quite low probability back to the original rovibronic level, but they will spontaneously decay in most cases to other levels. Thus by using molecules for matter wave interferometry we have the unique possibility to observe easily the two exits of the matter wave interferometer in ground and excited states at different time or places. In our case the molecular matter wave interferometer is realized with a supersonic beam, where we can neglect by interaction between the molecules and

their environment, this means that we can detect the ground state exit at large distances downstream the molecule beam.

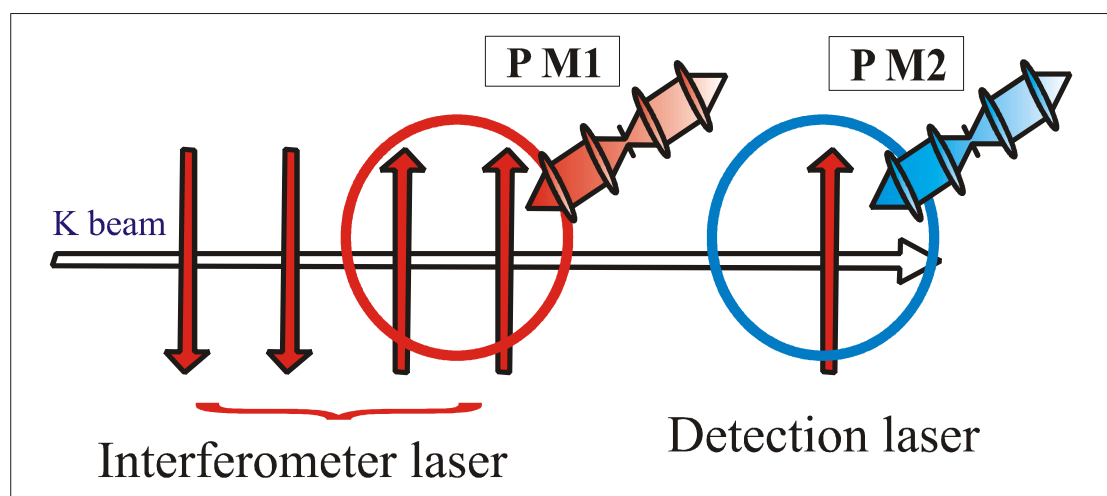


Figure 4.13 Scheme of the experimental setup for simultaneous observation of both exits of molecular matter wave interferometer

The principal scheme of the experimental setup is shown in Figure 4.13. The fluorescence detection by PM1 was used in section 4.2. The detection laser for the examination of the ground state exit crosses the molecular beam about ~300mm downstream the last pair of parallel laser beams. The laser induced fluorescence is detected by photomultiplier (PM2).

The traveling time for the molecules for the length of 300 mm is about 300 μ s.

Thus the molecules in the excited state have certainly ($e^{-\frac{300}{1}} \approx 10^{-130}$) decayed, when they arrive at the detection laser beam, and only the population information in the ground state is kept.

The tuning of the interferometer laser and recording of observed signals by PM1 and PM2 were done in the same manner as in section 4.2. The large separation between interferometer laser and detection laser of the ground state exit reduces the stray light background for the detection at PM2 significantly.

4.3.1. Ground state exit of molecular matter wave interferometer observed on the B-X transition

An unperturbed singlet – singlet transition is allowed and at the first glance a strong transition, with which a good detection efficiency is expected. The B $^1\Pi_u$ state is in a convenient energy range just above the b-A system and the B-X transition is known to be quite strong. The spectrum of the B-X band system has been analyzed by [50]. The transition Q(25) 4-0 B $^1\Pi_u \leftarrow X ^1\Sigma_g^+$ at 15655.36 cm^{-1} was chosen due to its large Franck-Condon factor. It shares the ground state level $v''=0 J''=25$ with the R(25) 27 – 0 b $^3\Pi_u(0^+) \leftarrow X ^1\Sigma_g^+$ transition used for the splitting of the matter wave. The dye laser for excitation of this transition was operated with DCM dye and was frequency stabilized by locking it to a confocal Fabry-Perot cavity, which is stabilized to an iodine stabilized HeNe laser (section 3.3). The spectral line width of this laser was about 2 MHz. The utilization of the dye laser had one disadvantage: the output power of the laser radiation had fluctuations caused by bubbles appearing in the dye jet. This typically reduces signal-to-noise ratio of the observed signals.

For the B-state the hyperfine splitting is small [50], and single hyperfine components are not resolved in the spectrum. Thus an excitation involves all hyperfine components simultaneously. Manipulation of the population of one of the 10 ground state hyperfine levels while leaving the other ones unchanged will accordingly lead to reduction of the changes by a factor of 10 of the whole laser induced fluorescence on the B-X transition. Thus a good signal-to-noise ratio is needed for this detection.

Simultaneous records of interference patterns observed with PM1 for the excited state exit of the MWI and with PM2 for the ground state exit are shown in Figure 4.14. The frequency of the interferometer beam splitters is tuned along the two uppermost hyperfine components.

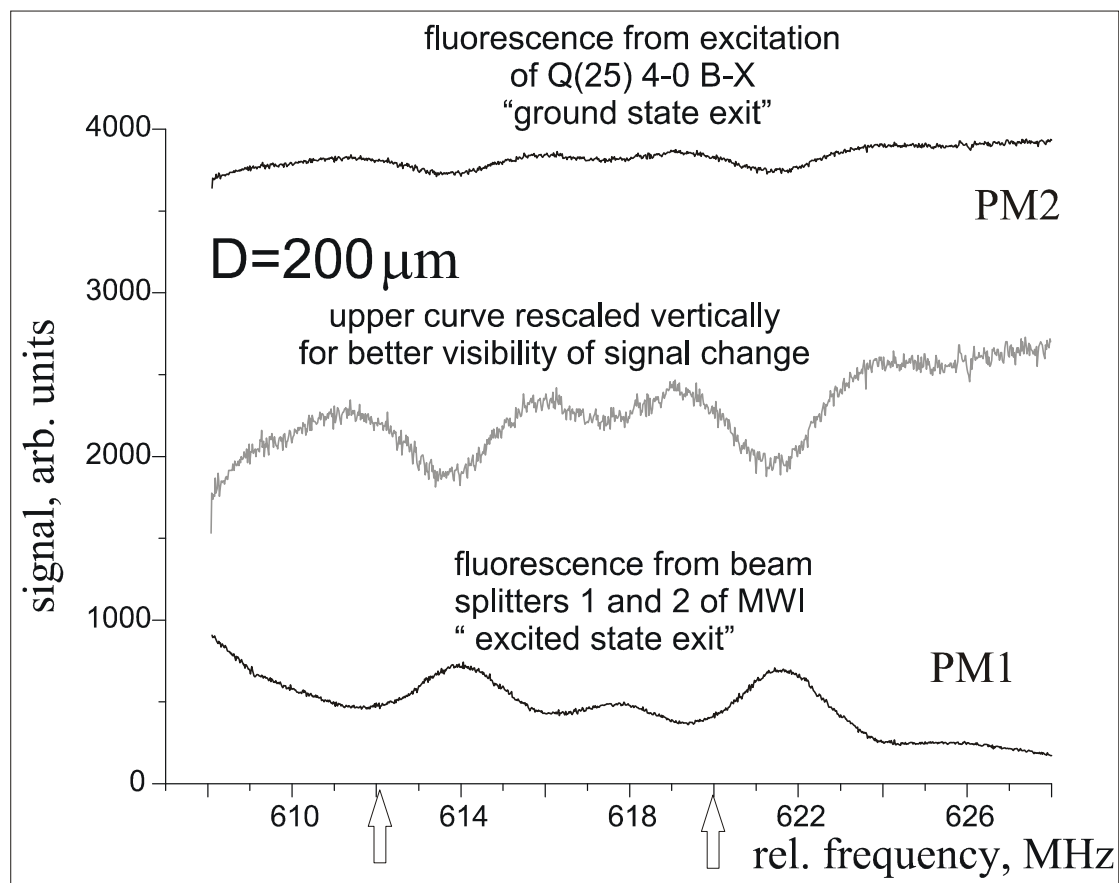


Figure 4.14 Simultaneous spectra of the interference patterns for the ground state and excited state exits of the two laser beam splitter interferometer. The ground state exit is realized by excitation on the $Q(25) 4-0 B^1\Pi_u \leftarrow X^1\Sigma_g^+$ transition of K_2

The upper and the lower traces correspond to the fluorescence by excitation on the B-X Q(25) (4-0) transition (ground state exit of MWI) and the R(25) (27-0) b-X transition in beam splitters 3 and 4 (excited state exit), respectively. The centers of the hyperfine components are located at about 612 MHz and 620 MHz on the picture and marked by arrows. The interference structure is due to the small length of the dark zone $D=200\ \mu\text{m}$ for a transverse matter wave interference created by beam splitters 1 and 2. Broadened by time of flight hyperfine components are overlapped and show interference fringes with frequency interval $1/P$ of about 4.5 MHz (see Figure 4.12). The signal changes according to the matter wave interference in the upper trace starts from a high background corresponding to simultaneous excitation of all 10 hyperfine components and is as expected opposite in sign compared to the lower trace. The middle trace shows the rescaled upper trace (not corresponding to the vertical scale) where the signal is magnified and shifted to have similar amplitude as the lower trace for better visibility of the structure. From the upper trace it is obvious that the signal contrast is much lower compared to the lower one, and from the middle trace one sees

that the signal-to-noise ration for this type of observation of the ground state exit is worse compared to the excited state exit. The reason for the observed noise on the signal was mainly intensity fluctuations of the dye laser used.

Using the B-X transition the matter wave interferences are observable, but due to the signal properties like high background and small contrast, and intensity fluctuations of the exciting laser there seems to be no advantage compared to the previous detection method using directly the fluorescence from the beam splitters. A better control of the intensity of the dye laser would improve the situation, but was not available at the time the experiments were undertaken.

4.3.2. Ground state exit of molecular matter wave interferometer observed with the b-X transition

Employing the b-X transition, in spite of having a much smaller transition moment than the B-X transition, has the important advantage that the hyperfine splitting can be readily resolved in this transition. For the observation the transit time broadening can be kept small, because no focusing is needed for good detection efficiency. Thus an excitation and detection of a single hyperfine component is possible. The various hyperfine components have only small remaining overlap in the hyperfine pattern, thus the fluorescence will show changes only when the interferometer laser is operating on the same hyperfine level of the ground state. Therefore, this method reduces also the overlapping interferences from neighboring hyperfine components, which are observed on the excited state exit.

From the stabilized master laser, from which already the radiation for the matter wave beam splitters is derived, a part of its radiation is used for injection lock of another slave laser. The frequency of this slave can be tuned via a RF-tuned AOM to the center of the same transition that is used in the interferometer. In Figure 4.15 the simultaneous records for both interferometer exits are shown. The b-X excitation laser frequency was fixed at the peak of the hyperfine component of highest frequency. The direction of the laser beam is carefully adjusted, perpendicular to that of the molecular beam. While the laser beam for the ground state detection has a diameter of 3.2 mm, one can see that the recorded hyperfine component has a width of about 8 MHz

defined by the beam profile of the focused interferometer laser. To increase signal-to-noise ratio each line in Figure 4.15 contains 15 averaged “typical scans”.

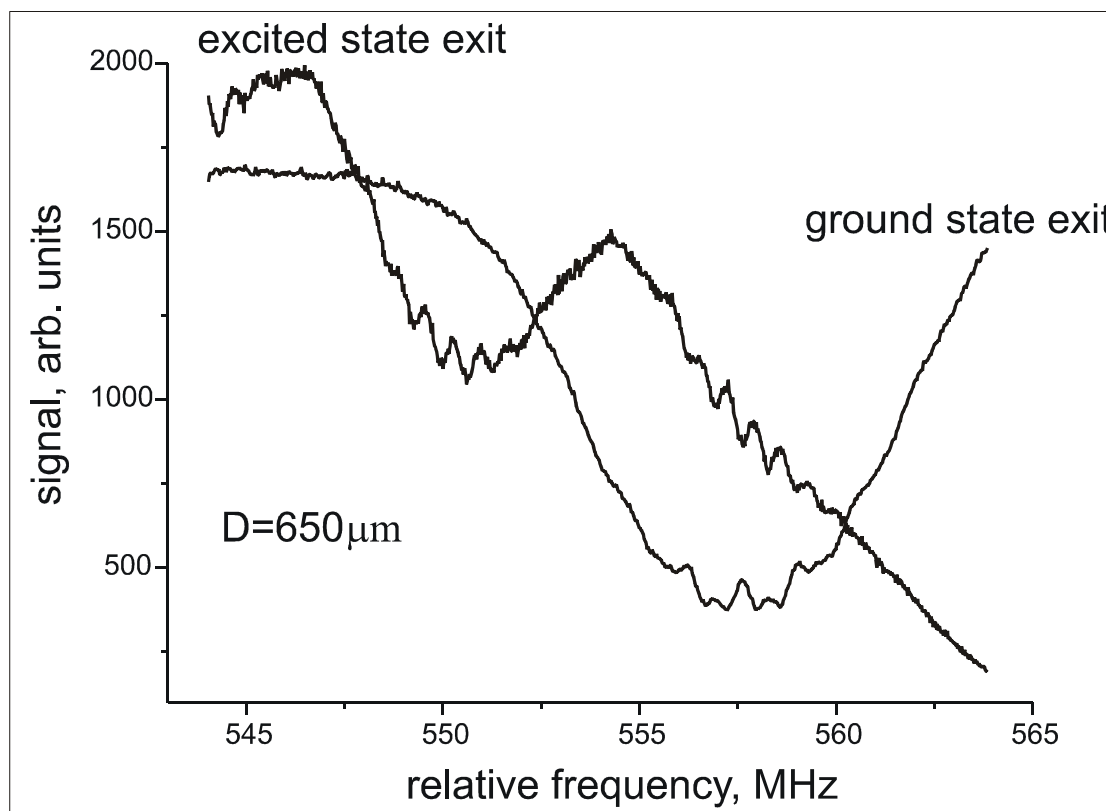


Figure 4.15 Simultaneous records of matter wave interference patterns from ground state exit detected by laser induced fluorescence on the highest frequency hyperfine component of the R(25) (27-0) b-X transition, and on the excited state exit. Note that the ground state exit shows the interference pattern and the background due to only one hyperfine component.

While the excited state exit shows clearly matter wave interferences due to at least two hyperfine components, the ground state exit starts from a high background, but shows a dip and an interference pattern located symmetrically in the dip due to one hyperfine component only. Essentially the interferences of excited state and ground state exit are opposite in phase, but for the ground state it appears more pronounced that the interferences are again a superposition of the Ramsey-Bordé interferences and transverse interferences with twice the period of the former. The S/N of the ground state exit detection is the same compared to that for the excited state exit. This is not obvious from the figure due to different kinds of preamplifiers with different bandwidths used, but was checked separately. As only one hyperfine component is involved, the signal appears symmetric on the background, which is of advantage for high precision determination of the phases and phase changes of interference pattern.

According to the selectivity for a specific hyperfine component and good signal-to-noise ratio the detection of the ground state exit using excitation in the b-X system

was further applied for comparison of the signals with the excited state exit. Systematic measurements with different settings of the dark zone length D , $200 \leq D \leq 950 \mu\text{m}$ were performed recording simultaneously both exits.

4.3.3. Excited vs. ground state exit: experimental advantages and complications

The signals observed (see e.g. Figure 4.15) for both exits are a superposition of the incoherent background and interference fringes from different interference phenomena, which lead to interference periods differing by a factor of two. While for the ground state exit the structure comprises only one hyperfine component, for the excited state exit we have a complicated superposition of more than one hyperfine component. For comparison of the phases of the interferograms of the different exits it is necessary to disentangle the interferences from the background and from each other. The result of such filtering is shown in Figure 4.16.

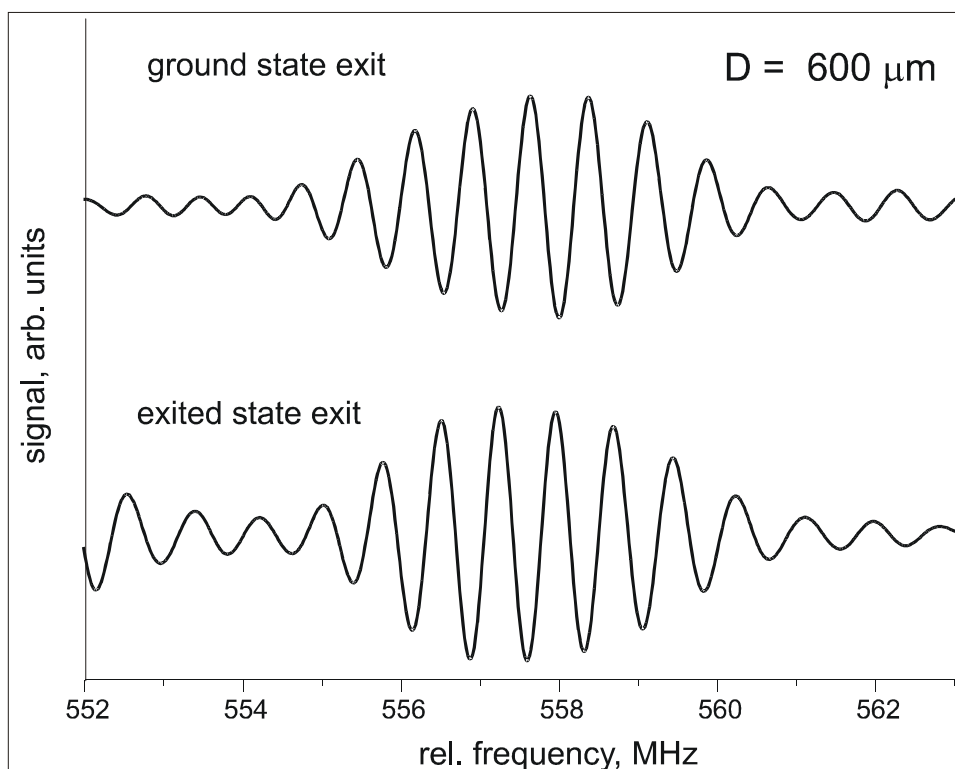


Figure 4.16 Result of narrow-band ($0.7 \mu\text{s}$) Fourier-filtering of the Ramsey-Bordé interferences of both interferometer exits

The central parts of the interferences can be well recognized. The nonzero amplitudes to higher and lower frequencies is the filtered noise remaining from the total noise.

For the excited state exit to low frequencies the amplitude raises again due to the interference pattern of the lower frequency hyperfine component. Such part is not visible in the signal of the ground state exit according to its selectivity to a single hyperfine component.

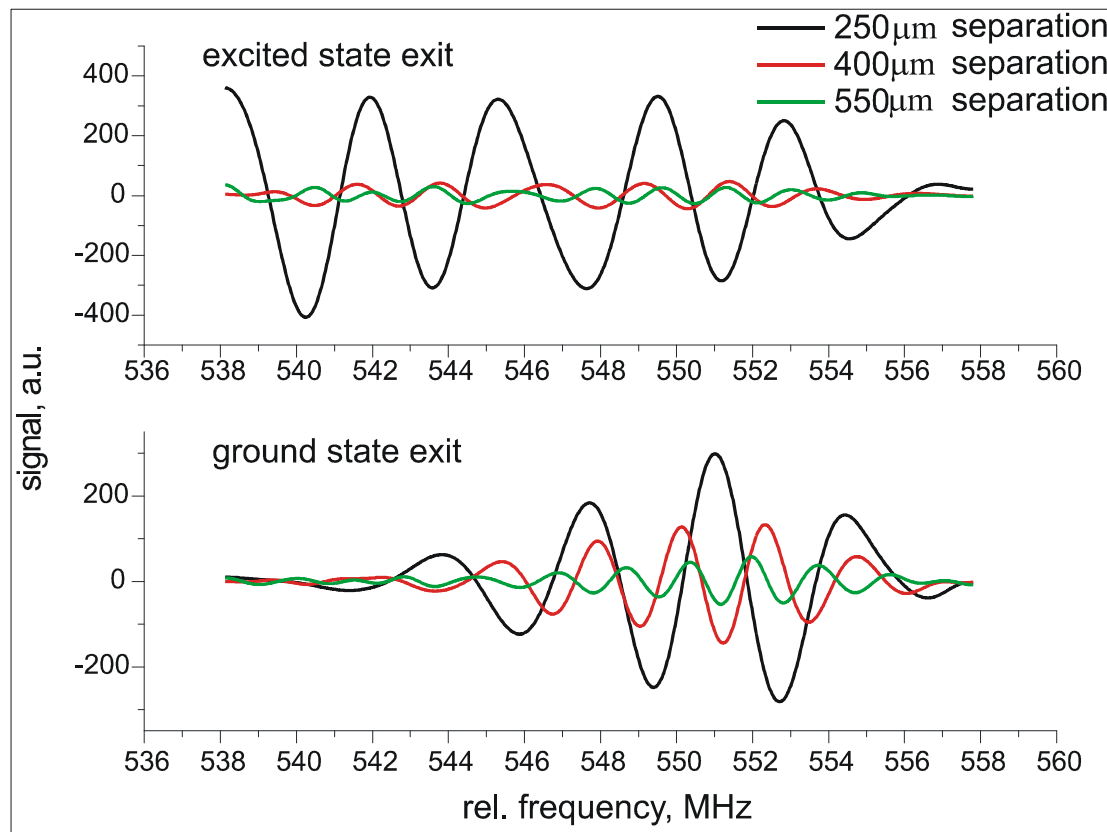


Figure 4.17 The optical Ramsey interferences observed for the ground and excited state exits of the molecular matter wave interferometer at different beam separations D

Another advantage of the ground state exit compared to the excited state exit is that it is better suited for the detection of the optical Ramsey interferences. Figure 4.17 shows the optical Ramsey interferences observed for the ground and excited state exits of the molecular matter wave interferometer at different beam separations D . One can see that the interference signals from different hyperfine components observed for the excited state exit are strongly overlapped, while for the ground state exit we have the interference patterns from only one hyperfine component and thus the smooth change of the contrast and oscillation period as a function of beam separation D is clearly visible. The determination of the phase and amplitude of the optical Ramsey interferences is possible in our experimental arrangement only by using the ground state exit of the molecular matter wave interferometer.

5. Cold collisions observed in a supersonic potassium beam

In this part of the thesis collision experiments within the supersonic potassium beam are described. The goal of this study was to verify the suitability of the molecular matter wave interferometer to observe low energy collisions between potassium atoms and molecules in well defined quantum states. In the section 5.1 some theoretical background of the collisional processes will be reviewed (in relation to expected interference of the matter wave). In the section 5.2 the experimental conditions for interferometric measurements in the supersonic beam of potassium atoms and molecules as collisional partners and the sequence of experimental steps are presented. In section 5.3 the results of the experiments of low energy collisions observation by matter wave interferometry with potassium molecules are reported.

5.1. Theoretical background

As it was described in section 3 we have a supersonic potassium beam where the main contribution to the particle density is given by K atoms with a small fraction of potassium molecules (about few percent). So because the mean free path at the present vacuum conditions is much large than the length of the vacuum apparatus we can neglect any interactions between the potassium beam and the environment. The density of the particles in the supersonic beam was estimated to be in the order of 10^{13} cm^{-3} at the interferometer location and they had a Gaussian velocity distribution with the mean velocity of about 1000 m/s and the width of ± 50 m/s. At such relatively high mean velocity the physical situation in the supersonic beam is viewed like potassium molecules slowly propagating through the medium of potassium atoms. And this image allows as to attribute an index of refraction for the molecular wave of $^{39}\text{K}_2$ to the potassium atomic medium [22, 27 and 28]

The plane matter wave can be described by $\Psi = A \cdot e^{ik_0x}$, where k_0 is the free space wave vector. Propagating through some refractive medium starting at $x = 0$, at the point $x = L$ the forward traveling wave function will gain some additional phase and be attenuated [26]

$$\Psi(x = L) = A \cdot e^{ik_0L} e^{i\varphi NL} e^{-\frac{\sigma}{2}NL} \quad (5.1)$$

Here N denotes density of scattering medium, $\frac{\sigma}{2}NL$ and φNL are attenuation and phase shift accumulated on the distance L . The quantities φ and σ are to be interpreted as cross section. We now introduce the new wave vector $k = nk_0$ with the complex index of refraction n defining the properties of the scattering medium

$$n = 1 + \frac{\varphi NL + i\sigma NL / 2}{k_0 L} = 1 + \frac{N}{k_0} (\varphi + i\sigma / 2) \quad (5.2)$$

The complex quantity $n - 1$ contains the necessary information to express both the phase shift and amplitude decay of the matter wave. It is proportional to the number density N .

The index of refraction is a macroscopic property of scattering media which defines the effect on the phase and amplitude of the matter wave by media. To describe the scattering process on the microscopic scale we introduce the scattering amplitude $f(\vec{k}, \vec{k}')$ [20], where \vec{k} and \vec{k}' are incoming and outgoing wave vectors. In case of elastic collisions $|\vec{k}| = |\vec{k}'|$ we can represent the scattering amplitude as $f(k, \theta)$, where θ is the angle between \vec{k} and \vec{k}' . In our experimental situation the Ramsey-Bordé matter wave interferometer is sensitive to the scattering process defined by forward scattering with $\theta=0$. Thus the relation between index of reflection and scattering amplitude can be written as [26, 29]

$$\begin{aligned} \sigma &= \frac{4\pi}{k_{cm}} \text{Im}(f(k_{cm}, 0)) \\ \varphi &= \frac{2\pi}{k_{cm}} \text{Re}(f(k_{cm}, 0)) \end{aligned} \quad (5.3)$$

where k_{cm} denotes the relative wave vector in the center of mass coordinate for the system $K + K_2$.

The matter wave interferometry method is sensitive to relative changes in the index of refraction and the measurable values by interferometer are changes of phase shift and contrast of the interferences due to changes of the medium. We can easily derive the relation of these directly observed quantities to the forward scattering amplitude [28, 29]

$$\Delta\phi = \phi(L) - \phi(0) = \frac{2\pi}{k_{cm}} NL \operatorname{Re}(f(k_{cm}, 0)) \quad (5.4)$$

$$\ln \frac{A(L)}{A(0)} = -\frac{2\pi}{k_{cm}} NL \cdot \operatorname{Im}(f(k_{cm}, 0)) \quad (5.5)$$

If we assume that the scattering process is described by a spherically symmetric potential the scattering amplitude can be written as a sum over angular momentum l [16,33]

$$f(k_{cm}, \theta) = \frac{1}{2ik_{cm}} \sum_{l=0}^{\infty} (2l+1)(e^{2i\delta_l} - 1)P_l(\cos\theta) \quad (5.6)$$

where δ_l is a phase shift for angular momentum l and $P_l(\cos\theta)$ are Legendre polynomials. In case of forward scattering, $\theta = 0$, $P_l(\cos\theta) = 1$ the separation of equation 5.6 in to real and imaginary parts leads to

$$\operatorname{Re}(f(k_{cm}, 0)) = \frac{1}{2k_{cm}} \sum_{l=0}^{\infty} (2l+1) \sin 2\delta_l \quad (5.7)$$

$$\operatorname{Im}(f(k_{cm}, 0)) = \frac{1}{k_{cm}} \sum_{l=0}^{\infty} (2l+1) \sin^2 \delta_l \quad (5.8)$$

Because of the velocity spread within the molecular beam we have to average over all wave vectors k_{cm} to calculate the index of refraction for the defined wave vector k_0

$$n(k_0) - 1 = \frac{2\pi N}{k_0} \left\langle \frac{f(k_{cm}, 0)}{k_{cm}} \right\rangle \quad (5.9)$$

The implementation of the index of refraction to the Ramsey-Bordé setup of the molecular matter wave interferometer can be easily illustrated by Figure 5.1. The splitted molecular wave packets in the dark zone D are in different quantum states and the indexes of refraction for excited and ground states are n_2 and n_1 .

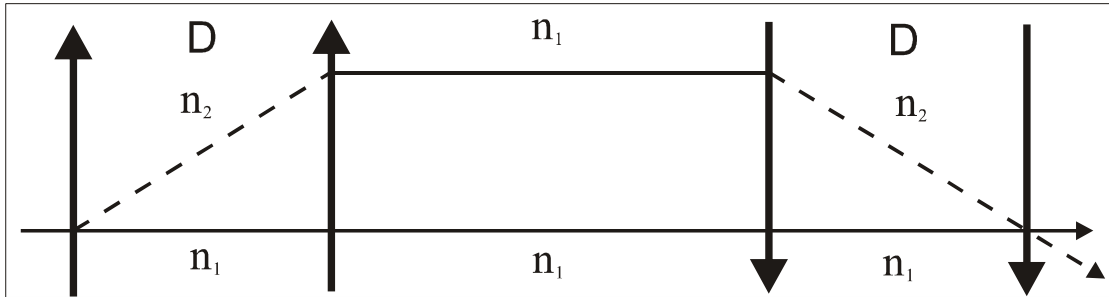


Figure 5.1 Indexes of refraction for the Ramsey-Bordé setup

Thus we can calculate the displacement between the partial matter waves the same way as it was done in eq. 2.4 but with presence of scattering medium. For the Ramsey-Bordé setup the two matter waves in the ground and excited states have momenta

$$\begin{aligned} p_x^g &= \hbar k_0 \\ p_x^e &= \hbar k_0 + \hbar \frac{m}{p_x^g} (\Delta - \delta) \end{aligned} \quad (5.10)$$

where k_0 is the wave vector of the incoming molecule matter wave. Than in each dark zone D we get

$$\begin{aligned} k_1 &= n_1 k_0 \\ k_2 &= n_2 k_0 + n_2 \frac{m}{p_x^g} (\Delta - \delta) \end{aligned} \quad (5.11)$$

The phase difference between two arms of the matter wave interferometer will be in this case

$$\Delta\phi = 2D \operatorname{Re}(k_1 - k_2) = 2k_0 D \cdot \operatorname{Re}\left(n_1 - n_2 + \frac{1}{k_0 v_x} n_2 (\Delta - \delta)\right) \quad (5.12)$$

As one can see in equation (5.12) the term $\operatorname{Re}(n_1 - n_2)$ determines the shift of the observed interference patterns while the factor n_2 in $\operatorname{Re}\left(\frac{1}{k v_x} n_2 (\Delta - \delta)\right)$, where $v_x = \frac{p_x^g}{m}$, produces a change of the period of the fringe structure as a function of detuning. It is also clear that the middle dark zone gives no contribution to the phase difference of the interferometer arms.

The direct connection between the observed phase shift and laser detuning can be derived from eq. (5.12) for two different physical situations, with and without presents of the scattering medium. As shown in Figure 5.1 in case of

no scattering medium: $n_1 = n_2 = 1$

with scattering medium: $n_1 \neq n_2$ and both unequal 1.

We get

$$\begin{aligned} \Delta\phi_{no} &= \operatorname{Re}\left(2Dk_0\left(\frac{1}{kv_x}(\Delta_0 - \delta)\right)\right) \\ \Delta\phi_{with} &= \operatorname{Re}\left(2Dk_0\left(n_1 - n_2 + \frac{n_2}{kv_x}(\Delta_s - \delta)\right)\right) \end{aligned} \quad (5.13)$$

where Δ_S and Δ_0 are laser detunings with and without presents of the scattering media. Thus the shift of a node ($\Delta\phi_{fix} = \pi/2$) on the detuning scale or for each desired position $\Delta\phi_{fix}$, which can be observed in experiment, gives

$$\Delta_S - \Delta_0 = \text{Re} \left(\frac{kv_x}{n_2} \left(n_2 - n_1 + \frac{\Delta\phi_{fix}}{2Dk_0} (1 - n_2) \right) \right) \quad (5.14)$$

The value of $\text{Re}(n_2 - 1)$ was estimated to be in the order of 10^{-10} for Na and K under experimental conditions described in [29,35] so we get the simplified formula for the difference of laser detunings

$$\Delta_S - \Delta_0 \approx kv_x \text{Re}(n_2 - n_1) \quad (5.15)$$

and with this well justified approximation the difference in phase shift for the conditions with and without scattering medium is

$$\delta\phi = \Delta\phi_{no} - \Delta\phi_{with} = 2Dk_0 \text{Re}(n_2 - n_1) \quad (5.16)$$

This is the quantity used for presenting the experimental results in the following figures.

Looking on eq. (5.15) one can directly see that the difference depends on the change of index of refraction for different arms of the matter wave interferometer. If we now assume that our interferometer has a precision of 100 kHz in the detuning a change of $\text{Re}(n_2 - n_1)$ in the order of 10^{-10} should be detectable, which is corresponding for $N = 10^{13} \text{ cm}^{-3}$ and $k_0 \approx 10^{10} \text{ cm}^{-1}$ to a difference in the cross section in the order of 10^{-13} cm^2 .

5.2. Switching atomic density inside supersonic potassium beam

Cold collisions between potassium atoms and molecules are an intrinsic feature of the supersonic molecular beam and thus phase shifts of the interferometric signals are expected for our matter wave interferometer. This effect is proportional to the particle density within the potassium beam and estimated to be quite small but should be observable due to high sensitivity of our matter wave interferometer, which will be discussed later. Since the interferometer is only sensitive to relative changes we have to vary collisional properties to observe cold collisions. The possible parameters to

manipulate could be the collisional cross section and the density of the colliding particles [eq. 5.2 and 5.3].

5.2.1. Potassium supersonic beam

We want to change the density of the colliding particles, and we will first consider experimental conditions of the potassium beam. For the supersonic jet out of a heated oven we use metallic potassium with natural abundance of the three isotopes ^{39}K , ^{40}K and ^{41}K with ratios 93.3%, 0.01% and 6.7%, respectively. The total molecular fraction of the beam is only few percent and consists mainly of $^{39}\text{K}_2$ and $^{39}\text{K}^{41}\text{K}$ dimers.

In order to detect collisions between potassium atoms and molecular dimers we want to manipulate the density of ^{39}K since it gives the main contribution to the collisional process and allows density switching of atoms up to a factor of 10. The variation of the density is obtained by deflecting most atoms out of the supersonic beam applying resonant laser light and we use this experimental situation as reference called “collision free” with $n = 1$.

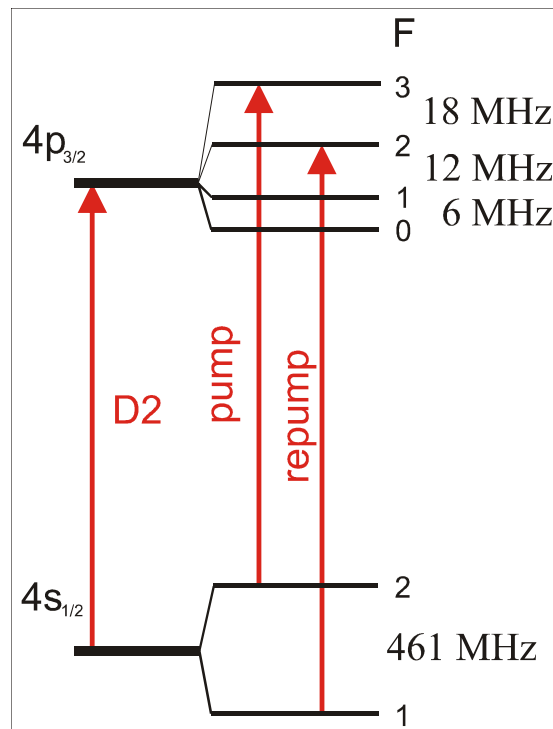


Figure 5.2 level diagram of ^{39}K D2 line

The level diagram of ^{39}K for the D2 line is shown in Figure 5.2. To deflect ^{39}K atoms as it was discussed in section 3.3.1 we use a Ti-Sa laser to produce two laser beams: pump and repump. The hyperfine splitting of the upper and lower levels are relatively small so the repump laser frequency can be easily obtained by a double path of the pump beam through an AOM operated at $\frac{1}{2} (461 - 18) \text{ MHz} = 221.5 \text{ MHz}$.

5.2.2. Experimental arrangement of the optical setup

The experimental setup for the investigation of cold collisions between potassium atoms and molecules is illustrated in Figure 5.3. The frequency stabilized a Ti-Sa laser system is split in two laser beams for pumping on the cycling transition $4S_{1/2} F = 2 \rightarrow 4P_{3/2} F = 3$ and repumping on the $4S_{1/2} F = 1 \rightarrow 4P_{3/2} F = 2$ transition. These two laser beams are mixed on the polarizing beam splitter BS and guided into the vacuum chamber.

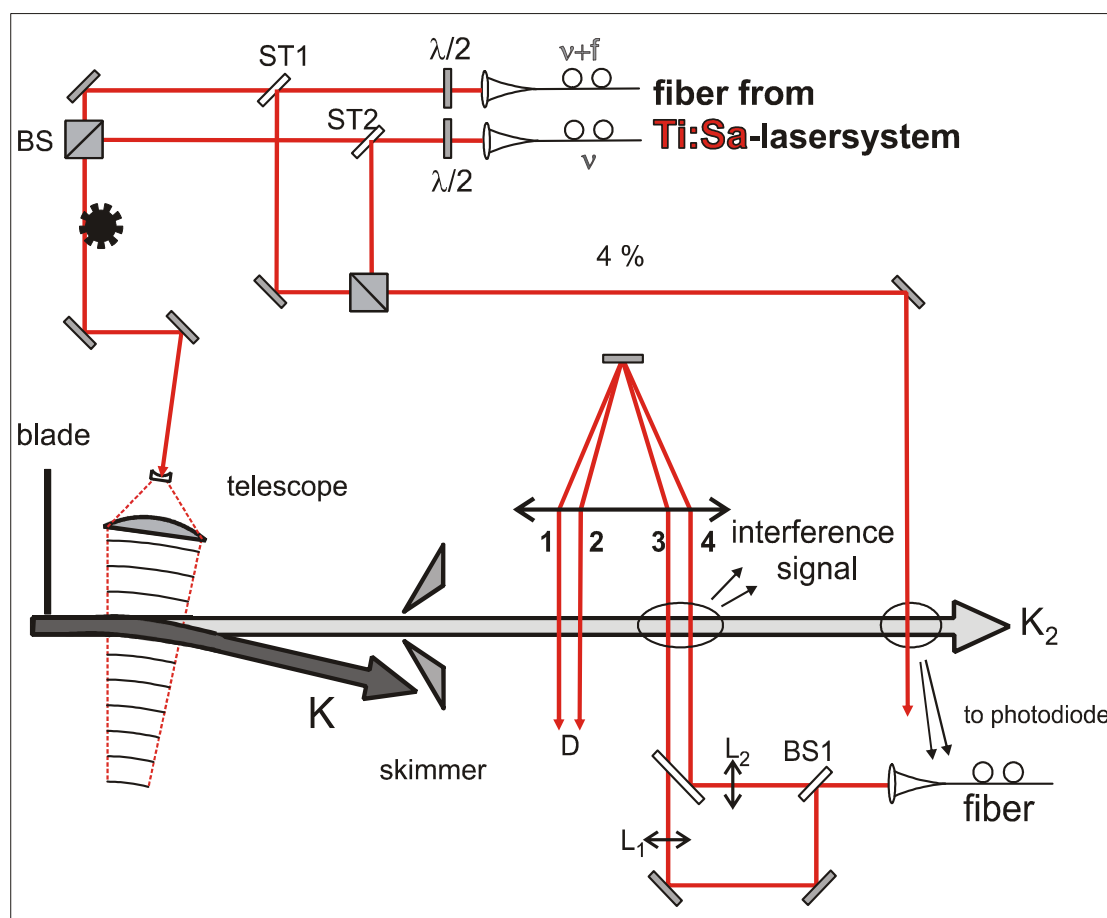


Figure 5.3 The optical setup for the collisional experiment

With the cylindrical telescope we can adjust the wave fronts of the laser radiation to follow the trajectories of the deflecting particles [32] in order to reach the best deflecting efficiency. The position of the deflection laser is about 40 cm upstream from the interferometer and deflected atoms are stopped by a skimmer separating the interferometer vacuum chamber from the intermediate one. The blade placed before the deflection zone prevents from deflecting a fraction of the divergent beam into the interferometer chamber through the skimmer.

About 4% of the mixed two frequency radiation (pump/repump) is split for online probing of the quality of the atomic density switching. The checking is placed after the region of the molecular matter wave interferometer and should not influence its detection system.

The typical powers of the pump and repump beams were 75 mW and 11 mW, respectively. The high long term stability of the frequency of the Ti-Sa laser was obtained by using He-Ne stabilization setup (see section 3.3.3) and allowed us to operate the complete system without readjustment for a full measuring day. Regularly more than 90% of ^{39}K atoms are deflected out of the supersonic beam, which means a change in density by the factor of ten.

5.2.3. Sequence of the experiment

To observe cold atom-molecule collisions we conduct measurements in the sequence illustrated in Figure 5.4. The interferometer laser was adjusted to be resonant to R(25) line of the $27 - 0$ band of $b^3\Pi_u(0^+) \leftarrow X^1\Sigma_g^+$ and was scanning over two hyperfine components highest in frequency. The intensity of the deflection laser was switched on and off by a mechanical chopper. The switching time of the chopper is 0.3 s and negligible compare to the time needed for one scan (~ 2 min). Each on/off interval contains a full interferometer scan.

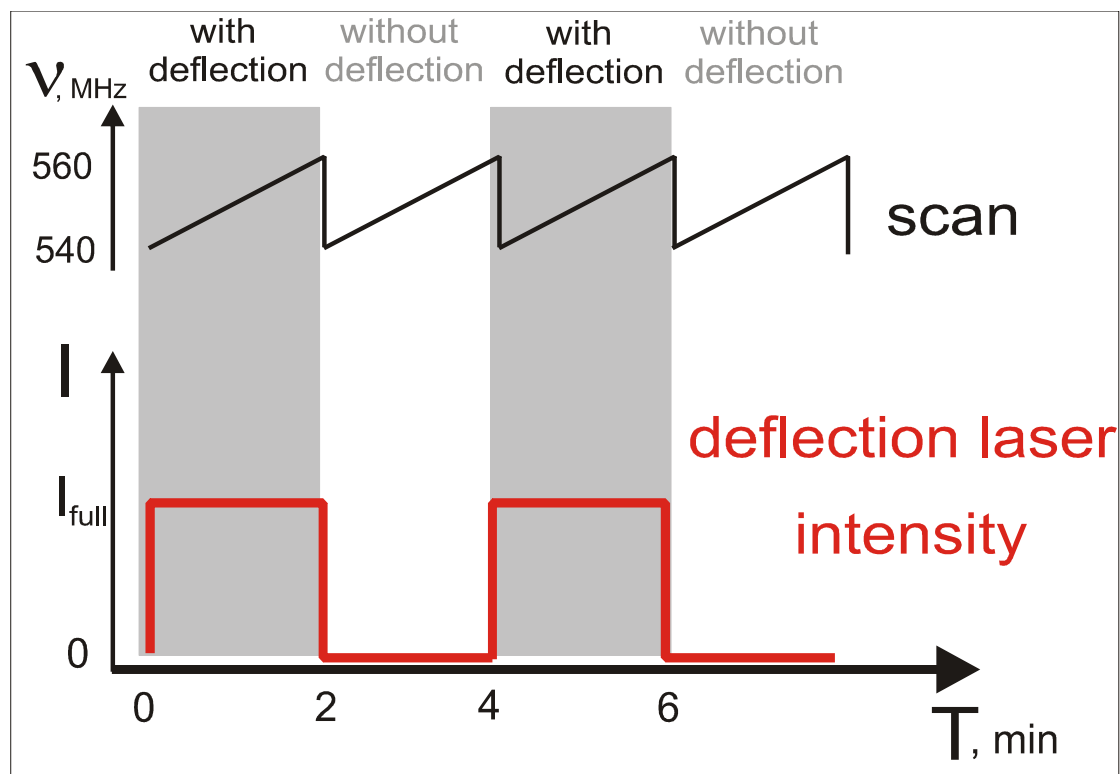


Figure 5.4 Sequence of the experiment to observe atom-molecule collisions in the potassium beam

The recorded scans corresponding to the different physical situations with and without presence of ^{39}K density in the supersonic beam are averaged independently. Typically about 30 scans for each different situation were taken and averaged to improve signal-to-noise ratio.

5.3. Low energy collisions examined by matter wave interferometry method

The derived phase shifts from measurements with switched off/on ^{39}K atomic density in the supersonic beam are presented in Figure 5.5. The recordings were done using the Ramsey-Bordé molecular matter wave interferometer with the dark zone length $D = 400 \mu\text{m}$ and the efficiency of the deflection of the ^{39}K atoms was between 85% and 95%.

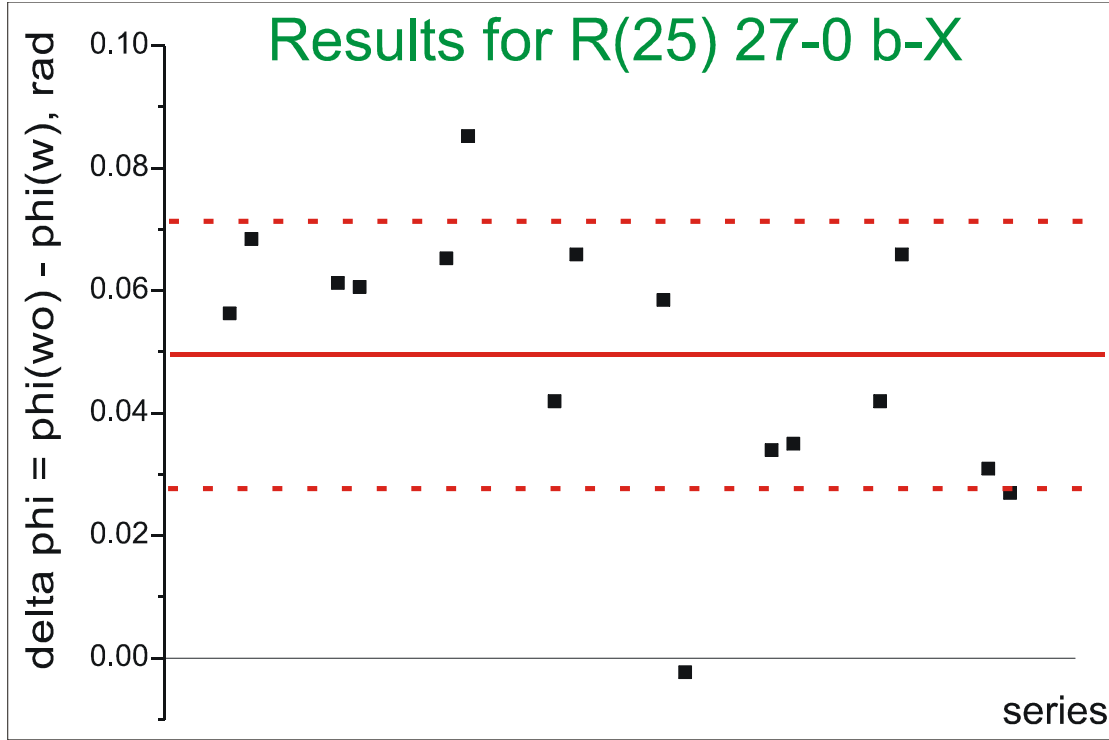


Figure 5.5 Observed phase difference between ^{39}K atoms present and deflected for the R(25) 27-0 b-X line measured for the dark zone length $D=400\ \mu\text{m}$ by the Ramsey-Bordé setup

All measurements in Figure 5.5 are divided into 8 pairs and were done on different days roughly within one year. Each pair of points corresponds to one measurement day and assumed to be an absolutely independent experimental result because the whole interferometer setup was readjusted since the last measurement event.

The grouping of the measurements of the phase difference in Figure 5.5 into the pairs is a result of fitting the averaged interference structure with formula (4.2)

$$I(\nu) = U + A \cdot \exp\left(\frac{(\nu - \nu_0)^2}{\nu_w^2}\right) \cdot \cos(2\pi P(\nu - \nu_0) + \varphi)$$

which we implement to define the phase of the observed interference patterns. In the beginning the recordings of the two classes of scans corresponding to physical situations with switched on and off atomic density are averaged independently. Typically per one measurement day we got about 30 scans for each scan class within 2 hours. The particle flux out of the potassium oven during a recording day is quite stable and the possible changes between different measurement days are less than 5%. This allows us to rescale all obtained experimental points in Figure 5.5 according only to quality of the atomic deflection and thus the density of atoms. The data in Figure 5.5 are rescaled to the deflection efficiency of 90 %.

As a first step of the fitting all parameters in formula (4.2) were released and fitted to determine the central frequency ν_0 , width of the Gaussian envelope ν_w , period of interference fringes P , background U , amplitude A and phase φ for only one particular class of scans (for example: class corresponding to situation with presents of atoms). Then all parameters except the amplitude A and phase φ were fixed and fitting was done for the second class of the scans. Finally, the phase difference between recordings with and without atomic density was calculated. The second point in each pair in Figure 5.5 is just the result of the same fitting strategy but starting now with the other type of scans. Using the average of each pair is equivalent to average over the fixed parameters for both types of records.

In Figure 5.5 one can see that the averaged phase difference marked by a solid line is 49.8 mrad which corresponds to the frequency shift of the molecular line $\nu_0^{wo} - \nu_0^w$ of -9.9 kHz. The standard deviation σ for the experimental points in Figure 5.5 counted as independent measurements is ± 21.5 mrad and is indicated by dashed lines.

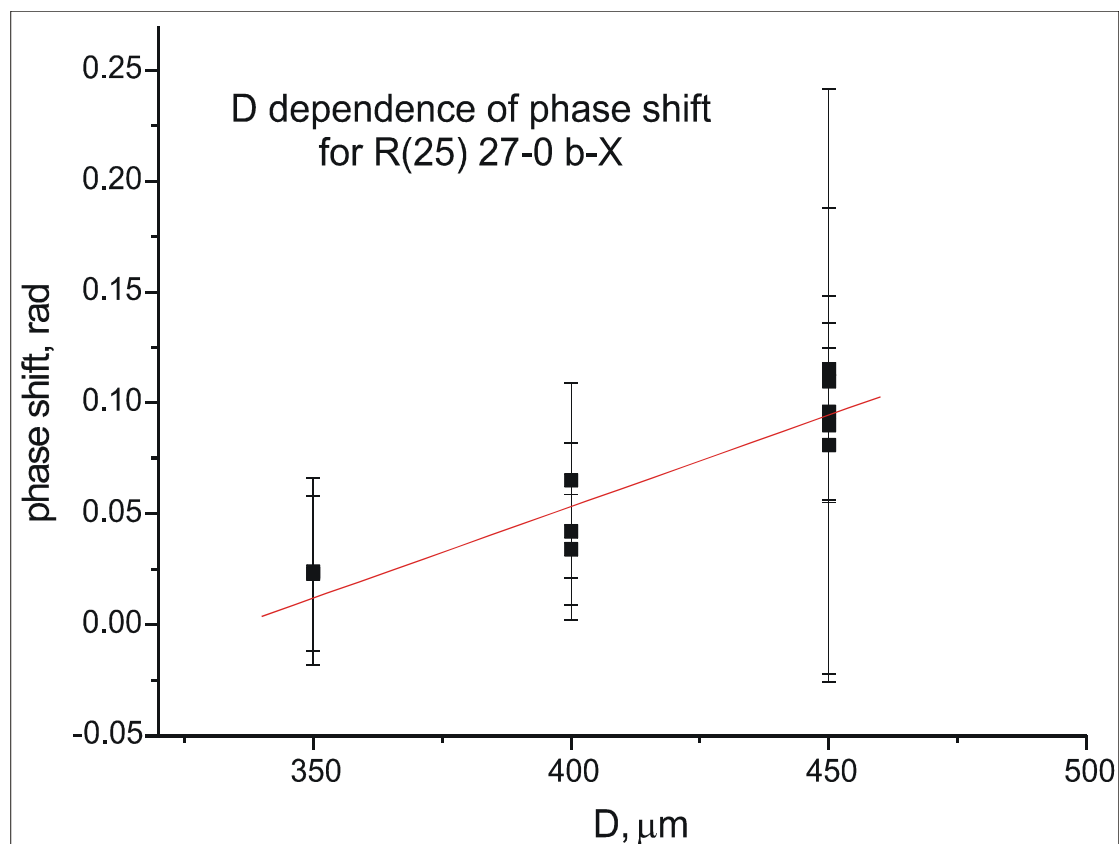


Figure 5.6 Dependence of the difference in the phase for the atomic density switched off/on as a function of the dark zone D observed for R(25) 27-0 b-X line by the Ramsey-Bordé setup

Figure 5.6 illustrates the dependence of the phase shift as a function of the dark zone D observed for R(25) 27-0 b-X line. The three examples chosen were measured several times which is indicated by multiple error bars, resulting from averaging for each measurement day. In total, 2 mean values of the recording pairs for $D = 350 \mu\text{m}$, 3 for $D = 400 \mu\text{m}$ and 5 for $D = 450 \mu\text{m}$ were taken. The solid line in Figure 5.6 is a fit of the experimental points to a linear function. By increasing the length D of the dark zone we increase the phase difference $\delta\phi$ between the molecular matter waves in different quantum states according to eq. (5.16). Figure 5.6 shows that the values of the observed phase shift increase as a function of the dark zone D .

From the fit one can learn more about the “real” length D' of our dark zone. By extrapolating the fitted solid line to its crossing with level $\delta\phi = 0$ we can say that the “real” length of the dark zone was $D' = D - 320 \mu\text{m}$ in our measurement. This effective shortening will probably come from the finite width of the laser beams used as the beam splitters. This width is about $150 \mu\text{m}$ and thus not negligible compared to the geometrical D .

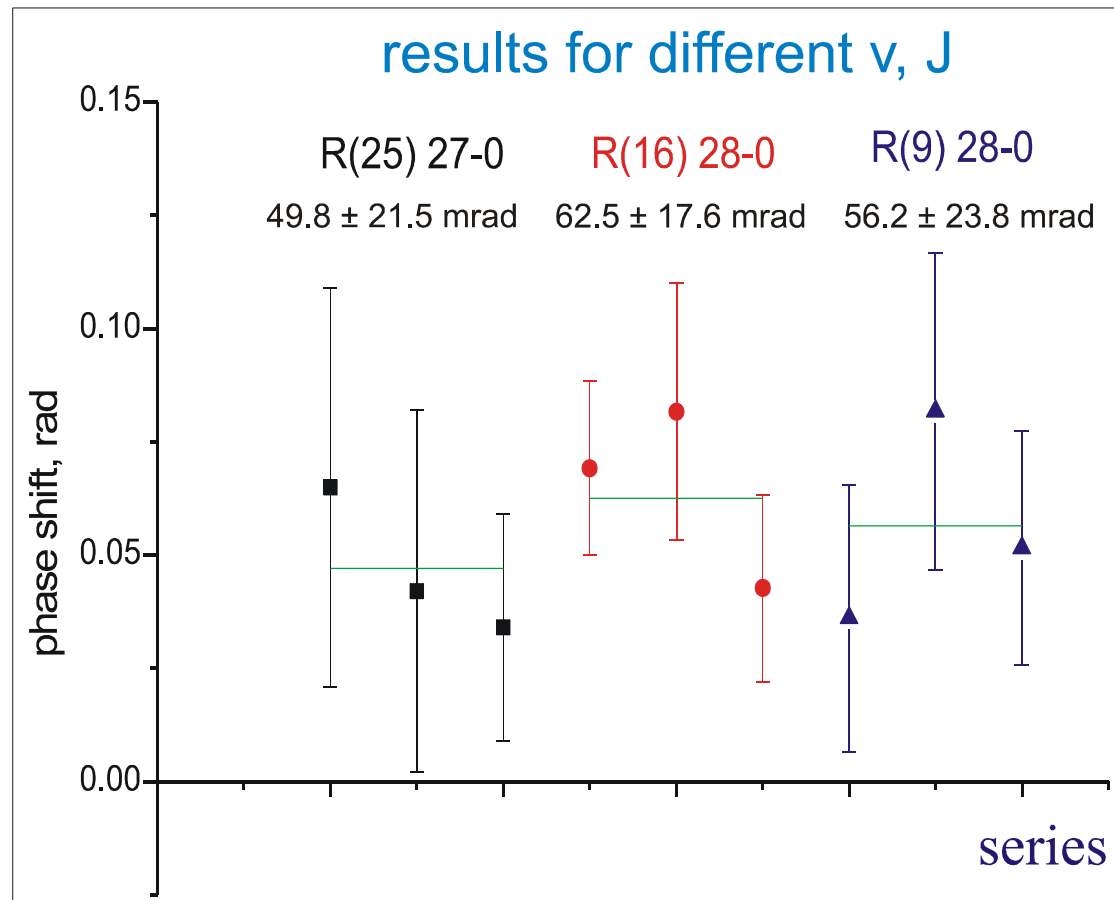


Figure 5.7 Observed phase difference between ^{39}K atoms present and deflected for several lines in the $b \ ^3\Pi_u(0^+) \leftarrow X \ ^1\Sigma_g^+$ system of K_2 measured for the dark zone length $D=400 \mu\text{m}$

Figure 5.7 shows the obtained phase shift for some other molecular lines with different v and J quantum numbers. The goal was a systematic study of the phase shift of molecular interferences for a typical set of quantum states but our choice was restricted by the frequency tuning range of the interferometer laser system. The experimental conditions for the result illustrated in Figure 5.7 are the same as for the measurements on the R(25) 27-0 b-X molecular line.

The obtained values of the phase shift for molecular lines with vibrational quantum numbers $v=27$ or $v=28$ and rotational quantum numbers J between 9 and 25 have the same value within error limits and same sign thus do not show any dependence on v or J .

5.4. Stability and precision of the interferometric measurements

The obtained results of the study of cold collisions in the potassium beam with the molecular interferometer raise the question of how reliable in general the interferometric measurements are. To answer this question we have to check the phase stability of our molecular matter wave interferometer which is directly connected with the precision of the interferometer comparing results over longer periods.

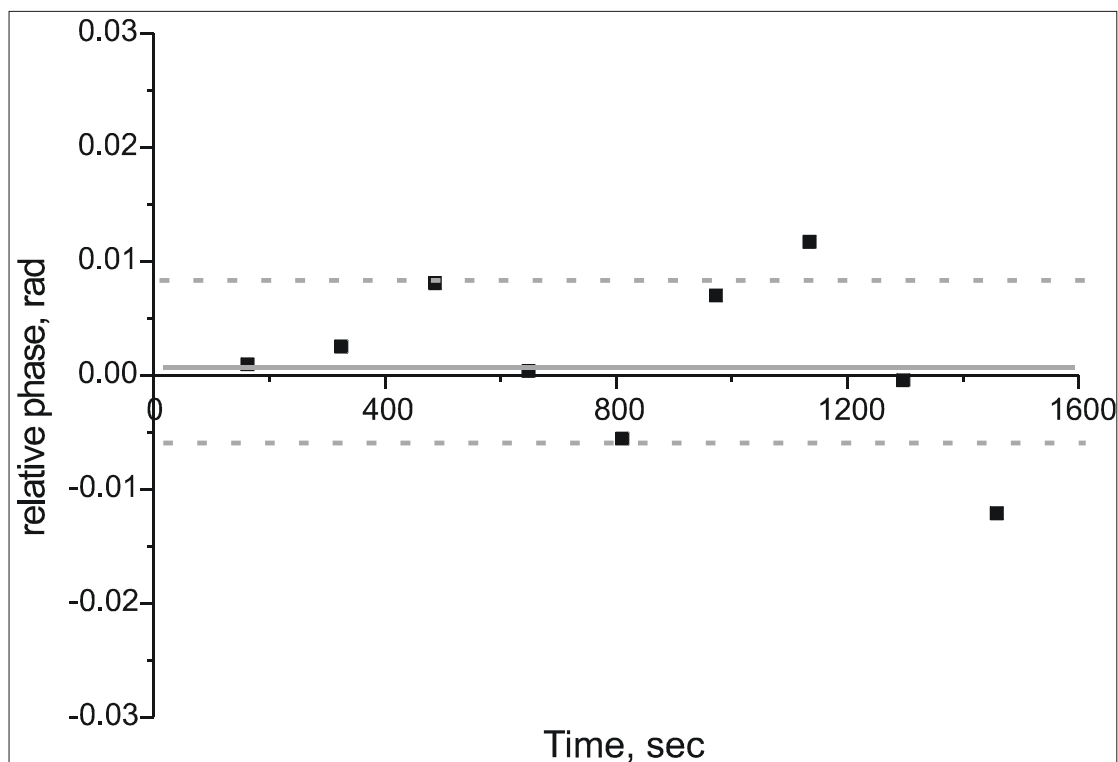


Figure 5.8 “Zero” measurement for the Ramsey-Bordé setup operated on the R(25) 27-0 b-X line with the dark zone length $D=400\ \mu\text{m}$.

To investigate the stability of our molecular Ramsey-Bordé interferometer we performed so called “zero” measurement for relative phase of the recorded fringes. We used the typical experimental sequence of the collisional measurement but with a different procedure of data evaluation. The evaluation was applied to only one class of scans with K atoms present in the beam and instead of averaging all scans we treated each scan of experimental sequence independently. The results of the “zero” measurement is shown in Figure 5.8. The relative phases of interferences were analyzed and plotted as independently measured on the time axis at each end of the scan. One can see that the stability of the molecular matter wave interferometer within half an hour and the standard deviation of the relative phase marked in Figure 5.8 as dashed line is $\pm 7\ \text{mrad}$ with mean value of $1\ \text{mrad}$. Thus, this stability is about a third of the standard deviation of the measured phase shifts. If only such phase fluctuations would play the role in the final results of Figure 5.5 and Figure 5.7 than the factor $\sqrt{2}$ would be expected. Unidentified fluctuations like atomic densities or laser pointing etc. should be considered.

6. Absolute frequency measurements of molecular transitions for matter wave interferometer

Here we present another way to observe cold atom-molecule collisions in the potassium supersonic beam. Instead of observing the change of the phase and contrast of the molecular matter wave interferences caused by interaction with the atomic medium we will measure directly the pressure shift of the resonance transition in the same experimental conditions as described in section 5.1. For this we perform absolute frequency measurements of the molecular transitions with and without the presence of the scattering medium.

6.1. Optical setup for the measurements with the frequency comb

The laser system for the spectroscopy of the molecular lines is based on highly stabilized extended cavity diode lasers (ECDL) used for matter wave interferometry. Figure 6.1 shows the schematic setup. Compared to the setup implemented for interferometry the output power of the ECDL (818 nm) is amplified only by one slave laser diode 1. It serves as a stabilized laser source for the spectroscopy. It has a bandwidth of about 30 kHz and its long term drift is less than 300 Hz/min.

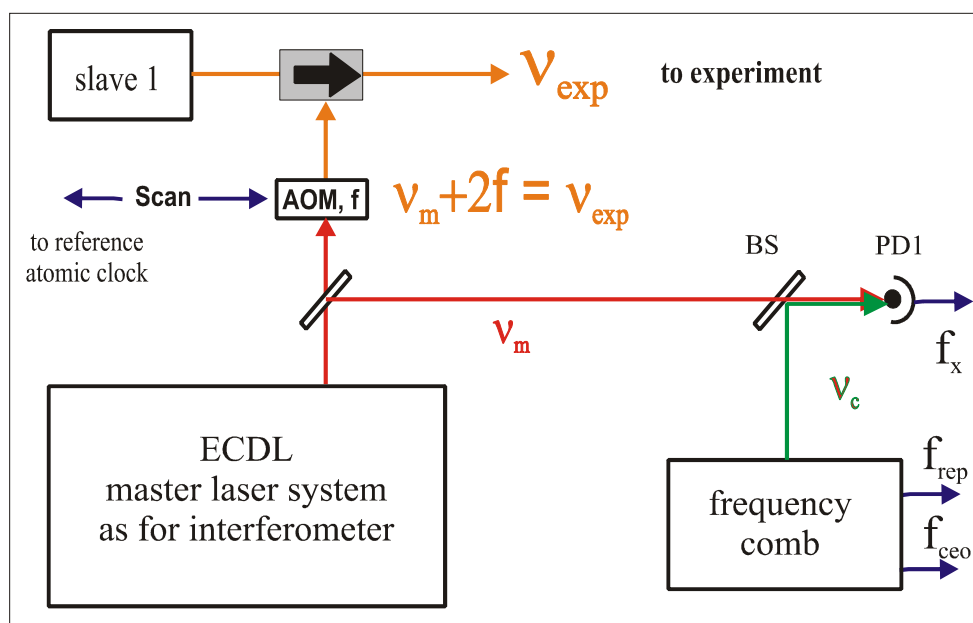


Figure 6.1 Scheme of the laser stabilization of the laser used for spectroscopy

A fraction of the laser intensity is guided in a double pass setup through an acousto-optical modulator (AOM). The frequency shifted laser field ν_{exp} is then used for the injection lock of the diode laser called slave 1. Frequency tuning of the slave 1 for spectroscopic purposes is obtained by tuning the RF frequency f of the synthesizer driving the AOM. The frequency of the synthesizer is phase locked to an atomic Cs clock. Another fraction (about 3 mW) of the output of ECDL is guided to the photo diode PD, where it is superimposed with the output spectrum of the self referencing frequency comb for obtaining the beat frequency f_x . The atomic Cs clock and Ti-Sa frequency comb as well as operation of them were provided by our coworker from Physikalisch - Technische Bundesanstalt (PTB) Harald Schnatz for what I am very thankful.

6.2. Frequency measurements with femtosecond comb

The basic function of a frequency comb is described in [55] and will not be detailed here. The repetition rate f_{rep} is phase locked to a commercial Cs clock, which provides also the reference frequency for all other rf-oscillators involved in the frequency measurements. The principal scheme for the frequency measurement is shown in Figure 6.2.

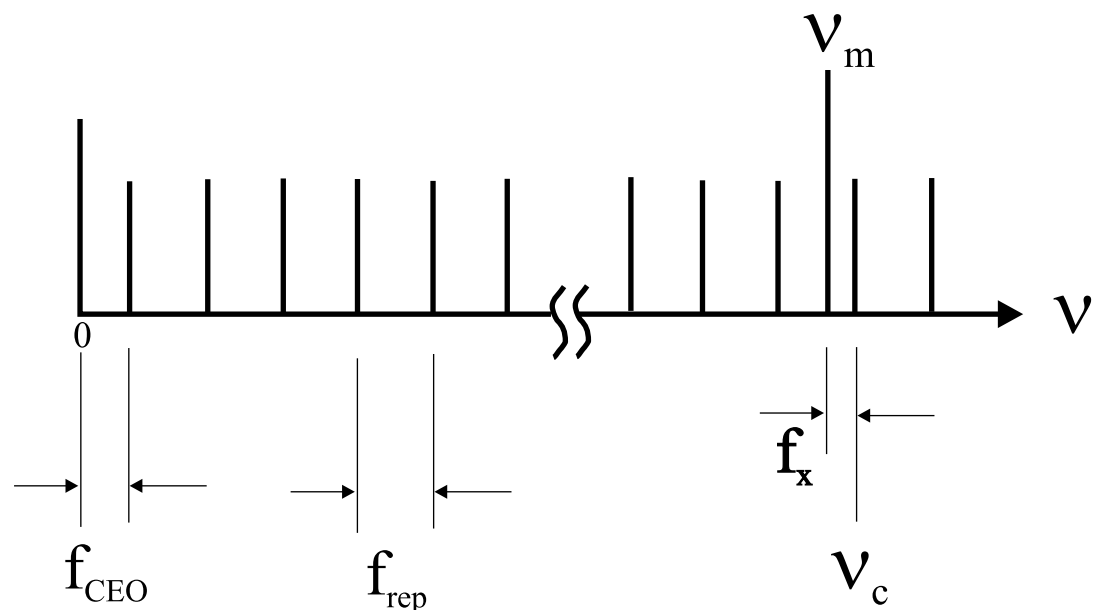


Figure 6.2 Frequency scheme for determination of absolute frequencies with the frequency comb

The carrier offset frequency f_{CEO} is chosen positive by proper choice of the comb tooth with number m , and f_x was chosen such that the nearest comb frequency ν_c is slightly above the unknown optical frequency ν_m , which is calculated from the following equation:

$$\nu_m = f_{CEO} + m \cdot f_{rep} - f_x \quad (6.1)$$

where the definitions of the frequencies are given in Figure 6.2 and m is the integer order of the comb tooth with frequency ν_m . For getting this choice one has to have a preset of frequency of ν_m at least a precision within half of f_{rep} . As f_{rep} is around 700 MHz, m could be determined uniquely by a measurement of the molecular transition frequency with a commercial wavemeter, which is calibrated to an absolute accuracy of ± 100 MHz (High Finesse WS7). The carrier-envelope-offset frequency f_{CEO} was not stabilized but counted with the help of a tracking oscillator. The laboratory conditions caused a continuous drift of the f_{CEO} which would limit the time of continuous measurement due to unlocking of the tracking oscillator. In the chosen configuration this results for a fixed f_{rep} to a drift of f_x by the same amount and direction. For better long term behavior we therefore mixed f_{CEO} and f_x and the difference frequency f_{dif} is phase locked to a tracking oscillator and then counted. The frequency ν_{exp} of the slave laser then simplifies to

$$\nu_{exp} = \nu_m + 2f_{AOM} = m \cdot f_{rep} + f_{dif} + 2f_{AOM} \quad (6.2)$$

with the frequency of the AOM f_{AOM} . While recording the molecular beam spectra f_{dif} and f_{rep} were recorded continuously and used later on for determination of the masters absolute frequency ν_m .

During the measurements the master laser frequency was stabilized to an external cavity and measured with the comb, while the RF synthesizer for the slave laser was tuned across a molecular line. For the spectroscopic measurements we use the Lamb-dip method and typical recordings are already given in Figure 4.3. Usually a power of 3 mW was applied in a laser beam with about 2 mm diameter. As was already discussed in section 4.1.2, lines of the $b^3\Pi_u(0^+) \leftarrow X^1\Sigma_g^+$ system of K_2 display magnetic hyperfine structure. The number of hyperfine components depends due to the Pauli principle on the rotational quantum number for the ground state J'' .

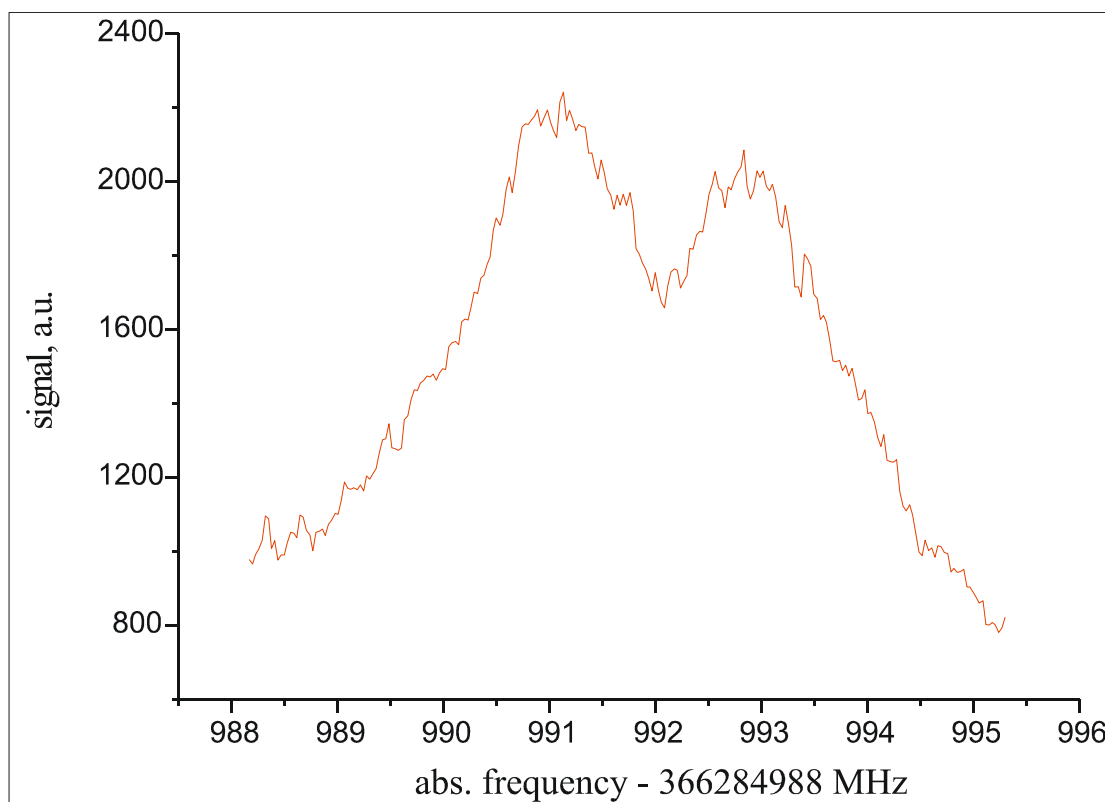


Figure 6.3 Spectrum of the highest frequency hyperfine component of the R(24) (27-0) line of $b \ ^3\Pi_u(0^+) \leftarrow X \ ^1\Sigma_g^+$ of K_2 . The Lamb dip in the line centre has a width of about 500 kHz due to natural linewidth and time of flight broadening.

For the frequency measurements we concentrated on the hyperfine component with the highest frequency. The slave laser was tuned across an interval of about 10 MHz around the line center, in order to include also parts of the background. In Figure 6.3 an example of such record is given. The central Lamb dip has a line width of about 500 kHz. Spectra were recorded tuning the laser frequency up and then down again to the starting frequency in order to have always two spectra with opposite shifts due to time constants of the detection system. Up to 30 samples of such frequency up/down pairs of spectra were collected, periodically changing the experiment from atoms present in the particle beam for one sample to the case that atoms are deflected from the beam for the next sample. Several such measurements were collected for the R(24) and R(25) lines of the $(v'-v'')=(27-0)$ band of the $b \ ^3\Pi_u(0^+) \leftarrow X \ ^1\Sigma_g^+$ on one experimental day.

The fitting of the scans up and down in frequency shows a difference in the position of central picks between these two classes of about 100 kHz. It was removed by simply averaging between the up and down scans. The recording of molecular

lines requires usage of the high sensitivity setting of the picoammeter thus large time constants what could be the reason for such frequency shift between different scan directions.

6.3. Results of the absolute frequency and relative measurement

Table 6.1 illustrates results of absolute frequency measurements done within one day. We concentrated on only two molecular lines from the band 27-0 of the $^3\Pi_u(0^+) \leftarrow X^1\Sigma_g^+$ system with odd and even quantum numbers J (R(24) and R(25)) since they are typically used for molecular matter wave interferometry.

Molecular line	Absolute frequency, MHz				Standard deviation, MHz	
	with atoms	N of scans	without atoms	N of scans	with atoms	without atoms
R(24) 27-0	366287448.092	14			0.0120	
R(24) 27-0	366287448.092	10			0.0051	
R(24) 27-0	366287448.100	28	366287448.098	28	0.0140	0.0101
R(24) 27-0	366287448.085	24	366287448.085	24	0.0086	0.0108
R(25) 27-0	366284992.039	10			0.0109	
R(25) 27-0	366284992.054	10			0.0115	
R(25) 27-0	366284992.026	6			0.0347	
R(25) 27-0	366284992.036	6			0.0051	
R(25) 27-0	366284992.035	10	366284992.031	10	0.0132	0.0133
R(25) 27-0	366284992.039	6	366284992.050	6	0.0197	0.0139
R(25) 27-0	366284992.039	30	366284992.040	30	0.0113	0.0110

Table 6.1 Results of absolute frequency measurements done for two molecular lines on one day

The results of the relative frequency measurements of the molecular lines for atomic density switched on/off in the experimental configuration described in section 5 are presented two columns. The quality of deflecting ^{39}K atoms out of supersonic beam was better than 80% what is giving us reduction in density by the factor of 5. It

allows us to estimate the expected pressure shift for the particle density in the potassium beam of about 10^{13} cm^{-3} to be about 5 kHz applying the results of the interferometer. In Table 6.1 one sees that the scatter of the measured shifts between the line frequencies with and without ^{39}K atoms is from +11 to -4 kHz and within the error bars which will be discussed below. Some large fluctuations in the value of the scatter for the results of the absolute frequency measurements shown in Table 6.1 are caused by a poor number of averaged scans.

6.4. Uncertainty budget for the absolute frequency measurements of molecular transitions

The precision of the described frequency measurements is limited by several effects so we have to estimate their influence in the total uncertainty budget. The main uncertainty in the performed measurements is coming from the residual first order Doppler effect. For the implemented saturation setup the parallelism of the counter propagating probe and saturation beams is determined by the alignment of the retroreflector. The residual angle between the laser beams and optical axis of the retroreflector can be derived from [36]

$$\alpha_{out} = 2 \frac{\varepsilon}{f^2} r_{in} - \left(1 + 2 \frac{\varepsilon}{f} \right) \alpha_{in} \quad (6.3)$$

where α_{in} and r_{in} are angle and radial displacement from the optical axis of the incoming beam, f is focal length of the lens of the retroreflector and ε is a deviation in the position of the mirror of the retroreflector from being in the focal plane of the lens. The main contribution in the angle α_{out} is coming in our case from the incoming angle α_{in} . So for the focal length $f = 300 \text{ mm}$, $r_{in} = 15 \text{ mm}$ and $\varepsilon = \pm 0.02 \text{ mm}$ the residual angle α_{out} can be estimated to be less than 30 μrad . This gives us an uncertainty for the absolute frequency measurements better than 50 kHz.

The second order Doppler shift for the frequency measurements was quite small. For the molecular velocity in the potassium beam of $950 \pm 100 \text{ m/s}$ it is calculated to be - 2.3 kHz.

The magnetic field is shielded in the interaction region by the μ -metal box (see section 3) which allows us estimate the residual magnetic field to be less than 20 mG. Because the molecular states we measured are mainly non-magnetic ($\Omega = 0$) we can

estimate the shift of a line to be less than 1 kHz because the effective g-factor is induced by rotation and should be in the order of several nuclear magnetons.

The recoil by the absorption of the photon causes two systematic frequency shifts. The first one is affecting a line center by $E_r = \hbar\omega_r = \frac{(\hbar\omega_0)^2}{2mc^2} \approx 3.8 \text{ kHz} \times h$ (see section 2). Here ω_0 is the frequency of molecular transition, h – Planck constant and m is the total mass of K dimer. The second contribution is coming from the average velocity $v_r = \frac{\hbar(\omega_0 + \omega_r)}{mc} \approx 0.7 \cdot 10^{-2} \text{ m/s}$ gained by molecule during a cycle of absorption and reemission. According to the Franck-Condon principle, in our experiment we assume that after one excitation – spontaneous decay cycle molecules are lost for further excitation and we have in average less than one photon scattered per molecule. The laser power during frequency measurements was close to $\pi/2$ conditions and the frequency shift caused by the total recoil effect can be estimated to be smaller than 5 kHz.

Following the arguments in [56] where highly precise frequency measurements of the D lines of potassium were performed we assume that the ac-Stark effect in our frequency measurement does not give significant contribution to the uncertainty budget. The ac-Stark shift ΔE_s in our frequency measurement can be estimated from the formula [57]

$$\Delta E_s = \frac{\Omega_0^2}{\Delta E_{hf}} \quad (6.4)$$

where Ω_0 and ΔE_{hf} denote the Rabi frequency and hyperfine splitting of a molecular transition. In spite of relatively high laser intensity compared to [56] in our case we have much smaller intensities for hyperfine transitions for given rotation quantum numbers $J = 24$ and 25 . So we estimate the ac-Stark shift of the molecular lines to be less than 1.5 kHz.

Another contribution to the uncertainty budget stems from the frequency measurement itself and coming from the signal-to-noise ratio (see section 6.3). The scatter of our measurements can be estimated from Table 6.1 and was below than 12 kHz.

7. Summary and outlook

This work presents experiments with a molecular matter wave interferometer based on $^{39}\text{K}_2$ molecules in well defined quantum states. Starting with the setup described in [35] further developments and systematic characterizations of the molecular interferometer and its implementation to study low energy collisions between potassium atoms and molecules were done. As an alternative way to look for collisional effects absolute frequency measurements of the molecular transitions typically used for the interferometer were performed to derive a pressure shift within the potassium beam.

7.1. Matter wave interferometry with potassium molecules

The development of the molecular matter wave interferometer reported in this work was mainly concentrated on getting into operation the ground state exit of the interferometer and the systematic analysis of the different types of molecular matter wave interferences.

7.1.1. Detection on ground state exit of interferometer

The choice of a molecular transition as a base for the realization of the matter wave interferometer in well defined quantum state opened for us many additional possibilities. For example, compared to atoms, molecules have a higher number of internal degrees of freedom. According to the Franck-Condon principle, mostly the molecules in the excited state decay back with quite low probability to the original rovibronic level, but they will spontaneously decay to other levels. Thus by using molecules for matter wave interferometry it is much simplified to observe simultaneously two exits of molecular matter wave interferometer in ground and excited states. In our case of a matter wave interferometer realized in a supersonic beam, where we can neglect by interaction between the matter wave and the particle environment, in the vacuum chamber we can detect the ground state exit at any distance downstream the molecule beam from the laser interaction zones.

We made systematical analysis and comparison of the results obtained for two different transitions in the $B\ ^1\Pi_u \leftarrow X\ ^1\Sigma_g^+$ and $b\ ^3\Pi_u(0^+) \leftarrow X\ ^1\Sigma_g^+$ molecule systems. The fluorescence from $B\ ^1\Pi_u \leftarrow X\ ^1\Sigma_g^+$ molecular system can be easily detected by the photomultiplier implemented in our experimental setup so, in principle, transitions in the $B\ ^1\Pi_u \leftarrow X\ ^1\Sigma_g^+$ system can be used for detecting ground state exit of the molecular matter wave interferometer. But the interference patterns recorded on a transition in the $B\ ^1\Pi_u \leftarrow X\ ^1\Sigma_g^+$ system are located on a large background produced by its unresolved hyperfine structure which makes a practical application of such transitions quite complicated.

Alternatively transitions in the $b\ ^3\Pi_u(0^+) \leftarrow X\ ^1\Sigma_g^+$ molecule system are spin forbidden and relatively weak, but its large splitting between hyperfine components of excited state makes it extremely useful for detecting ground state exit of the interferometer. By setting a second photomultiplier with fluorescence collecting optics downstream the interaction region of the K_2 interferometer and exiting only one separated hyperfine component we obtained interferences with the same signal-to-noise ratio and opposite in phase relative the ones by excited state exit. The main advantages of ground state exit operated on transitions in the $b\ ^3\Pi_u(0^+) \leftarrow X\ ^1\Sigma_g^+$ molecule system compared to the excited state exit and the ground state exit on transitions of the $B\ ^1\Pi_u \leftarrow X\ ^1\Sigma_g^+$ system is to resolve easily without any additional effort [35] interference patterns of only one hyperfine component and to obtain a symmetric background on which interferences appear, and which are much easier to deal with during the data processing.

7.1.2. Observation of different types of interferences

Our matter wave interferometer with $^{39}K_2$ is, to my knowledge, unique compared to other types of molecular and atomic matter wave interferometers in the world. In our molecular matter wave interferometer one observes simultaneously and distinguishes by appropriate fitting two different types of molecular matter wave interferences: longitudinal and transversal. Due to the high collimation of the molecular beam we have quite narrow velocity distribution in transversal direction.

This leads to an enormous transversal coherence length of the matter wave packet of about 6 nm compare to de Broglie wave length for potassium molecules in the supersonic beam, which is about 5 pm in our case. So as resulting signals of our matter wave interferometer with four laser beam splitters we obtain superimposed transversal optical Ramsey and longitudinal Ramsey-Bordé interferences. We developed the procedure of the evaluation of such complicated interferometric signals and made systematic investigations and comparison of longitudinal and transversal types of molecular matter wave interferences.

In our Ramsey-Bordé interferometer setup the longitudinal interferences are produced by all four laser beam splitters while the transversal ones are the result of interaction with only one pair copropagating laser beams. Thus the period of the transversal optical Ramsey interferences is exactly two times the period of the longitudinal Ramsey-Bordé interferences. Thus the interference structure looks like the time dependence of two beating frequencies with a frequency ratio of 1 : 2.

Because of the difference in origin of these two types of matter wave interferometers their phase stability is also quite different. The longitudinal Ramsey-Bordé interferences obtained by interaction of molecules with two counter propagating pairs of laser beams where one of these pairs is produced by the retroreflector are less sensitive to phase fluctuation of partial laser beams due to cancellation compared to the transversal optical Ramsey interferences. The phase stability of the Ramsey-Bordé interferences obtained in the experiment was ± 7 mrad in half an hour while the phase of the optical Ramsey interferences could have deviations in the same time interval more than $\pi/2$ rad.

7.2. Collisional experiments with molecular matter wave interferometer and absolute frequency measurements

We implemented the $^{39}\text{K}_2$ matter wave interferometer to study cold atom-molecular collisions within supersonic potassium beam. The frequency stabilized Ti-Sa laser system was developed and implemented to switch the density of ^{39}K atoms, which gives the main contribution to the particle density in the potassium beam. The frequency of the Ti-Sa laser was set resonant to the ^{39}K atomic cycling transition which allows us to deflect between 85% and 95% of ^{39}K atoms out of the potassium

beam corresponding to a density change of factor 10. By comparing the phases of the interferograms with switched on/off atomic density we observed the phase shift $\delta\phi$ due to atom-molecule collisions of 50 ± 21 mrad on interferometric transition R(25) $27-0 \ b \ ^3\Pi_u(0^+) \leftarrow X \ ^1\Sigma_g^+$, corresponding to a pressure shift of -9.9 ± 4.2 kHz for atom's particle density in the potassium beam of about 10^{13} cm⁻³.

The measurements of the value of $\delta\phi$ for different length of the dark zone D shows clear the linear dependence expected from theory [1]. We also measured the value of the phase shift due to atom-molecular collisions for different molecular states in order observe the dependence on v and/or J molecular quantum numbers. By varying the rotation quantum number J between 9 and 25 and vibration v of 27 and 28 we obtained the same absolute values within the limits of the experimental error bars and sign of the phase shift.

In general, there is another way how to observe cold atom-molecule collisions in a potassium supersonic beam [59]. Instead of observing the change of the phase and contrast of the molecular matter wave interferences caused by interaction with the atomic medium we measured directly the pressure shift of the resonance molecular transition under same experimental conditions as for interferometric measurements. We used Ti-Sa frequency comb kindly provided by Physikalisch - Technische Bundesanstalt to observe differences of absolute transition frequencies between the physical situations with switched on and off atomic density of ³⁹K. The pressure shifts obtained for changing the particle density in the potassium beam by a factor of 5 were from +11 to -4 kHz which is in the order of the precision of the frequency comb measurement (10 kHz) and much smaller than its absolute accuracy (65 kHz). So we have not observed a contradiction between interferometric and direct absolute frequency measurements.

It is also worth while to mention the quality of the key component in our experimental setup for the interferometric measurements as well as for absolute frequency measurements of molecular transitions, which has direct influence on the precision of the measurements, - the interferometer laser system. By developing and improving the frequency stabilized diode laser system we achieved a reliable radiation source for interferometric and absolute frequency measurements with linewidth of 30 kHz and long term frequency drift better than 260 Hz per min.

The precision of the interferometric measurements in present experimental conditions was about 5 kHz, while the precision of the relative frequency measurements with the frequency comb was about 10 kHz and the main contribution to the uncertainty budget was coming from signal-to-noise ratio. This could be a one possible reason why we have not seen clearly the pressure shift due to atom-molecule collisions. We could, in principle, reach the precision of 1 kHz for the relative frequency measurements with the frequency comb but for this we have to make recording over 100 times longer time period, which is impossible with present long term stability of the laser system. Another reason of the disagreement in results obtained by the interferometer and the frequency comb could be a difference in the deflection quality (90% for interferometric compare to 80% for frequency comb measurements).

7.3. Outlook

The construction of our matter wave interferometer based on the potassium dimers where we can observe simultaneously longitudinal and transversal spatial interferences on both ground and excited state exits opens large variety of possible applications to study weak interactions of molecules with its environment. The interferometrically obtained results for cold atom-molecule collisions in the supersonic beam excite us to continue collisional study.

We have analysed the cold atom-molecule collisions in the supersonic beam by reducing the density of the colliding atoms and observing the difference for the gained phase of interference patterns between these two situations. So if we now increase the density in the potassium beam we can expect also change in the contrast of interferences and phase shift. As a realization of this idea we want to use again resonant to ^{39}K atoms radiation but this time we want to cool atoms and compress in two dimensions (2D MOT [60, 61, 62] or 2D Raman cooling [63]). By increasing atomic density by factor of 10 we should be able to observe 10 times bigger phase shifts compare to switching of atomic density but with opposite sign.

Until now we discussed changes in the refractive index for the molecular matter wave caused by changes in the particle density in the beam. Another possibility to vary the index of refraction is to change the cross section between colliding particles.

Systematic investigation of cold collisions between potassium molecules and atoms in Rydberg states [35] will be continued. We want to examine collisional effects for different Rydberg states (8s, 12s, 13s, etc.) and several v and J quantum numbers within potassium b-X molecular system. The preparation of Rydberg states will be done by two steps excitation: the first excitation laser should be resonant to 4s-4p atomic transition and the second laser frequency will be in blue part of the spectra to excite from 4p state to long living Rydberg state. In order to avoid uncontrolled state mixing we have control to precisely light polarization and residual magnetic field for preparation of Rydberg states, which significantly simplified after installation of the μ -metal box shielding the magnetic field in the interferometer chamber down to 20 mG.

The interesting topic under the theme of suitability of the molecular matter wave interferometry to examine weak interactions can be the study of light shift on potassium molecules caused by near resonant light. If we apply in one of the dark zones of the Ramsey-Bordé interferometer setup light which couples near resonantly either the ground or the excited state, the molecular path of the respective state will feel an additional potential which leads to an extra phase shift. The aim of such experiment will be measurement of change of contrast and phase of interference patterns as a function of the frequency detuning and intensity of near resonant light.

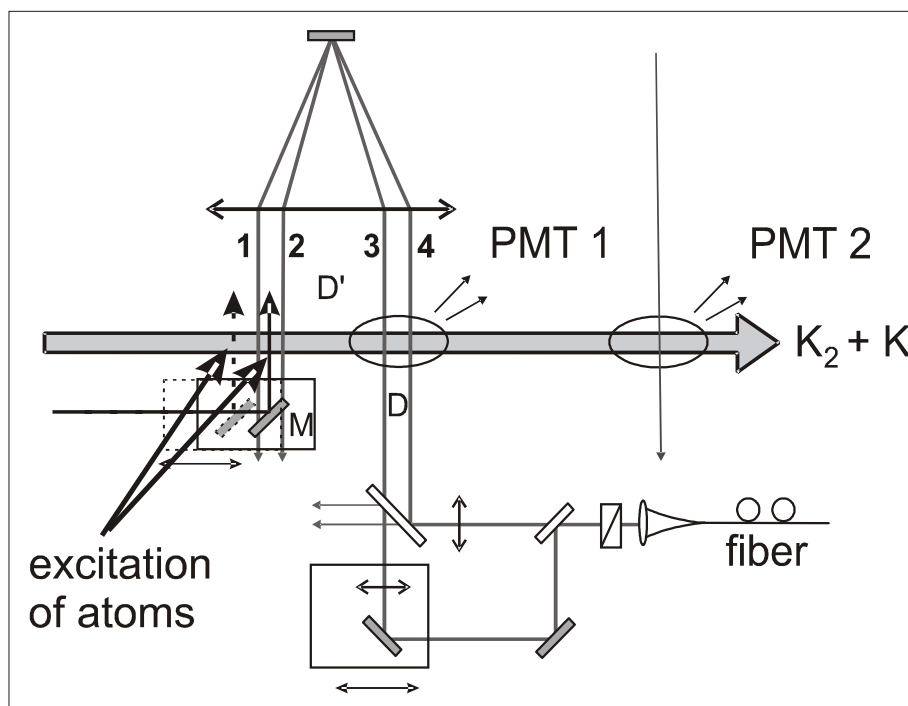


Figure 7.1 Perspective setup for study collisions with K atoms in Rydberg states and influence of near resonant light on the properties of molecular matter wave interferometer

The possible scheme of the experimental setup to study cold collisions between $^{39}\text{K}_2$ molecules and ^{39}K atoms in Rydberg states or influence of near resonant light on interferences is presented in Figure 7.1. By installing the additional mirror M mounted on a translational stage we can guide laser light inside or outside of the interferometer. In principle, to increase an effect of the light-particle interaction we can introduce laser light in both dark zones, but its presence in the dark zone between interferometer laser beams 3 and 4 could cause some unwanted background observed by the excited state exit detection.

While at all the time we simultaneously record both, the longitudinal and transversal, types of interferences, only the longitudinal Ramsey-Bordé interferences were used in applications to investigate cold collisions in the potassium beam. The atom-molecule collisions are relatively small effect and their influence on the characteristics of the transversal optical Ramsey interferences was not investigated mainly because of the high sensitivity of the optical Ramsey interferometer to laser or optical instability causing large deviations in phase and because the expected phase shift is two times smaller compared to the longitudinal interferometer due to the length of the dark zone. But for relatively short length of the dark zone the recorded signals of the optical Ramsey interferences anyway show quite good signal-to-noise ratio and can reach the contrast of 100 %. So we want to improve significantly the mechanical stability of the optical Ramsey matter wave interferometer by passive (better isolation of all optical components of the interferometer from the environment) and/or active (stabilization of the phase difference of the laser beam splitters by optical interferometer) means and implement it in the same way as the longitudinal one.

Literature

1. Paul R. Berman: *Atom interferometry*, Academic Press 1997
2. L. Marton: *Electron Interferometer*, Phys. Rev. **85**, 1057–1058, 1952
3. H. Maier-Leibnitz, T. Springer, Z. Phys. **167**, 368, (1962)
4. G. Badurek, H. Rauch, W. Bauspiess, U. Bonse, and A. Zeilinger: *Phase-shift and spin-rotation phenomena in neutron interferometry*, Phys. Rev. D **14**, 1177–1181, (1976)
5. F. Riehle, A. Witte, Th. Kisters and J. Helmcke: *Interferometry with Ca Atoms*, Appl. Phys. B **54**, 333-340 (1992)
6. David W. Keith, Christopher R. Ekstrom, Quentin A. Turchette, and David E. Pritchard: *An interferometer for atoms*, Phys. Rev. Lett. **66**, 2693–2696 (1991)
7. C. Degenhardt, H. Stoehr, C. Lisdat, G. Wilpers, H. Schnatz, B. Lipphardt, T. Nazarova, P.-E. Pottie, U. Sterr, J. Helmcke, and F. Riehle: *Calcium optical frequency standard with ultracold atoms: Approaching 10^{-15} relative uncertainty*, Phys. Rev. A **72**, 062111 (2005)
8. J. J. Hudson, B. E. Sauer, M. R. Tarbutt, and E. A. Hinds: *Measurement of the Electron Electric Dipole Moment Using YbF Molecules*, Phys. Rev. Lett. **89**, 023003 (2002)
9. Klaus Hornberger, Stefan Uttenthaler, Björn Brezger, Lucia Hackermüller, Markus Arndt, and Anton Zeilinger: *Collisional Decoherence Observed in Matter Wave Interferometry*, quant-ph/0303093, (2003)
10. M. Arndt, O. Nairz, J. Vos-Andreae, C. Keller, G. van der Zouw, A. Zeilinger: *Wave – particle duality of C_{60} molecules*, Nature **401**, 680 (1999)
11. E. M. Rasel, M. K. Oberthaler, H. Batelaan, J. Schmiedmayer, A. Zeilinger: *Atom wave interferometry with diffraction gratings of light*, Phys. Rev. Lett. **75**, 2633 (1995)
12. S. Dettmer, D. Hellweg, P. Ryytty, J. J. Arlt, W. Ertmer, D. S. Petrov, G. V. Shlyapnikov, H. Kreutzmann, L. Santos, M. Lewenstein and K. Sengstock: *Observation of Phase Fluctuations in Elongated Bose-Einstein Condensates* Phys. Rev. Lett. **87**, 160406 (2001)

13. T. Weber, J. Herbig, M. Mark, H.-C. Nagerl, and R. Grimm, *Science* **299**, 232 (2003)
14. A. Wicht, E. Sarajlic, J. M. Hensley, and S. Chu: *Phase shifts in precision atom interferometry due to the localization of atoms and optical fields*, *Phys. Rev. A* **72**, 023602 (2005)
15. R. A. Cornelussen, R. J. C. Spreeuw, and H. B. van Linden van den Heuvell: *An atom interferometer enabled by spontaneous decay*, *Phys. Rev. A* **71**, 033627 (2005)
16. Richard B. Bernstein: *Atom-molecule collision theory*, Plenum Press 1979
17. G. Scoles: *Atomic and molecular beam methods*, Vol. 1, Oxford Univ. Press 1988
18. G. Herzberg: *Molecular spectra and molecular structure, I. Spectra of diatomic molecules*, van Nostrand Reinhold Company, 1950
19. N. F. Ramsey: *Molecular beams*, Oxford University Press 1956
20. A. S. Davydov: *Quantum mechanics*, Pergamon Press 1965
21. Ch. Bordé: *Atomic interferometry with internal state labelling*, *Phys. Lett. A* **140**, 10 (1989)
22. A. Lenef, T. D. Hammond, E. T. Smith, M. S. Chapman, R. A. Rubenstein, D. E. Pritchard: *Rotation sensing with an atom interferometer*, *Phys. Rev. Lett.* **78**, 760 (1997)
23. M. Kasevich, S. Chu: *Measurement of the gravitational acceleration of an atom with a light-pulse atom interferometer*, *Appl. Phys. B* **54**, 321 (1992)
24. T. L. Gustavson, A. Landragin, M. A. Kasevich: *Rotation sensing with a dual atom-interferometer Sagnac gyroscope*, *Class. Quantum Grav.* **17**, 2385 (2000)
25. T. L. Gustavson, P. Bouyer, M. A. Kasevich: *Precision rotation measurements with an interferometer gyroscope*, *Phys. Rev. Lett.* **78**, 2046 (1997)
26. T. D. Hammond, M. S. Chapman, A. Lenef, J. Schmiedmayer, E. T. Smith, R. A. Rubenstein, D. Kokorowski, D. E. Pritchard: *Matter-wave index of refraction, inertial sensing, and quantum decoherence in an atom interferometer*, *Braz. J. Phys.* **27**, 193 (1997)
27. C. Champenois, E. Audouard, P. Dupl a, J. Vigu e: *Refractive index for atomic waves: Theory and detailed calculations*, *J. Phys. II France* **7**, 523 (1997)

28. J. Vigué: *Index of refraction of dilute matter waves in atomic interferometry*, Phys. Rev. A **52**, 3973 (1995)
29. J. Schmiedmayer, M. S. Chapman, C. E. Ekstrom, T. D. Hammond, S. Wehinger, D. E. Pritchard: *Index of refraction of various gases for Sodium matter waves*, Phys. Rev. Lett. **74**, 1043 (1995)
30. Ch. Bordé, Ch. Salomon, S. Avrillier, A. Van Lerberghe, Ch. Bréant, D. Bassi, G. Scoles: *Optical Ramsey fringes with travelling waves*, Phys. Rev. A **30**, 1836 (1984)
31. Ch. Bordé, N. Courtier, F. du Burck, A. N. Goncharov, M. Gorlicki: *Molecular interferometry experiments*, Phys. Lett. A **188**, 187 (1994)
32. Sebastian Jung: *Untersuchungen zur Manipulation von Stoßbedingungen zwischen Atomen und Molekülen in einem Materiewelleninterferometer*, Diplomarbeit, Universität Hannover, 2002
33. Sha Liu: *Molecular matter wave interferometry: laser systems, method of detection and applications*, diploma work, Universität Hannover 2005
34. Ch. Lisdat: *Experimente zum kohärenten Besetzungstransfer mit zwei Lasern am K_2 -Molekülstrahl*, Diplomarbeit, Hannover 1997
35. Christian Lisdat: *Realisation eines Materiewelleninterferometers für Moleküle und neue Möglichkeiten zur Beobachtung von Atom-Molekül-Stößen*, Doktorarbeit, Universität Hannover, 2001
36. K. Sengstock: *Ramsey Atominterferometrie an lasermanipulierten, kalten Atomen*, Dissertation, Bonn 1993
37. Matthias Frank: *Aufbau eines frequenzstabilisierten Diodenlaserpaares mit großer kontrollierbarer Differenzfrequenz*, Diplomarbeit, Universität Hannover, 1999.
38. Ch. Lisdat, M. Frank, H. Knöckel, E. Tiemann: *Modulation techniques in a molecular Ramsey-Bordé interferometer*, Appl. Phys. B **73**, 99 (2001)
39. Ch. Lisdat, M. Frank, H. Knöckel, M.-L. Almazor, E. Tiemann: *Realization of a Ramsey-Bordé matter wave interferometer on the K_2 molecule*, Eur. Phys. J. D **12**, 235 (2000)
40. Ch. Lisdat, H. Knöckel, E. Tiemann: *First observation of hyperfine structure in K_2* , J. Mol. Spec. **199**, 81 (2000)

41. R. W. P. Drever, J. L. Hall, F. V. Kowalsky, J. Hough, G. M. Ford, H. Munley, H. Ward: *Laser phase and frequency stabilization using an optical resonator*, Appl. Phys. B **31**, 97 (1983)
42. W. T. Hicks: *Evaluation of Vapor-Pressure Data for Mercury, Lithium, Sodium, and Potassium*, The Journal of Chemical Physics **38**, 8, 1873-1880, (1963)
43. R. V. Pound: *Electronic frequency stabilization of microwave oscillators*, Rev. Sci. Instr. **17**, 490 (1946)
44. O. Stern, Naturwiss. **17**, 391 (1929)
45. R. Delhuille, C. Champenois, M. Büchner, R. Mathevet, C. Rizzo, C. Robilliard and J. Vigué: *Atom interferometry: principles and applications to fundamental physics*, Quantum Electrodynamics and the Physics of the Vacuum, QED 2000, AIP Conference Proceedings **564**, 192-199 (2001)
46. Christian J. Bordé: *Quantum Theory of Atom-Wave Beam Splitters and Applications to Multidimensional Atomic Gravito-Inertial Sensors*, General Relativity and Gravitation, **36**, 3, (2004)
47. Bordé, Ch. J. (2001). *C. R. Acad. Sci. Paris, t. 2* (Série IV), 509–530.
48. H. L. Bethlem, and G. Meijer: *Production and application of translationally cold molecules*, Int. Reviews in Physical Chemistry, **22**, 1, (2003) 73–128
49. U. Sterr, K. Sengstock, J. H. Müller, D. Bettermann, W. Ertmer: *The Magnesium Ramsey interferometer: Applications and prospects*, Appl. Phys. B **54**, 341 (1992)
50. J. Heinze and F. Engelke: *The $B^1\Pi_u$ potential energy curve and dissociation energy of $^{39}K_2$* , J. Chem. Phys. **89**, 1, (1988)
51. William H. Press, Brian P. Flannery, Saul A. Teukolsky, William T. Vetterling: *Numerical Recipes in C: The Art of Scientific Computing*, Cambridge University Press 1988
52. Christian Samuelis: *Spektroskopie und optische Manipulation kalter Stöße in einem Natrium-Molekülstrahl*, Doktorarbeit, Universität Hannover, 2003
53. Harold J. Metcalf, Peter van der Straten: *Laser Cooling and Trapping*, Springer 1999
54. K. Davis, M-O. Mewes, M. Andrews, M. van Druten, D. Durfee, D. Kurn, and W. Ketterle: *Bose-Einstein Condensation in a Gas of Sodium Atoms*, Phys. Rev. Lett. **75**, 3969 (1995)

55. H. Schnatz, B. Lipphart, C. Degenhart, E. Peik, T. Schneider, U. Sterr, Chr. Tamm: *Optical frequency measurements using fs-comb generators*, IEEE Trans. Instrum. and Meas., **54**, 750-753 (2005)
56. Stephan Falke, Eberhard Tiemann, Harald Schnatz, Gesine Grosche and Christian Lisdat: *The transition frequencies of the D lines of ^{39}K , ^{40}K and ^{41}K measured with femtosecond laser frequency comb*, submitted to PRA
57. C. H. Townes, A. L. Schawlow: *Microwave Spectroscopy*, Dover Publications, Inc. 1975
58. Shannon Blanchard, Dave Civello, and Robert C. Forrey: *Index of refraction for sodium matter waves traveling in a cold noble-gas medium* Phys. Rev. A **67**, 013604 (2003)
59. A. F. J. van Raan, J. E. M. Haverkort, and J. Korving: *Self-shift and foreign-gas-induced shift of molecular Rydberg states measured in a thermionic heat-pipe oven*, J. Phys. B: At. Mol. Phys. **17**, L823-L827, (1984)
60. J. Catani, P. Maioli, L. De Sarlo, F. Minardi, and M. Inguscio: *Intense slow beams of bosonic potassium isotopes*, Phys. Rev. A **73**, 033415 (2006)
61. J. Schoser, A. Batär, R. Löw, V. Schweikhard, A. Grabowski, Yu. B. Ovchinnikov, and T. Pfau: *Intense source of cold Rb atoms from a pure two-dimensional magneto-optical trap*, Phys. Rev. A **66**, 023410 (2002)
62. K. Dieckmann, R. J. C. Spreeuw, M. Weidemüller, and J. T. M. Walraven: *Two-dimensional magneto-optical trap as a source of slow atoms*, Phys. Rev. A **58**, 3891-3895 (1998)
63. Nir Davidson, Heun Jin Lee, Mark Kasevich, and Steven Chu: *Raman cooling of atoms in two and three dimensions*, Phys. Rev. Lett. **72**, 3158–3161 (1994)

Curriculum Vitae

Name: Ivan V. Sherstov
Date and place of birth: November 10, 1979, Moscow, USSR (Russian Federation)
Parents: Elena I. Sherstova, Valeriy I. Sherstov
Family status: married, wife Yulia Sherstova, son Alexander Sherstov
Citizenship: Russian

Study

09.1986 – 11.1993 secondary school № 941, Moscow, Russia
11.1993 – 06.1996 experimental school № 1073, Moscow, Russia
09.1996 – 03.2002 Moscow Engineering Physics Institute (State University), got a national degree “engineer-physicist” in the field of “Solid state physics”
09.2000 – 03.2002 prediploma and diploma work in Frequency standards laboratory, P.N. Lebedev Physical Institute, Russian Academy of Science, Troitsk, Russia
07.2002 – 10.2002 guest coworker in PTB, Braunschweig, Germany
12.2002 – 07.2006 member of European Graduate College and PhD student in Prof. Tiemann working group, Hannover University (Hannover, Germany)

Thanks, Danke, Спасибо

Many persons contributed to the success of this work in many different ways, for which I am very grateful. My special thanks to:

- Mr. Professor Dr. Eberhard Tiemann, that I could make this work in his research group. I appreciate greatly and learned a lot from all helpful discussions with him and valuable advices. I will always remember his professionalism, honesty and, especially, his patience to me during my work in his group. Danke!
- Mr. Dr. Horst Knöckel for his invaluable support in the experimental work and his humaneness. Although we belong to different generations and cultures I will always consider him as my dear friend. Danke!
- Mr. at the time when I'm writing this yet Dipl.-Phys. ☺ Sebastian Jung. I probably will never able fully cover that several billions euro dept for your help which appeared since my stay in Germany, but I promise to do my best! ☺ Danke!
- Mrs. Dipl.-Phys. Sha Liu for her help in running the experiment. I learn a lot in the process of supervising you. Thanks!
- Dr. Asen Pashov for his help and moral support during my stay in Hannover, especially, in the first months. Благодаря!
- All present and former members of the small society called "Tiemann AG": Dipl.-Phys. Andreas Gerdes, Dipl.-Phys. Stephan Falke, Dr. Christian Lisdat, Dr. Olivier Allard, Dr. Christian Samuelis, Dipl.-Phys. Matthias Frank, Dipl.-Phys. Frau Kirsten Jaspers, Alexander Stein, Marcin Nowak for discussions and shearing with me day by day the lab life. You showed me how interesting and many-sided could be humans' relationships. Thanks, Danke, Merci!!!
- Моей семье за моральную поддержку. Особенно, моей жене Юлии за то, что она так многим пожертвовала и так много сделала, чтобы дать мне возможность сделать эту работу. Огромное Спасибо!!!